

**DEVELOPMENT OF 2D TESTBEDS AND
IMPLEMENTATION OF HELIX ANTENNAS USING
FREQUENCY AND TIME DOMAIN
MEASUREMENTS FOR ASSESSMENT OF CWR
TECHNOLOGIES**

by

Jonathan Toro Vázquez

A thesis submitted in partial fulfillment of the requirements for the degree of

MASTER OF SCIENCES
in
ELECTRICAL ENGINEERING

UNIVERSITY OF PUERTO RICO
MAYAGÜEZ CAMPUS
2012

Approved by:

Ingrid Padilla, PhD
Member, Graduate Committee

Date

José Colom, PhD
Member, Graduate Committee

Date

Rafael Rodríguez-Solís, PhD
President, Graduate Committee

Date

Hector Rosario, PhD
Representative of Graduate Studies

Date

Pedro I. Rivera, PhD
Chairperson of the Department

Date

ABSTRACT

The contamination of underground systems causes serious detriment to the environment and can pose a serious threat to human health. The challenge of locating many common contaminants creates the need to develop technologies that enhance our ability to detect and characterize underground contamination. Cross-Well Radar (CWR) is being evaluated as a potential technology for detection of hazardous contaminants, such as Dense Non-Aqueous Phase Liquids (DNAPLs), present in underground environments. This work addresses the development of enabling CWR technologies that rely on the use of transmission and reflection measurements to detect changes in soil electromagnetic (EM) properties caused by the presence of underground target elements, such as DNAPL contamination. Time- and frequency-domain measurements and simulations are applied to assess the performance of antennas and design testbeds for proper estimation of EM properties in soil systems. Results indicate that proper development of CWR testbeds must account for wave propagation near sharp EM boundaries. Time-domain analysis shows that transmission and reflection measurements in a properly developed testbed can be applied to accurately estimate EM properties of bulk soil. The integrated use of soil testbeds with time- and frequency-domain EM modeling, thus, lead to enhanced CWR enabling technologies for DNAPLs detection in underground environments.

RESUMEN

La contaminación de suelos causa serios deterioros a la calidad ambiental y presenta una amenaza a la salud humana. El reto de localizar estos contaminantes potentes ha llevado a desarrollar tecnologías que tengan potencial para la localización y caracterización en suelos de estos peligrosos contaminantes. “Cross-Well Radar” (CWR por sus siglas en inglés) es evaluado como una tecnología con potencial para detectar peligrosos contaminantes como lo son compuestos más densos que el agua (“Dense Non-Aqueous Phase Liquids”-DNAPLs por sus siglas en inglés) presentes en ambientes subterráneos. Este trabajo trata del desarrollo de aplicar “CWR” el cual se basa en medidas de transmisión y reflexión de ondas electromagnéticas (EM) para detectar cambios en las propiedades electromagnéticas de suelo causado por la presencia de “DNAPLs”. Medidas y simulaciones en el dominio en frecuencia y tiempo fueron realizados para poder estudiar el rendimiento de antenas en suelo y para el diseño de tanques para realizar medidas apropiadas de suelo con el fin de obtener estimados apropiados de las propiedades electromagnética del suelo estudiado. Los resultados indican que es necesario el desarrollar tanques apropiados para poder obtener que la onda electromagnética al propagarse cerca de las fronteras del tanque sean adecuadas para tener buenos estimados de las propiedades del suelo. El análisis en el dominio del tiempo nos demostró que las medidas de transmisión y reflexión en un tanque apropiado puede aplicarse para obtener unos estimados precisos de las propiedades electromagnéticas del suelo estudiado. La

integración de usar modelaje en el dominio del tiempo y frecuencia en tanques para realizar pruebas de suelo demuestra el poder utilizar tecnologías como “CWR” para detectar “DNAPLs” presentes en ambientes sub-superficiales.

To my family . . .

ACKNOWLEDGEMENTS

During the development of my graduate studies here in the University of Puerto Rico at Mayagüez, several persons and institutions collaborated directly and indirectly with my research. Without their support it would have been impossible for me to finish my work.

I want to start my sincere acknowledgement to my advisor Dr. Rafael Rodríguez Solís for giving me the opportunity to work on this research and for giving me guidance, supervision, support, and learning experiences all this time as a graduate student. I also want to acknowledge Dr. Ingrid Padilla for letting me be part of this research team, and also for given me the support, guidance, and confidence since the beginning of this research. I am very grateful with both of them and I feel truly very fortunate to have them as supervisors. I want to thank Dr. Henrick Mario Ierkic for its support and collaboration during my research. I want to thank Dr. José Colom who motivated and inspired me to explore the world of microwave engineering; it has been a wonderful experience learning from him since I was an undergraduate student. An important acknowledgement goes to Dr. Nelson Sepúlveda who encouraged and motivated me to the work on research. I had a great experience learning from him.

I want to thank my brothers Gianni Pablos, Juan Casillas, and Jose Cordero (Gaki Crew) who were together with me since we were undergraduate students. We learned, we grew up, we enjoyed every midnight moment working hard at the labs and all the experience that we developed as undergraduate and graduate students. I sincerely want to

thank my friend Ledinés Hernández for supported me during these final moments of my research and for giving me her unconditional friendship when I most needed it during difficult situations.

I want to thank my parents Monserrate and Miriam who supported and encouraged me to go to the university and get educated. This has been the best gift I received from them, the experience of being educated and becoming a better person to contribute to this world. They gave me the knowledge and the counseling to keep fighting in every battle to reach my goals. I also want to sincerely thank my aunt Nora who was the person that did her maximum to be able to be accepted here to University of Puerto Rico at Mayagüez. Without her I would probably be somewhere else.

I want to thank Perla Torres, Ángel Anaya, Zalleris Escobar, María de Lourdes, and the rest members of the Environmental Engineering Laboratory and also to Victor Asencio, Samuel Rosario, and Marie Ayala from LARSIP for their support and collaboration throughout my graduate studies. Also I want sincerely acknowledge Dr. Scott Tsai for his help, counseling, and guidance during difficult situations through my graduate studies.

I want to acknowledge to the U.S. Department of Energy Savannah River (Grant Award No. DE-FG09-07SR22571) and Gordon-CenSSIS, the Bernard M. Gordon Center for Subsurface Sensing and Imaging Systems, under the Engineering Research Centers Program of the National Science Foundation (Award Number EEC-9986821) for providing the funding resources for this research.

Table of Contents

ABSTRACT	II
RESUMEN	III
ACKNOWLEDGEMENTS	VI
TABLE OF CONTENTS	VIII
TABLE LIST	X
FIGURE LIST	XI
1 INTRODUCTION.....	1
1.1 JUSTIFICATION	1
1.2 OBJECTIVES	4
1.3 THESIS STRUCTURE.....	4
2 LITERATURE REVIEW	6
2.1 OVERVIEW	6
2.2 THEORETICAL BACKGROUND.....	7
2.2.1 <i>Electromagnetic Wave Propagation</i>	7
2.2.2 <i>S-parameters</i>	9
2.2.3 <i>Antennas</i>	10
2.2.4 <i>Electromagnetic Properties of a Material</i>	12
3 METHODOLOGY	18
3.1 OVERVIEW	18
3.2 TESTBED DESIGN	18
3.2.1 <i>Design Considerations</i>	19
3.2.2 <i>Design Limitations;</i>	20
3.3 HELIX ANTENNA MODELING	21
3.3.1 <i>Antenna Design</i>	22
3.3.2 <i>Soilbed Model</i>	23
3.3.3 <i>S-parameters Preliminary Results of the Simulated Model for Different Assigned EM Properties</i>	26
3.4 HELIX ANTENNA FABRICATION AND SOILBED SETUP	28
3.4.1 <i>Antenna Fabrication</i>	29

3.4.2	<i>Tank Construction</i>	30
3.5	EXPERIMENTAL MEASUREMENTS	31
3.5.1	<i>Frequency Domain Measurements</i>	33
3.5.2	<i>Time Domain Measurements</i>	35
3.6	ESTIMATION OF THE ELECTROMAGNETIC PROPERTIES USING FREQUENCY DOMAIN MEASUREMENTS	40
3.6.1	<i>Transmission and Reflection Equations for Lossy Media</i>	41
3.6.2	<i>EM Properties Estimates using Two Frequency Points</i>	42
3.6.3	<i>Channel Transfer Function Method</i>	43
3.7	TIME DOMAIN MODELING	44
3.8	ESTIMATION OF ELECTROMAGNETIC PROPERTIES IN TIME DOMAIN	47
4	ANALYSIS AND RESULTS	52
4.1	OVERVIEW	52
4.2	ESTIMATION OF THE EM PROPERTIES	52
4.2.1	<i>Estimates Using Transmission and Reflection Equations for Lossy Media</i> .	53
4.2.2	<i>Estimates of the EM Properties Using Two Frequency Points</i>	53
4.2.3	<i>Estimates of the EM Properties Using Channel Transfer Function Method;</i> 56	
4.2.4	<i>Analysis in the Phase Component of the Transmission Response</i>	57
4.2.5	<i>Estimates of the Relative Permittivity using a Modified Phase Shift</i>	60
4.3	DESIGN OF HELIX ANTENNA FOR SOILBED TESTING.....	77
4.3.1	<i>Effect of Helix Diameter in the S-parameters Results</i>	78
4.3.2	<i>Effect of Number of Turns</i>	79
4.3.3	<i>Effect of Width Strip in the S-parameters Response</i>	80
4.3.4	<i>S-parameters Response under Different Assigned EM Properties</i>	81
4.3.5	<i>Final Design of the Helix Antenna</i>	82
4.4	PRELIMINARY S-PARAMETERS MEASUREMENTS OF DRY SAND SOILBED USING HELIX ANTENNAS	84
4.4.1	<i>Helix Antenna Measurements</i>	84
4.4.2	<i>Estimates of the Relative Permittivity of Helix Antenna Measurements</i>	89
4.5	TIME DOMAIN EXPERIMENTS.....	95
4.6	FREQUENCY MODELING OF THE EXTENDED TESTBED	101
4.7	ESTIMATES OF THE RELATIVE PERMITTIVITY FOR THE SIMULATED EXTENDED TESTBED MODEL IN TIME DOMAIN	112
5	CONCLUSIONS AND RECOMMENDATIONS.....	125
5.1	CONCLUSIONS.....	125
5.2	RECOMMENDATIONS.....	126
	REFERENCES.....	127

Table List

Tables	Page
Table 3.1 Summary of the Dimensions for the Designed Tank.....	21
Table 3.2 Helix Antenna Design Physical Limitations.....	22
Table 3.3 Assigned EM Properties Used to Model the Helix Antenna.....	23
Table 3.4 Assigned Relative Permittivity of the Simulated Testbed Model Using Transient Network Analysis.....	46
Table 4.1 Relative Permittivity Estimates Using the Equations on Lossy Media.....	54
Table 4.2 Estimates of the Relative Permittivity Using Two Frequencies Points.....	55
Table 4.3 Estimates of the Relative Permittivity Using Channel Transfer Function.....	57
Table 4.4 Estimates of the Relative Permittivity for Dry Sand Soilbed Measurements.....	69
Table 4.5 Estimates of the Relative Permittivity for Dry Sand Soilbed Measurements.....	70
Table 4.6 Estimates of the Relative Permittivity of Dry Sand Soilbed Measurements With TCE Injected for 50 Minutes.....	71
Table 4.7 Estimates of the Relative Permittivity for Dry Sand Soilbed Measurements (Saturated Sand Background).....	73
Table 4.8 Estimates of the Relative Permittivity for Saturated Sand Soilbed Measurements.....	74
Table 4.9 Estimates of the Relative Permittivity for Saturated Sand Soilbed Measurements With TCE Injected for 45 Minutes.....	75
Table 4.10 Final Geometry Dimensions of the Designed Helix Antennas.....	83
Table 4.11 Estimates of the Relative Permittivity of the Simulated Extended Testbed Model.....	113
Table 4.12 Estimates of the Relative Permittivity for the Simulated Testbed Model in Air Medium.....	119
Table 4.13 Estimates of the Relative Permittivity for the Simulated Extended Testbed Model of Air Medium With the Antennas Placed at Different Height Boreholes.....	122

Figure List

Figures	Page
Figure 2.1 Illustration of the Electromagnetic Wave Propagation.....	9
Figure 2.2 Illustration of a Parallel-Plate Waveguide.....	10
Figure 2.3 Two Port Network Representation of the S-parameters.....	11
Figure 2.4 Illustration of a Helix Antenna Configuration.....	13
Figure 3.1 Diagram of the Design Tank for Soilbed Testing.....	19
Figure 3.2 Diagram of the Simulated Soilbed Model in HFSS.....	24
Figure 3.3 Waveport Used to Feed the Soilbed Model in HFSS.....	25
Figure 3.4 Input Parameters of the Assigned Excitation Used to Feed the Soilbed Model in HFSS.....	26
Figure 3.5 Simulated Return Loss for the Helix Antenna in Dry Sand Soilbed.....	27
Figure 3.6 Simulated Insertion Loss for the Helix Antenna in Dry Sand Soilbed.....	28
Figure 3.7 Fabricated Helix Antennas Made With Delrin Rod, Copper Strip, and SMA Connectors.....	29
Figure 3.8 Constructed Tank for Soilbed Testing filled With Dry Sand Soil.....	31
Figure 3.9 Agilent's Vector Network Analyzer Model ENA 5071C.....	32
Figure 3.10 Protective Well-Casing Pipe.....	33
Figure 3.11 Return Loss Measurements of Dry Sand Soilbed Using the Fabricated Helix Antennas.....	34
Figure 3.12 Insertion Loss Measurements of Dry Sand Soilbed Using the Fabricated Helix Antennas.....	34
Figure 3.13 Measured Reflection Response of Air Medium Testbed Using Helix Antennas.....	36
Figure 3.14 Measured Transmission Response of Air Medium Testbed Using Helix Antennas.....	36
Figure 3.15 Metal Plates Placed on the Testbed for Boundary Conditions Experiments.....	37
Figure 3.16 Illustration of the Constructed Testbed With a Metal Plate Place at Top of the Testbed Used for the S-parameters Measurements.....	38
Figure 3.17 Illustration of the Constructed Testbed With Horizontal Metal Plates Placed at the Faces of the Mesh Plates of the Testbed Used for the S-parameters Measurements.....	38
Figure 3.18 Illustration of the Constructed Testbed With Vertical	

Metal Plates Placed at the Faces of the Mesh Plates of the Testbed Used for the S-parameters Measurements.....	39
Figure 3.19 Borehole Locations of the Testbed Where the Helix Antennas Were Placed for the Time Domain Experiments.....	40
Figure 3.20 Simulated Testbed Model Used for Transient Network Analysis.....	45
Figure 3.21 Input Signal Used for Transient Network Analysis of the Simulated Testbed Model.....	46
Figure 3.22 Transmission Response and Variable Selection for the Simulated Model Using Transient Network Analysis.....	49
Figure 3.23 Reflection Response and Variable Selection for the Simulated Model Using Transient Network Analysis.....	50
Figure 3.24 Reflection Response for the Simulated Model of Air Medium Testbed.....	50
Figure 3.25 Transmission Response for the Simulated Model of Air Medium Testbed.....	51
Figure 4.1 Phase Component of the Measured Transmission Response for Dry Sand Soilbed.....	61
Figure 4.2 Phase Component of the Measured Transmission Response (S51) for Dry Sand Soilbed.....	64
Figure 4.3 Phase Component of the Measured Transmission Response (S82) for Dry Sand Soilbed.....	64
Figure 4.4 Phase Component of the Measured Transmission Response (S51) for Saturated Sand Soilbed.....	65
Figure 4.5 Phase Component of the Measured Transmission Response (S82) for Saturated Sand Soilbed.....	65
Figure 4.6 Phase Component of the Measured Transmission Response (S52) for Saturated Sand Soilbed.....	66
Figure 4.7 Phase Component of the Measured Transmission Response (S71) for Saturated Sand Soilbed.....	66
Figure 4.8 Phase Component of the Measured Transmission Response (S53) for Saturated Sand Soilbed With TCE Injected for 45 Minutes.....	67
Figure 4.9 Phase Component of the Measured Transmission Response (S71) for Saturated Sand Soilbed With TCE Injected for 45 Minutes.....	67
Figure 4.10 Phase Component of the Measured Transmission Response (S51) for Dry Sand Soilbed After Applying Channel Transfer Function Method.....	76
Figure 4.11 Phase Component of the Measured Transmission Response (S62) for Dry Sand Soilbed After Applying	

Channel Transfer Function Method.....	77
Figure 4.12 Simulated Return Loss Response for the Helix Antenna in Dry Sand Soilbed With a Helix Diameter of 0.64cm.....	78
Figure 4.13 Simulated Return Loss Response for the Helix Antenna in Dry Sand Soilbed With a 1 Turn (Blue Trace) and 3 Turns (Green Trace).....	79
Figure 4.14 Simulated Return Loss Response for the Helix Antenna in Dry Sand Soilbed With a Width Strip of 0.8cm (Blue Trace) and 1.4cm (Green Trace).....	81
Figure 4.15 Simulated Return Loss Response for the Helix Antenna in Dry Sand Soilbed (Blue Trace), Saturated Sand Soilbed (Green Trace), and Distilled Waterbed (Red Trace).....	82
Figure 4.16 Simulated Return Loss for the Designed Helix Antenna in Dry Sand Soilbed.....	84
Figure 4.17 Simulated and Measured Return Loss Response of Dry Sand Soilbed.....	85
Figure 4.18 Simulated and Measured Insertion Loss Response of Dry Sand Soilbed.....	86
Figure 4.19 Protective Well-Casing Pipe with the Constructed Helix Antenna Used in the S-parameters Measurements.....	86
Figure 4.20 Simulated Model Diagram of the Helix Antennas Placed Inside the Protective Well-Casing Pipe.....	88
Figure 4.21 Simulated and Measured Return Loss Response of Dry Sand Soilbed Including a Protective Well-Casing Pipe.....	88
Figure 4.22 Simulated and Measured Insertion Loss Response of Dry Sand Soilbed Including a Protective Well-Casing Pipe.....	89
Figure 4.23 Insertion Loss Response (Top), Expanded Phase Component (Middle) and Estimate of the Relative Permittivity (Bottom) for Dry Sand Soilbed With the Helix Antennas Placed at Middle Borehole Location.....	91
Figure 4.24 Expanded Phase Component (Top) and Estimate of the Relative Permittivity (Bottom) for an Air Medium Testbed Using Gating Option and Antennas Placed at Middle Borehole Location.....	93
Figure 4.25 Expanded Phase Component (Top) and Estimate of the Relative Permittivity (Bottom) for an Air Medium Testbed Using Gating Option and Antennas Placed Below Middle Borehole Location.....	93
Figure 4.26 Expanded Phase Component (Top) and Estimate of the Relative Permittivity (Bottom) for an Air Medium Testbed using Gating Option and Antennas Placed at Top Borehole Location.....	94

Figure 4.27 Expanded Phase Component (Top) and Estimate of the Relative Permittivity (Bottom) for an Air Medium Testbed Using Gating Option and Antennas Placed Above Middle Borehole Location.....	94
Figure 4.28 Expanded Phase Component (Top) and Estimate of the Relative Permittivity (Bottom) for an Air Medium Testbed Using Gating Option and Antennas Placed at Bottom Borehole Location.....	95
Figure 4.29 Measured Reflected Response of an Air Medium Testbed. Helix Antennas Located at Top (Blue Trace), Middle (Green Trace), and Bottom (Red Trace) Borehole Location.....	96
Figure 4.30 Measured Transmitted Response of an Air Medium Testbed. Helix Antennas Located at Top (Blue Trace), Middle (Green Trace), and Bottom (Red Trace) Borehole Location.....	97
Figure 4.31 Measured Transmission Response of Air Medium Testbed. Helix Antennas Located at Top (Blue Trace) and at Top with Metal Plate Placed on Top (Green Trace) Borehole Locations of the Testbed.....	98
Figure 4.32 Measured Transmission Response of Air Medium Testbed. Helix Antennas Located at Bottom (Blue Trace) and at Bottom with Metal Plate Placed on Top (Green Trace) Borehole Location of the Testbed.....	99
Figure 4.33 Measured Transmission Response of Air Medium Testbed. Helix Antennas Located at Middle (Blue Trace) and at Middle With Extended Vertical Metal Plates (Green Trace).....	100
Figure 4.34 Measured Transmission Response of Air Medium Testbed. Helix Antennas Located at Middle (Blue Trace) and at Middle with Extended Horizontal Metal Plates (Green Trace) Borehole Location.....	101
Figure 4.35 Simulated Model Diagram of Air Medium Testbed With the Horizontal Metal Plates Placed at the Faces of the Mesh Plates.....	102
Figure 4.36 Measured (Green Trace) and Simulated (Blue Trace) Insertion Loss Response of an Air Medium.....	103
Figure 4.37 Simulated-Model Diagram of an Air Medium Testbed.....	103
Figure 4.38 Measured (Green Trace) and Simulated (Blue Trace) Insertion Loss Response of an Air Medium.....	104
Figure 4.39 Simulated Insertion Loss of Extending the Mesh Plates Length for Air Medium Testbed. The Mesh Length's are; 1 (Blue Trace), 2 (Green Trace), 3 (Red Trace), 4 (Cyan Trace), and 5 (Magenta Trace) Times the Separation d.....	106
Figure 4.40 Simulated Return Loss of Extending the Mesh Plates Length for an Air Medium Testbed. The Mesh Length's are; 28 cm (Blue Trace), 56 cm (Green Trace), 92 cm (Red Trace), 120 cm (Cyan Trace), and 148 cm (Magenta Trace).....	107
Figure 4.41 Simulated Insertion Loss of an Air Medium Testbed.	

Ideal Testbed (Blue Trace), 112cm Long Extended Testbed (Green Trace), and 140cm Long Extended Testbed (Red Trace).....	108
Figure 4.42 Simulated-Model Diagram of an Air Medium Testbed Without Air Radiation Boundaries at the Extent of the Tank.....	109
Figure 4.43 Simulated Insertion Loss Response of Air Medium Testbed. Testbed Heights are; 58cm High (Blue Trace), 87cm High (Green Trace), 116cm High (Red Trace), and 145cm High (Cyan Trace).....	110
Figure 4.44 Simulated Extended Testbed Model Diagram.....	111
Figure 4.45 Simulated Insertion Loss Response for an Air Medium Extended Testbed (122cm Wide, 107cm High, and 2.54cm Deep). Helix Antennas Located at Top (Blue Trace), Middle (Green Trace), and Bottom (Red Trace) Borehole Locations.....	112
Figure 4.46 Simulated-Model Result of the Reflected Response for Air Medium of the Extended Testbed.....	114
Figure 4.47 Simulated-Model Result of the Transmitted Response for Air Medium of the Extended Testbed.....	114
Figure 4.48 Simulated-Model Result of the Reflected Response for Dry Sand of the Extended Testbed.....	115
Figure 4.49 Simulated-Model Result of the Transmitted Response for Dry Sand of the Extended Testbed.....	115
Figure 4.50 Simulated-Model Result of the Reflected Response for a Relative Permittivity of 10 of the Extended Testbed.....	116
Figure 4.51 Simulated-Model Result of the Transmitted Response for a Relative Permittivity of 10 of the Extended Testbed.....	116
Figure 4.52 Simulated-Model Result of the Transmitted Response for a Relative Permittivity of 10 of the Extended Testbed (Closer Look).....	117
Figure 4.53 Simulated-Model Result of the Reflected Response for a Relative Permittivity of 20 of the Extended Testbed.....	117
Figure 4.54 Simulated-Model Result of the Transmitted Response for a Relative Permittivity of 20 of the Extended Testbed.....	118
Figure 4.55 Simulated-Model Result of the Transmitted Response for a Relative Permittivity of 20 of the Extended Testbed (Closer Look).....	118
Figure 4.56 Simulated-Model Result of the Reflected Response for Air Medium of the Ideal Testbed.....	120
Figure 4.57 Simulated-Model Result of the Transmitted Response for Air Medium of the Ideal Testbed.....	120
Figure 4.58 Simulated-Model Result of the Reflected Response for Air Medium of the Real Testbed.....	121
Figure 4.59 Simulated-Model Result of the Transmitted Response for Air Medium of the Ideal Testbed.....	121

Figure 4.60 Simulated-Model Result of the Reflected Response for Air Medium of the Extended Testbed With Antennas Located at Top Borehole.....	122
Figure 4.61 Simulated-Model Result of the Transmitted Response for Air Medium of the Extended Testbed With Antennas Located at Top Borehole.....	123
Figure 4.62 Simulated-Model Result of the Reflected Response for Air Medium of the Extended Testbed With Antennas Located at Bottom Borehole.....	123
Figure 4.63 Simulated-Model Result of the Transmitted Response for Air Medium of the Extended Testbed With Antennas Located at Bottom Borehole.....	124

1 INTRODUCTION

Contamination of soils and groundwater by accidental spills, poor storage facilities, and inadequate disposal practices causes serious detriment to the environment and can pose a serious threat to human health. Common contaminants found in underground environments include many Dense Non-Aqueous Phase Liquids (DNAPLs). These contaminants pose particular threats because of their heterogeneous distribution and long-term perseverance in the environment. Moreover, they are difficult to locate, characterize, and remediate [NRC 2000]. It is, therefore, necessary to develop new technologies that will enhance our ability to characterize contaminated sites, locate underground contaminants, evaluate fate and transport processes, and remediate these contaminated sites.

1.1 Justification

DNAPLs are hazardous substances commonly found in underground systems. These substances affect the environment and are very harmful to human health. Persistent underground contamination has created the need to develop cost effective technologies to detect and monitor underground contamination. Traditional approaches for locating and characterizing contaminated sites rely on invasive techniques which require drilling, testing, and sampling. While these techniques provide the most direct access to the subsurface, they are generally expensive, only provide measurements at some spatial points, and may promote further spread of contaminants. Non-invasive techniques such

as electromagnetic and acoustic methods, offer rapid and relatively inexpensive characterization, but may suffer lack of resolution and specificity. Improvement of these technologies will enhance our ability to detect and monitor plumes and sources of organic contaminants, form a better understanding of the process affecting their fate and transport in subsurface environments, and assess remediation schemes in contaminated sites.

Cross well radar (CWR) is a new technology that may serve as a non-invasive method with minimal soil disruption for locating and characterizing underground contamination. It involves placing antennas into distant boreholes and emitting radar waves from the transmitting antennas in one borehole, through soil, to receiving antennas in other locations. The propagation characteristics of the waves depend on the materials present under the ground surface, and their distribution, and are assessed through electromagnetic (EM) wave reflection and transmission measurements. These measurements should therefore reflect the composition and distribution of materials in underground environments.

Previous work indicates that CWR technologies may be used to detect changes in fluid distribution, including DNAPLs, in homogeneous sandy soil [Serrano 2008]. Transmission and reflection measurements indicate that the EM response is affected when a fluid is introduced into the system. This effect is caused by changes in dielectric properties of the bulk soil in the presence of the fluid, object, or soil heterogeneities. Further studies are, however, necessary to evaluate frequency dependence, boundary effects, and quantify changes in dielectric properties caused by the presence of soil heterogeneities and contamination. The presence of DNAPLs in the underground environments may induce changes in the electromagnetic properties of the bulk soil.

Previous efforts to estimate bulk-soil EM properties from transmission and reflection (s-parameters) measurements using loop antennas interfaced with a Network Analyzer in a sandy soilbed under different degrees of contamination [Serrano 2008] have shown high variability in the results. This variability may be attributed to the antenna's radiation characteristics and performance, energy coupling to the receiving port around the borders of the soilbed tank, and non-ideal wave propagation characteristics near sharp EM boundaries.

This work applies time- and frequency- domain measurements and simulations to assess the performance of helix antennas, evaluates the effects of the testbed's boundaries on EM response, and redesigns testbeds for proper estimation of EM properties in soil systems. It also implements a time-domain method to estimate EM properties of a soilbed under different EM bulk conditions of the medium from transmission and reflection responses. This method will lead to the development of CWR technologies to detect EM changes caused by variable distribution of fluids with different EM properties, and ultimately it will enhance our ability to characterize and locate underground contamination of different EM properties.

1.2 Objectives

- Design, simulate, fabricate, and test helix antenna to obtain adequate performance of the antenna's response in soilbeds used for assessment of CWR technologies under different soil conditions.
- Assess the performance of the helix antennas and evaluate the effects of the testbed's boundaries on the wave propagation response in CWR systems.
- Evaluate helix antenna's frequency domain experimental measurements by using time domain measurements.
- Applies time- and frequency- domain measurements and simulations to redesigns testbeds for proper estimation of EM properties in soil systems.
- Implements a time-domain method to estimate EM properties of a soilbed under different EM bulk conditions.

1.3 Thesis Structure

This thesis consists of 5 chapters. This chapter (Chapter 1) introduces the problem and addresses the objective of this work. Chapter 2 consists of literature review and background theory of Cross Well Radar technology, electromagnetic wave propagation, antennas, scattering parameters and the electromagnetic properties of a material. The third chapter presents the methods for design and implementation of the testbed for

soilbed testing, and for the antenna configuration. Additionally, methods to estimate the electromagnetic properties for soil measurements using frequency and time domain are described. Analysis and Results of the methods performed for the modeling and experiments are presented in Chapter 4. Conclusions and recommendations are presented in Chapter 5.

2 LITERATURE REVIEW

2.1 Overview

Cross Well Radar (CWR) is evaluated as a potential minimally invasive technology for detection of DNAPL pollutants in underground environments. CWR relies on electromagnetic (EM) wave reflection and transmission (s-parameters) measurements in underground systems. It involves placing antennas into distant boreholes and emitting radar waves from the transmitting antennas in one borehole, through the soil, to the receiving antennas in other locations. CWR technologies have been applied to locate underground tunnels [Kim et al. 2009, Farid et al. 2003a], voids [Farid et al. 2003b], and objects [Serrano et al. 2007, Takahashi et al. 2006, Rappaport et al. 1999], identify bedrock fractures [Sato et al. 2009, Day-Lewis et al. 2003], characterize subsurface soils [Sagnard et al. 2010], characterize lithology and hydrogeological properties [Jang et al. 2007, Kim et al. 2004], and delineate flow zones and tracer movement [Lane et al. 2003]. Previous work indicates that CWR technologies may be used to detect changes in fluid distribution, including DNAPLs, in homogeneous sandy soil [Serrano 2008]. Transmission and reflection measurements indicate that the electromagnetic (EM) response is affected when a fluid is introduced into the system. This effect is caused by changes in dielectric properties of the bulk soil in the presence of fluid, object, or soil heterogeneities. Further studies are, however, necessary to evaluate frequency dependence, boundary effects, quantify changes in dielectric properties, and the response

of similar experiments under water saturated systems, and soil properties and heterogeneities.

2.2 Theoretical Background

This section provides a brief theoretical background on EM concepts important for the development of CWR technologies. These include concepts on wave propagation, scattering parameters, antennas, and EM properties of materials.

2.2.1 Electromagnetic Wave Propagation

An electromagnetic wave is radiation of energy through free space or matter by form of an electric and magnetic field arrangement. A transverse electromagnetic (TEM) wave consists of the electric and magnetic field components oscillating orthogonal to each other and to the direction of propagation (Figure 2.1). EM waves can interact with and travel through different media at the speed of light (3×10^{10} cm/s in vacuum). EM radiation can be present at different frequency ranges. Microwave radiation is a type of EM wave which covers a range from 300 MHz to 300 GHz region of the electromagnetic spectrum.

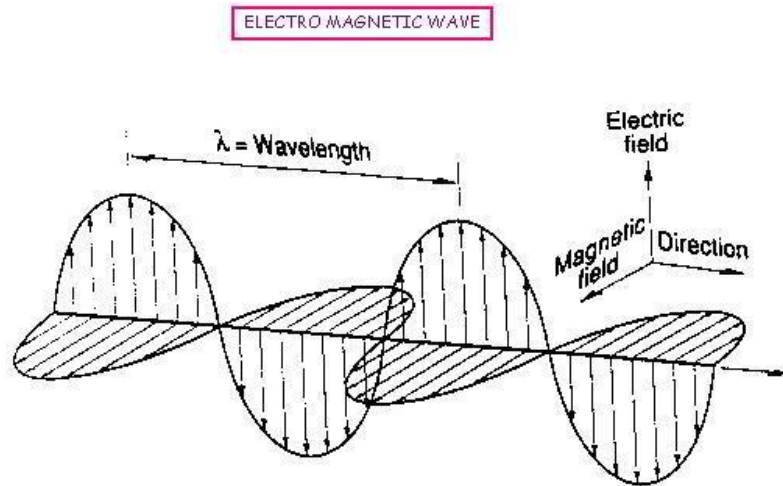


Figure 2.1 Illustration of the Electromagnetic Wave Propagation.
Source: <http://www.tutorvista.com>.

A parallel plate waveguide is the simplest waveguide structure, and also supports TEM wave mode (Figure 2.2). In order to preserve a TEM wave mode for the parallel plate waveguide, the cut-off frequency (f_c) of the high order propagating modes must be determined. The first high order mode in a parallel plate waveguide is TE_{01} . The cut-off frequency of this mode also indicates the largest frequency where there is only a TEM wave mode (which has a DC cut-off). For a parallel-plate waveguide, f_c depends on the filling medium and the separation between plates (d). The cut-off frequency f_c is determined by using equation 2.1;

$$f_c = c / (2 * (d) * (\mu_r \epsilon_r)^{1/2}) \quad 2.1$$

where c is the speed of light (3×10^{10} cm/s in vacuum), and ϵ_r and μ_r are the relative permittivity and relative permeability, respectively.

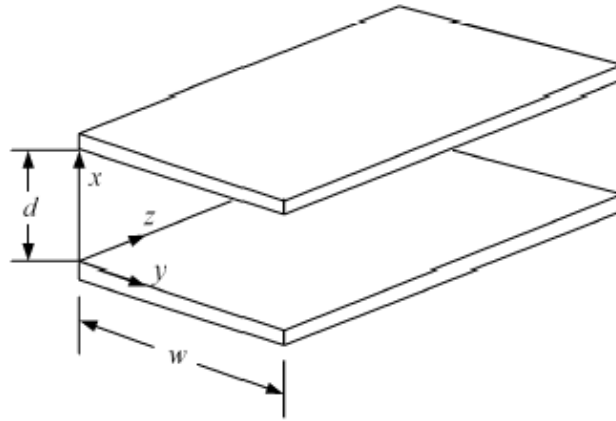


Figure 2.2 Illustration of a Parallel-Plate Waveguide.
Source: <http://cc.ee.ntu.edu.tw>.

2.2.2 S-parameters

The scattering parameters or s-parameters are used to provide a complete description of a network at high frequencies. At microwave frequencies the analysis of a network relies on traveling waves which can be represented as incident voltages (V_i^+) and reflected voltages (V_i^-) on the input and output ports. Information of the transmitted and the reflected electromagnetic waves are provided from the s-parameters (S_{ij}). S_{ij} is defined as the ratio of the reflected voltage (V_i^-) from the wave traveling on port i over the incident voltage (V_j^+) at port j. When i is equal to j, the response represents the reflection coefficient response at that port. For different values of i and j, the response represents the transmission coefficient of the analyzed network. Figure 2.3 shows a diagram of a two-port network with the incident and the reflected voltages. The underground soilbed system can be represented as a two-port network.

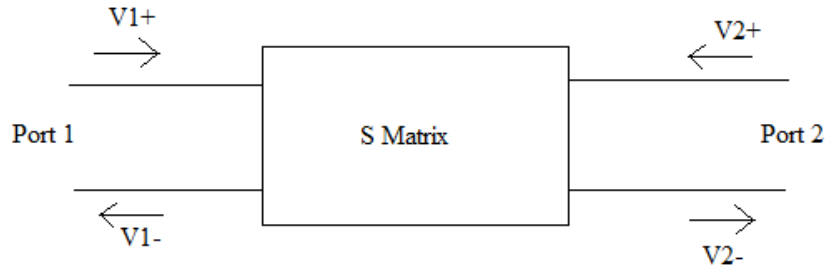


Figure 2.3 Two-Port Network Representation of the S-parameters.

For a two-port network, the relation between the incident (V_j^+) and reflected (V_i^-) voltages with the s-parameters is represented by equation 2.2 in the vector form and equation 2.3 in matrix form (equation 2.3);

$$\begin{aligned} V_1^- &= S_{11} V_1^+ + S_{12} V_2^+ \\ V_2^- &= S_{21} V_1^+ + S_{22} V_2^+ \end{aligned} \quad 2.2$$

$$\begin{bmatrix} V_1^- \\ V_2^- \end{bmatrix} = \begin{bmatrix} S_{11} & S_{12} \\ S_{21} & S_{22} \end{bmatrix} \begin{bmatrix} V_1^+ \\ V_2^+ \end{bmatrix} \quad 2.3$$

The S matrix represents the measurements of the transmitted and reflected traveling wave along the studied medium. This S matrix is obtained using a network analyzer.

2.2.3 Antennas

An antenna is a passive structure used as a transition device between a waveguide and free space [Balanis 2005a]. The antenna radiates to free space the electromagnetic

energy coming from the waveguide. Many antenna configurations have been used for target detection using CWR in underground systems [Sagnard 2009, Serrano 2008, Ebihara et al. 2007, Farid 2004]. Sagnard [2009] designed a bow-tie monopole antenna to perform soil moisture measurements using borehole radar between 500 MHz to 1.5 GHz. Wire loops have been used for detection of DNAPLs in sandy soilbeds under different environmental conditions [Serrano 2008]. Ebihara et al. [2007] performed an analysis of dipole antennas in cross borehole radar to ensure similarities between the simulated models with the field experiments of the studied medium. Also, Farid [2004] used monopoles antennas to assess potential detection of DNAPLs.

Another antenna configuration is the helical or helix antenna (Figure 2.4). The helical antenna was invented by John Kraus in 1946 [Kraus 1988]. This configuration is based on a wire wound forming a helix [Balanis 2005b, Kraus 1988]. The helix provides the advantage to select the desired type of propagation of the electromagnetic wave in two different modes; the axial mode and the normal mode. Another advantage of the helix antenna is that it provides broadband characteristics in axial mode, which is very suitable for broader frequency range analysis on the study area.

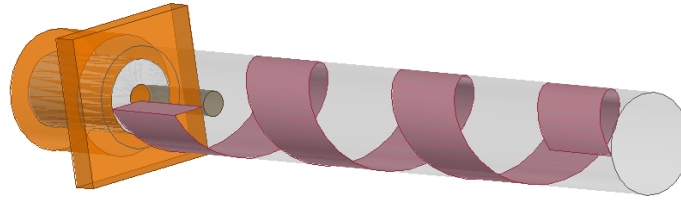


Figure 2.4 Illustration of a Helix Antenna Configuration.

Previous work using helix antennas was a modified counter-wound helix antenna for land mine detection [Shivandas 2004] using Ground Penetrating Radar (GPR) technology. This modification of the helix antenna was made to achieve a broader bandwidth, greater than 5:1, and also obtain linear polarization.

The use of a helix antenna in a 2D EM soilbed system is suitable for soilbed testing due to the physical design limitations imposed by the system, which are the separation of the parallel-plate waveguide, the borehole diameter where the antenna is inserted, and the length used to immerse the antennas into the soilbed. Also it is considered to provide enhanced performance and lower variability for the estimates of the EM properties for an experimental frequency range between 500 MHz and 1.5 GHz.

2.2.4 Electromagnetic Properties of a Material

The EM properties of a material in a macroscopic scale can be described using Maxwell equations [Chen et al. 2004]. There are three parameters that determine the spatial extent that an EM field can penetrate a material at a given frequency; the permittivity (ϵ), the permeability (μ), and the conductivity (σ). In order to determine these

parameters, a relationship between the transmitted and reflected energy wave must be established.

A diversity of methods have been proposed and developed to perform estimates of the EM properties for soil measurements or material properties [Chen et al. 2004]. Chen et al. [2004] developed methods using reflection measurements only and transmission and reflection measurements for soil and/or material characterization. Experimental and simulated methods for soil and/or material characterization were proposed considering frequency and/or time domain techniques.

Several frequency domain techniques have been applied to determine EM parameters of materials [Panzner et al. 2010, Maio et al. 2009, Hasar 2009, Gunasekaran et al. 2008, Chung 2007, Abbas et al. 2001]. Panzner et al. [2010] applied frequency domain to determine EM parameters of dry sand using GPR and resonances at the microwave frequency region. Maio et al. [2009], estimated permittivities from scattering responses using TEM waveguides. Others [Hasar 2009, Gunasekaran et al. 2008, Chung 2007, Abbas et al. 2001] have also applied waveguide techniques used to estimate the permittivity of materials.

Time domain techniques, such as Time Domain Reflectometry (TDR), have been very popular to estimate the dielectric properties of material and soil parameters [Igel et al. 2011, Nakano et al. 2009, Savi et al. 2007, Robinson 2004]. Igel et al. [2011] used TDR to measure EM properties and generate soil models for realistic Ground Penetrating Radar (GPR) data. TDR measurements were performed using transmission lines to determine the dielectric permittivity of homogeneous materials [Nakano et al. 2009,

Robinson 2004]. Savi et al. [2007] studied the waveform responses of TDR's measurements in order to improve the estimates of the permittivity. Other time domain techniques besides TDR were used in order to estimate the dielectric properties of a material [Ratto et al. 2010, Will et al. 2009]. Will et al. [2009] used waveguides and dielectric obstacles of time delay responses to determine the permittivity of materials and soil. Ratto et al. [2010] performed GPR modeling to estimate the soil permittivity from raw time domain data.

2.3 Effect of Underground Composition on Wave Propagation and Characteristics

CWR has been applied for detection of target objects that exhibit significant contrast of dielectric properties in soils [Farid et al. 2006, Farid 2004, Serrano 2008, Serrano et al. 2007].

Serrano [2008] developed and evaluated CWR technology to detect and monitor DNAPLs contamination in subsurface environments under transient flow conditions. This work involved developing and testing CWR and signal processing technologies. A methodology was applied to detect EM changes caused by the presence of fluids with different EM properties in a 2D flow and EM soilbed with loop antennas. The method was validated through multi-fluid experiments in a 2D soilbed. Experiments were conducted in dry sand, saturated sand, and dry and saturated sand with TCE. Saturation

was accomplished by pumping distilled water at the bottom of the soilbed. For DNAPL experiments, TCE was injected at the top center of the soilbed, below the soilbed surface.

Transmitting and receiving antennas imbedded in the soilbed were used to assess changes on s-parameters measurements as DNAPL and other fluids entered and flow through the system.

A method was developed to estimate the relative permittivity of bulk soil along raypath between transmitting and receiving antennas from s-parameters measurements. This method assumed lossless medium, and perfectly coupled and identical radiation characteristics of the antennas. The determined estimates from water and DNAPL flow experiments indicated that variable and temporal distribution of fluids with different EM properties cause detectable changes in the dielectric properties of the bulk soil. It was concluded that there was sufficient contrast between the EM properties of uncontaminated and DNAPL contaminated soil to apply CWR for contaminant detection. The contrast, however, depends on water content, frequency range of analysis, fluid movement, distribution, heterogeneities, and the presence of physical and fluid interfacial areas. The estimated values, however, showed high variability and deviated from expected values published in the literature [Serrano 2008]. This variability may be attributed to differences on the antenna's characteristics and performance, energy coupling to the receiving port around the soilbed tank, and non-ideal wave propagation characteristics near EM boundaries. The assumptions related to lossless medium, straight raypaths, and equal radiation properties of antennas must, therefore, be revised for more accurate estimates.

Certuche [2008] developed an electromagnetic model for the 2D soilbed setup implemented by Serrano [2008] to verify the possibility of detecting DNAPLs using CWR. Two EM simulators were used to develop the EM soilbed model: Ansoft's HFSS and Remcom's XFDTD. Simulations of the developed model were done for dry sand and saturated sand, with or without DNAPL. Different shapes were used to represent the DNAPL pool in the simulated model, and they were placed at different locations inside the soilbed. Certuche [2008] studied the electric field distribution and the s-parameters for different transmitter port positions inside the soilbed at three different frequencies of 285 MHz, 515 MHz and 1.5 GHz. The results of the electric field distribution for the EM model showed different behavior under different soil conditions (degree of saturation, water table level) of the soilbed. The analysis of the s-parameters were performed by using the s-parameters simulations of dry sand and saturated sand as reference and comparing with the s-parameters simulations of dry sand with DNAPL and saturated sand with DNAPL, respectively. The detection was possible using this comparison for both dry and saturated sand. Certuche [2008] concluded that the detection of DNAPLs using CWR is possible depending on the frequency of operation, the position and amount of ports used to have a better spatial resolution.

Serrano's [2008] and Certuche's [2008] work showed the understanding and the significance which they provide to develop and accomplish the objectives for this work. They both demonstrated significant contrasts for the CWR s-parameters response when DNAPLs are present in sand soilbed as water content varies, the position of the antennas changes, and the frequency changes. These contrasts in the s-parameters consequently

contrast the EM properties estimates of the bulk soil. Both works shared that CWR could be use as a potential technology to detect and monitor DNAPL in homogeneous soils.

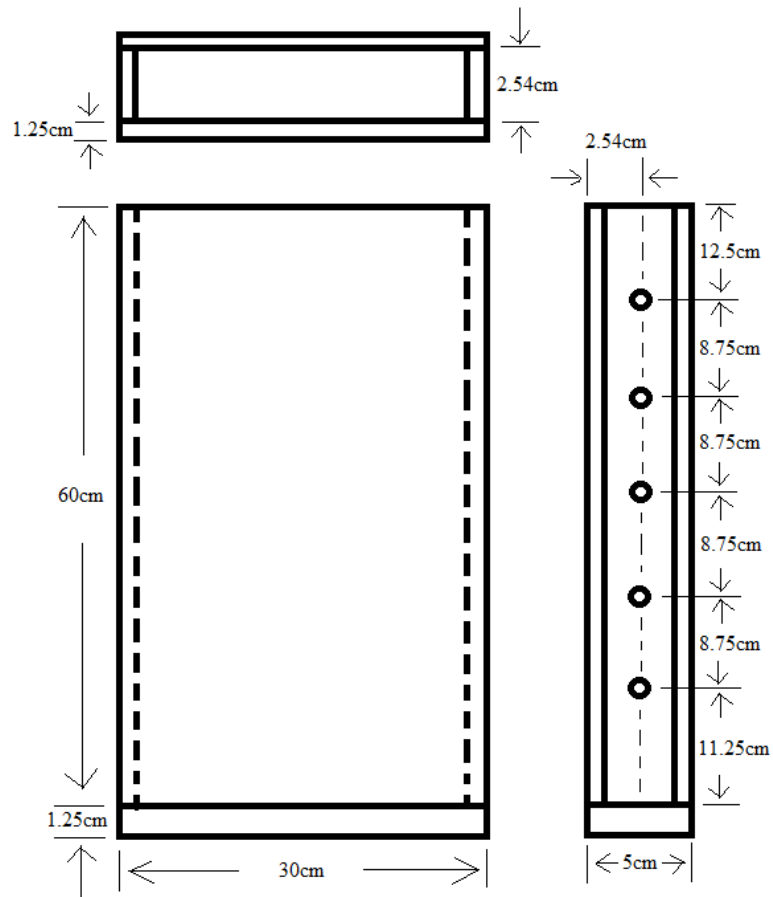
3 METHODOLOGY

3.1 Overview

This chapter focuses on: development of a 2D parallel plate waveguide testbed for soilbed testing; development of suitable helix antennas for the enhancement of the experimental measurements of the soilbed; development of appropriate methods to estimate the electromagnetic properties of the soilbed by using different techniques. Simulations and experimental measurements were performed in frequency and time domain to get a better understanding of the studied soilbed system.

3.2 Testbed Design

A soilbed was designed to the system environmental conditions for experimental purposes. A diagram for the considered design of the new tank is shown in Figure 3.1. This soilbed follows a similar design to the one previously used by Serrano [2008]. Considerations from these previously fabricated tanks are used to preserve similarities in geometry dimensions, their design physical limitations, and analysis limitations. Additional considerations were performed to enhance the experimental measurements of the soilbed.



NOTES:

- 1) Plexiglass Sheet Thickness = 1.25cm
- 2) Holes Diameter = 1.12cm

Figure 3.1 Diagram of the Designed Tank for Soilbed Testing.

3.2.1 Design Considerations

The first consideration from the previous tank was to keep the same internal geometry dimensions. The internal geometry dimensions represent the area of study where the experiments were performed (soilbed medium). The selected geometry dimensions of the tank were 28 cm wide, 60 cm high and 2.5 cm deep (Figure 3.1).

An important consideration for the design of the new tank was how the electromagnetic wave propagates through the soilbed. The approach was to use a transversal electromagnetic (TEM) waveguide for wave propagation through the soilbed in order to simplify the electromagnetic analysis of the studied soilbed. Parallel plate waveguides were used to propagate the EM wave through the soilbed because this type of waveguide configuration permits a TEM propagation mode. A metal mesh was considered as a representation of the parallel plate. The purpose of using a mesh instead of a sheet is to allow visibility of fluid flow inside the soilbed.

3.2.2 Design Limitations

The separation between the parallel mesh plates, the diameter of the boreholes and the aperture size of the mesh plates require to be accounted for in the experimental measurements. Table 3.1 shows a summary of the selected physical dimensions values considered for the design of the new soilbed tank. The selected separation between the parallel mesh plates was 2.54 cm. This separation was selected to preserve the TEM wave propagation mode, which depends in turn of the highest frequency applied for the experiments and the relative permittivity of the studied medium. The aperture length for the mesh plates selected was less than a tenth of wavelength ($\lambda/10$). For a frequency of 1.5 GHz, which is the largest used for the experiments, and an expected maximum relative permittivity for saturated sand soilbed of 40 (highest considered), the largest aperture length of the mesh used is 0.316 cm. The limitation of the separation between the mesh plates leads to limitation of the diameter of the boreholes. The antennas will be

introduced through boreholes to take measurements of the studied soilbed. The diameter of the borehole was restricted to less than 1.12 cm.

Table 3.1 Summary of the Dimensions for the Designed Tank

Geometry	Size (cm)
Tank Height	60
Tank Width	28
Separation Between Parallel Plates	Less than 2.54
Mesh Aperture Length	Less than 0.316
Boreholes Diameter	Less than 1.12

3.3 Helix Antenna Modeling

The helix antenna configuration was designed using Ansoft's High Frequency Structure Simulator (HFSS) version 13. HFSS analyzes the electromagnetic wave modeling of a desired 3-D structure. For frequency domain analysis, the electromagnetic wave simulation is based on Finite Element Method (FEM). FEM is a numerical technique used to find approximate solutions of a problem using partial differential equations or integral equations. In a structure, FEM cuts the structure in multiple finite elements and then reconnects them as nodes to hold the elements together and resulting in a set of simultaneous equations [de Weck 2004]. Then, the simultaneous equations are solved for the parameters of choice. For HFSS, the simulations solve the electromagnetic fields.

The model was performed in HFSS using different geometries. By creating and combining different shapes, a desired structure was build. Each built structure was then assigned a property (e.g., waveport excitation, dielectric material, perfect electrical conductor boundary, or air radiation boundary) in order to define a physical interpretation or a particular characteristic of the structure for the simulations. After the model was implemented, the type of analysis was configured. Simulations then were performed and the results were obtained. The analysis of these results was performed using tables, plots or other tools such as Matlab (software used for high level computing to perform numerous of tasks) using the exported data.

3.3.1 Antenna Design

The helix antenna was implemented using a copper strip, a delrin rod ($\epsilon_r=1.7$) to support the copper strip, and a SMA connector. The cylinder length (L) and the diameter (D) were design limitations established in the simulations, based on the required physical limitations to be used for the experiments of the constructed testbed (Table 3.2).

Table 3.2 Helix Antenna Design Physical Limitations

Antenna Geometry	Dimension (cm)
Diameter	Less than 1.12
Length	Less than 4

3.3.2 Soilbed Model

The soilbed model used to design the helix antenna consists of a two parallel-plates waveguides with properties set as a perfect electrical conductor (PEC). Inside the waveguide, a box was placed representing the soil medium. The soil medium properties assigned in the model were the relative permittivity, the relative permeability, and the electrical conductivity. The values of the assigned properties were obtained from previous experimental properties [Serrano 2008]. Table 3.3 shows the assigned values of different soil properties used for the simulations. A box at the top and bottom of the soilbed was placed to represent air radiation boundaries. Air radiation boundaries cause energy flux of the electromagnetic wave through the soilbed and outside of the testbed. An illustration of the soilbed model used is shown in Figure 3.2.

Table 3.3 Assigned EM Properties used to Model the Helix Antenna

Type of Material	Relative Permittivity	Electrical Conductivity
Dry Sand	4	10^{-4}
Saturated Sand	40	10^{-3}
Distilled Water	81	10^{-4}

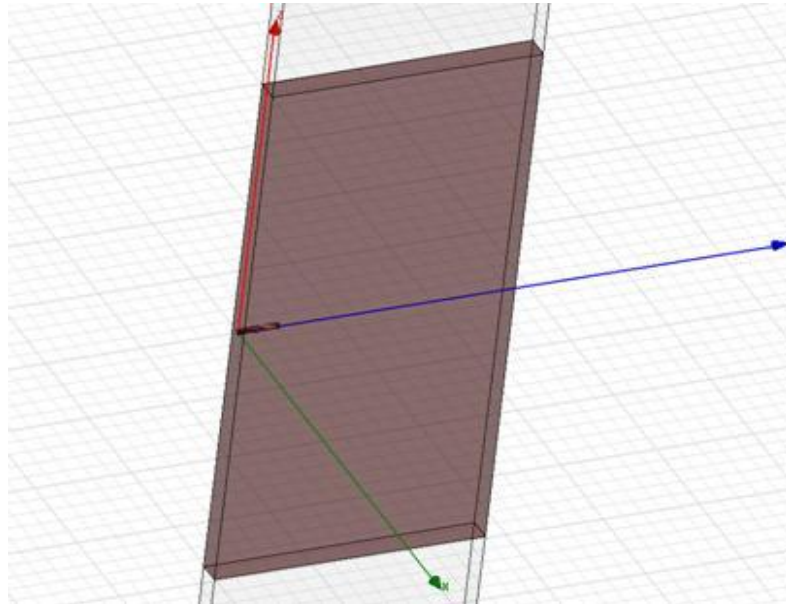


Figure 3.2 Diagram of the Simulated Soilbed Model in HFSS.

The excitation port used as the input for the helix antennas is of type waveport. The waveport consists of a 2D object where it arranges the orientation of the electric field of the applied signal. The shape of the 2D object used to represent the waveport was a circle with a small hole in the center of it and the direction of the applied electric field was represented as a small red vector (Figure 3.3). To fulfilled the appropriate applied excitation, input parameters such as the deembed distance, the number of propagation modes and renormalize of the simulated results were provided (Figure 3.4). The deembed distance is the distance between the point where the excitation was placed physically and the point where actually the simulation was performed and the simulated results were obtained. The number of propagation modes represents the number of EM wave modes to be applied to the system. TEM wave propagation was the only applied mode used for the simulations. Renormalize is an option to decide if the simulated results will be provided with the full-impedance of the system or normalized results will be provided after the

simulation was performed. The simulated results were renormalized to 50 Ohm impedance because it represents the impedance of the simulated model.

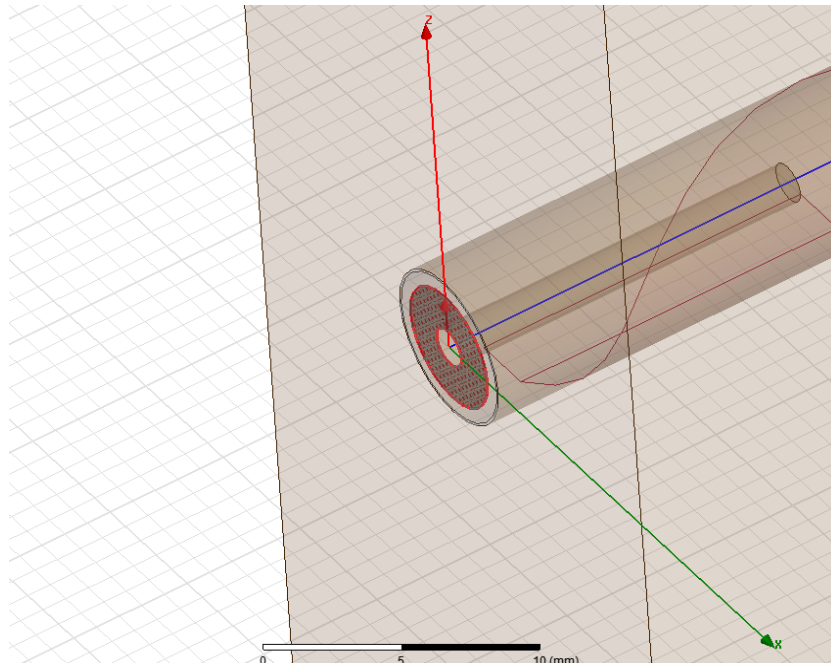


Figure 3.3 Waveport Used to Feed the Soilbed Model in HFSS.

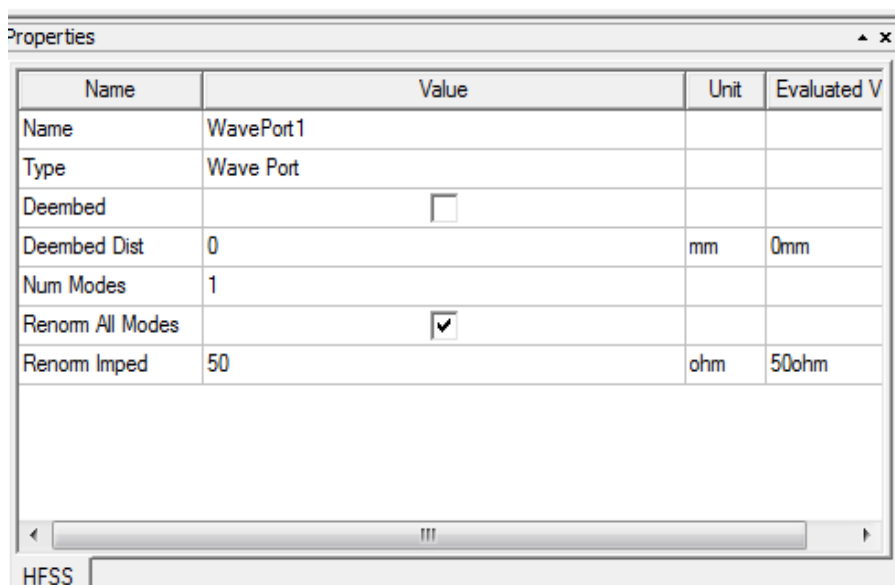


Figure 3.4 Input Parameters of the Assigned Excitation Used to Feed the Soilbed Model in HFSS.

3.3.3 S-parameters Preliminary Results of the Simulated Model for Different Assigned EM Properties

The s-parameters for the helix antenna were simulated inside the soilbed model to take into account the effects of the waveguide in the antenna impedance and the generated fields. The simulated results of the helix antenna response were obtained for the soilbed model under different assigned EM properties for a desired frequency range. The return loss (S_{11}) and the insertion loss (S_{21}) represent the s-parameters results of the simulated model. The return loss represents the helix antenna response for the assigned medium (Figure 3.5). This response shows the performance of the antenna at the assigned medium over the desired frequency range. In order to achieve a good performance in the antenna, the return loss for a desired frequency range must be less than -6 dB. This represents at least 67% percent of the input power distributed from the antenna to radiate

enough EM energy through the soilbed. The insertion loss represents the soilbed response for the assigned EM property over the desired frequency range (Figure 3.6).

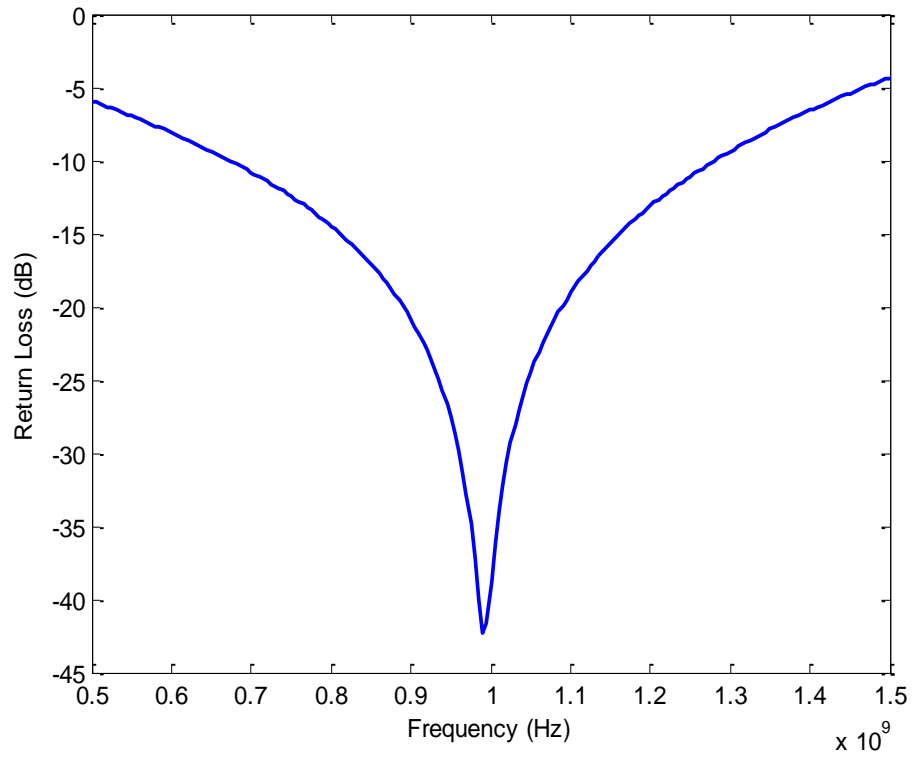


Figure 3.5 Simulated Return Loss for the Helix Antenna in Dry Sand Soilbed.

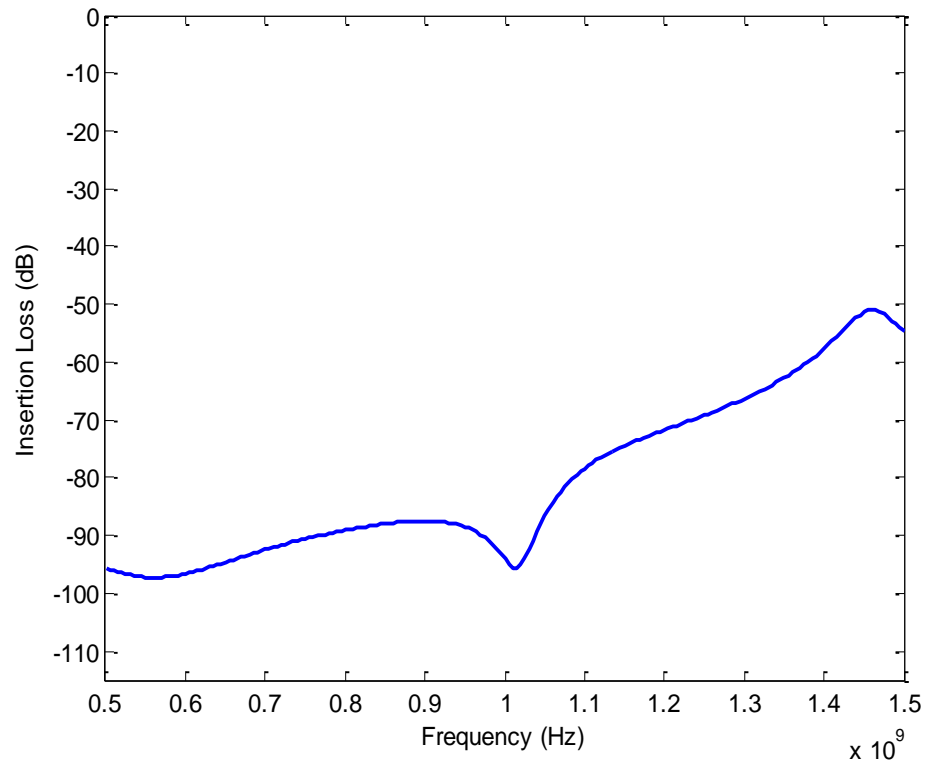


Figure 3.6 Simulated Insertion Loss for the Helix Antenna in Dry Sand Soilbed.

3.4 Helix Antenna Fabrication and Soilbed Setup

The helix antennas were fabricated and tested in a soilbed built with the same specifications as the designed tank (Figure 3.1). The corresponding dimensions of the fabricated helix antennas were selected from the s-parameters results of dry sand soilbed model, which provided the best performance. The tank was built to allow measurements of s-parameters in air and dry sand, with the antennas placed at different heights throughout the setup. Air medium experiments, were conducted by making measurements in an empty (air-filled) tank. For dry sand experiments, the tank was filled and packed with dry sand soil from Isabela, P.R.

3.4.1 Antenna Fabrication

The helix antennas shown in Figure 3.7 were fabricated using delrin rods, copper strip, and SMA connectors. The delrin rods (4 cm long, 0.64 cm of diameter and a relative permittivity ($\epsilon_r=1.7$)) were used to support the helix antenna structure. The helix form was made using a copper strip and a 50 ohm SMA connector (Mouser Electronics) was placed at one end of the antennas to establish a connection with the equipment to take the s-parameters measurements.



Figure 3.7 Fabricated Helix Antennas Made With Delrin Rod, Copper Strip, and SMA Connectors.

3.4.2 Tank Construction

The constructed tank for soilbed testing is shown in Figure 3.8. The dimensions of the constructed tank were identical to the designed tank (30 cm wide, 60 cm high, and 2.54 cm deep). The tank was constructed with plexiglass sheets. A stainless steel mesh was placed on each face inside the tank to create a parallel plate waveguide with TEM wave mode behavior as the wave travels through the soilbed. The aperture length of the mesh plates is 0.24 cm, which is less than the largest permitted. Also a protective well-casing was placed at each borehole where the antennas are inserted to take the measurements of the studied soilbed. This protective well-casing protects the antennas from physical contact with the soil, and avoids soil disturbances. Boreholes were placed along each panel tank at 11.25 cm, 20 cm, 28.75 cm, 37.5 cm, and 46.25 cm from the bottom of the tank (Figure 3.8). The mesh plates were glued at the faces of the plexiglass. This ensures the plates stay flat when the soil is packed in the tank. The constructed tank was used air-filled (empty) for air experiments, and packed with dry sand at a density of 1.6 g/cm^3 for the soil experiments.

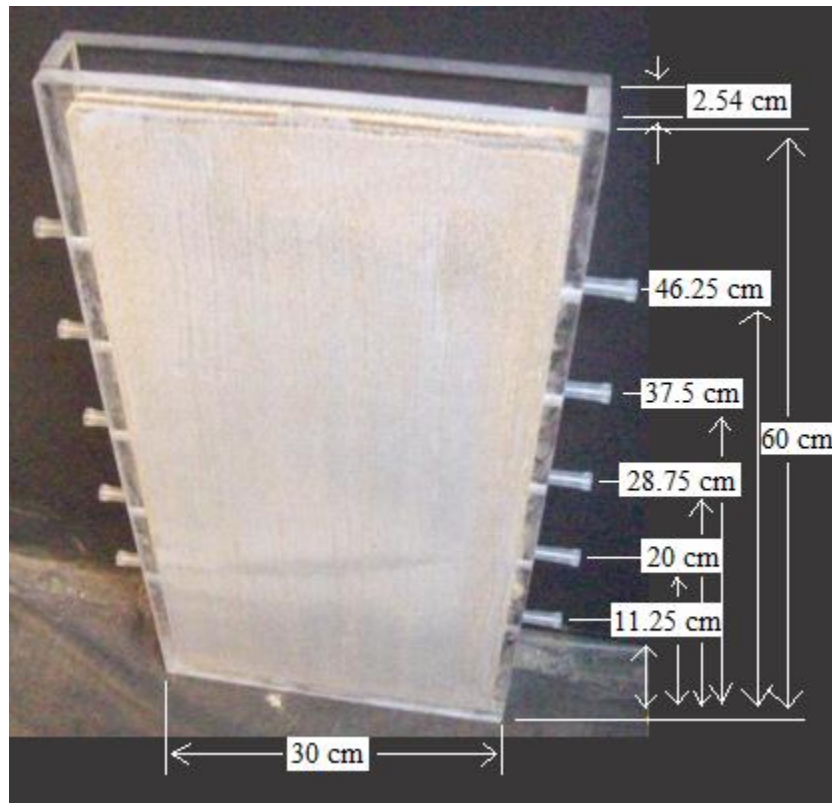


Figure 3.8 Constructed Tank for Soilbed Testing Packed With Dry Sand Soil.

3.5 Experimental Measurements

Experimental measurements were performed using the designed helix antenna configuration and the constructed tank for soilbed testing. The measurements were taken using a vector network analyzer model ENA 5071C from Agilent Technologies (Figure 3.9). This network analyzer provides the option to take measurements in frequency and time domain. Measurements using this instrument can be taken from 100 kHz to 4.5 GHz, the system dynamic range is better than 100 dB, and the maximum applied input power is 10 dBm. The input power applied to take the measurements was 1 mW (0 dBm) which is enough to radiate energy from the transmitting antenna, spread through the soilbed, and

detect enough energy at the receiving antenna. Calibration measurements were performed before the experiments to eliminate undesired effects caused by addition of external coaxial lines, and by the network analyzer. The calibration was performed using different types of loads (short circuit, open circuit, and broadband 50 Ohms load) from Agilent's calibration kit set 50033. The selected frequency range for calibration was between 500 MHz to 1.5 GHz with a total of 801 frequency points. By calibrating the network analyzer, appropriate measurements of the soilbed using the helix antennas are obtained.



Figure 3.9 Agilent's Vector Network Analyzer Model ENA 5071C.

The antennas were placed inside a protective well casing pipe (Figure 3.10) pointing directly one to the other with a separation of 19.8 cm. S-parameters measurements were taken with antennas located at different height locations (11.25 cm, 20 cm, 28.75 cm, 37.5 cm, and 46.25 cm from the bottom of the tank), but keeping the same separation between them.



Figure 3.10 Protective Well-Casing Pipe.

3.5.1 Frequency Domain Measurements

S-parameters measurements were taken at the same frequency range selected for calibration of the network analyzer (500 MHz- 1.5 GHz). Both return loss (S_{11}) and insertion loss (S_{21}) measurements in frequency domain were taken for air medium and dry sand soilbeds at middle borehole location of the testbed. An illustration of S_{11} and S_{21} measurements are shown in Figures 3.11 and 3.12, respectively.

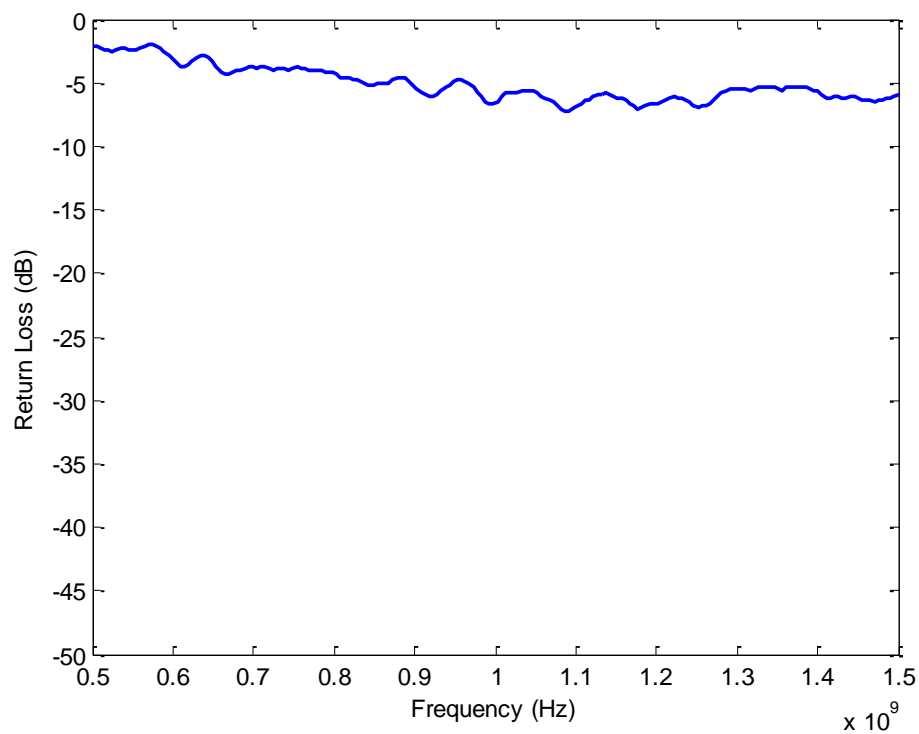


Figure 3.11 Return Loss Measurements of Dry Sand Soilbed Using the Fabricated Helix Antennas.

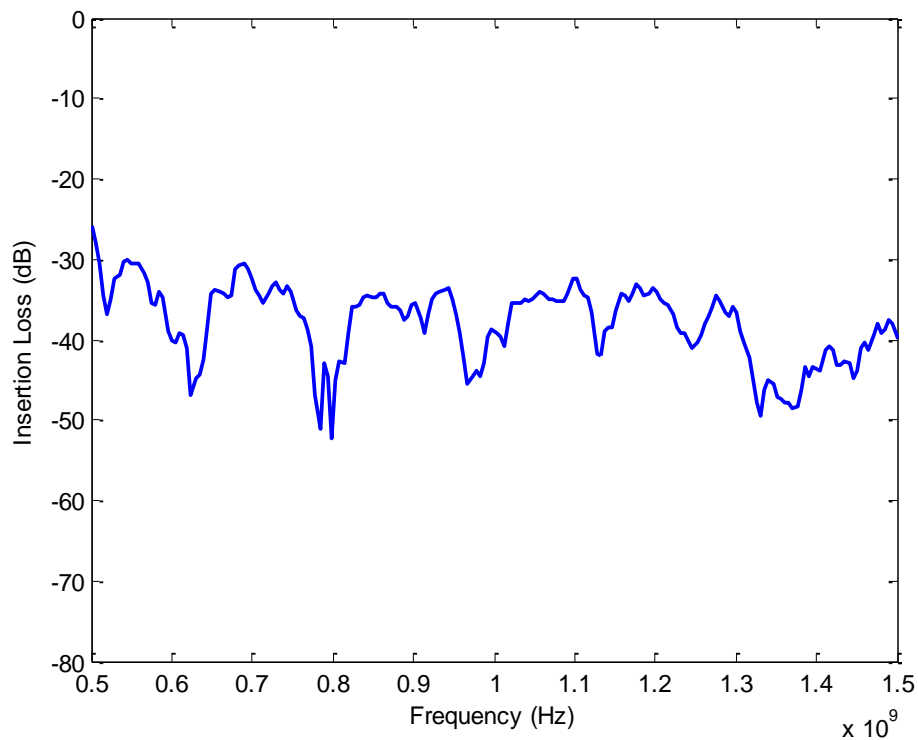


Figure 3.12 Insertion Loss Measurements of Dry Sand Soilbed Using the Fabricated Helix Antennas.

3.5.2 Time Domain Measurements

Time domain measurements represent a transformation of the s-parameters measurements using Fourier transforms. By using time domain measurements, a detail of the EM wave propagated through the medium is obtained. The advantage of using time domain measurements is the ability to create time windows where undesirable effects present in the reflection and transmission measurements of the soilbed can be eliminated. This option is called gating. Time domain measurements were taken considering the same calibration method used as for frequency domain. Reflection and transmission measurements of the EM wave propagated through the soilbed were performed for a time of 10 ns. Time domain measurements were performed for air medium. Preliminary reflection and transmission measurements are illustrated in Figures 3.13 and 3.14, respectively.

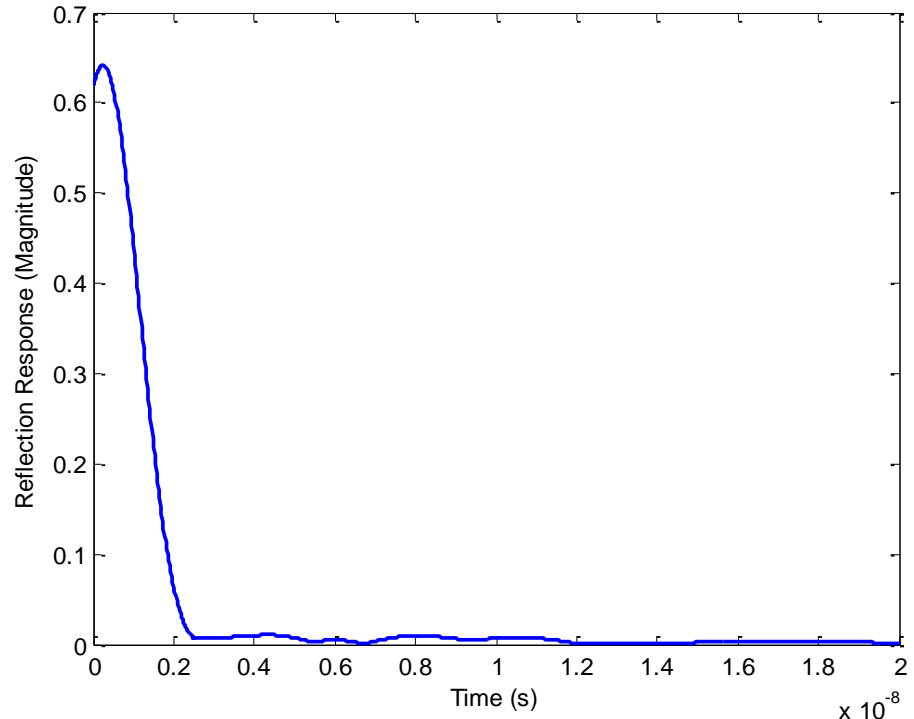


Figure 3.13 Measured Reflection Response of Air Medium Testbed Using Helix Antennas.

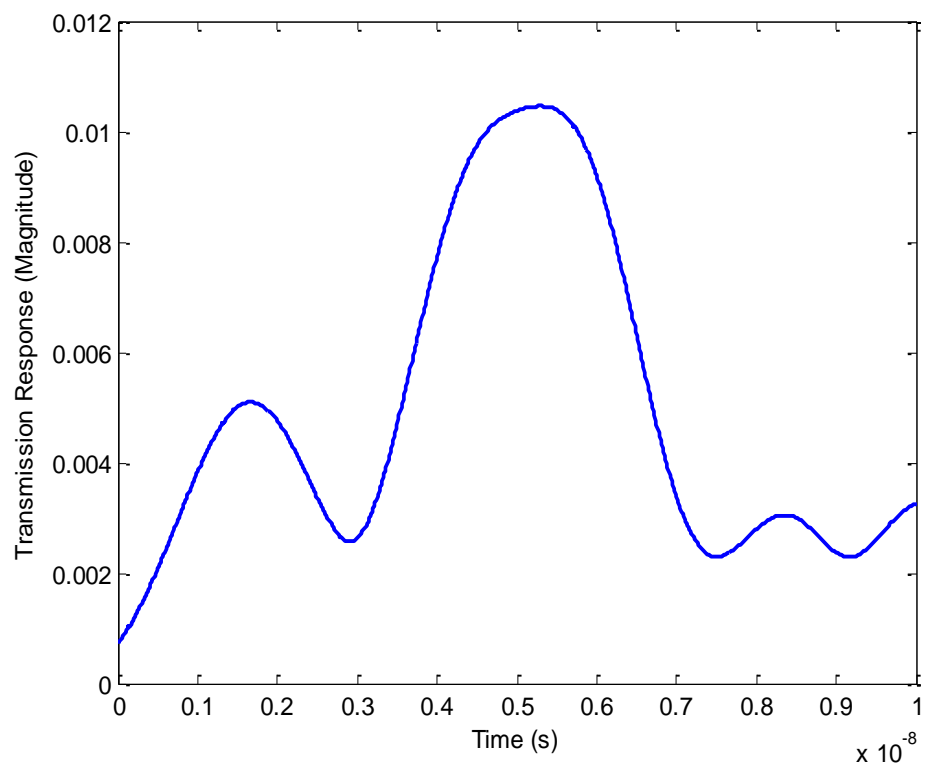


Figure 3.14 Measured Transmission Response of Air Medium Testbed Using Helix Antennas.

3.6 Boundary Conditions Experiments Using Metal Plates

To assess the potential effects of boundary conditions, metal plates (Figure 3.15) were placed over the top of the testbed (Figure 3.16), and beyond the horizontal (Figure 3.17) and vertical (Figure 3.18) extent of the tank. Time domain measurements were taken in an air medium for a period of 10 ns. The constructed testbed (30 cm wide, 60 cm high, and 2.54 cm deep) was used for these experiments. The helix antennas were placed at different borehole locations (Figure 3.19) and pointing directly one to the other. The reflected response and transmitted response were analyzed to assess these potential effects.



Figure 3.15 Metal Plates Placed on the Testbed for Boundary Conditions Experiments.



Figure 3.16 Illustration of the Constructed Testbed With a Metal Plate Placed at Top of the Testbed Used for the S-parameters Measurements.



Figure 3.17 Illustration of the Constructed Testbed With Horizontal Metal Plates Placed at the Faces of the Mesh Plates of the Testbed Used for the S-parameters Measurements.

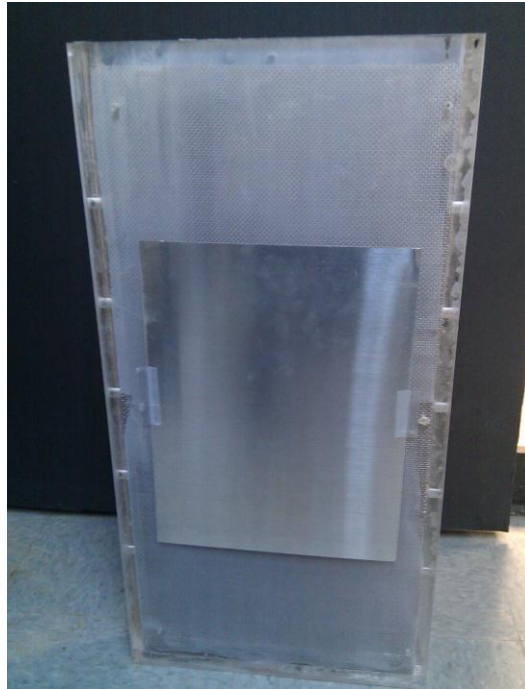


Figure 3.18 Illustration of the Constructed Testbed With Vertical Metal Plates Placed at the Faces of the Mesh Plates of the Testbed Used for the S-parameters Measurements.

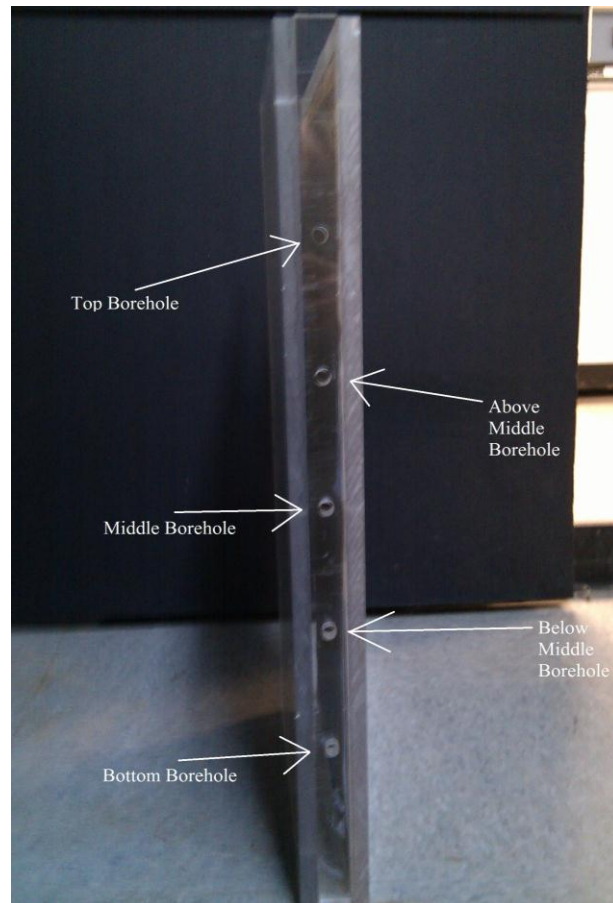


Figure 3.19 Borehole Locations of the Testbed Where the Helix Antennas Were Placed for the Time Domain Experiments.

3.7 Estimation of the Electromagnetic Properties using Frequency Domain Measurements

Previous estimates of the EM properties from frequency domain s-parameters measurements [Serrano 2008] of sandy soilbed have shown uncertain results [Toro et al. 2011]. In order to achieve good estimates of the EM properties from frequency domain measurements, three different techniques were performed. Two of the three techniques use the raw s-parameters measurements taken directly to perform the estimates of the EM

properties. The other method incorporates the antenna effect for the raw s-parameters measurements in order to obtain the s-parameters which correspond to the soil medium.

3.7.1 Transmission and Reflection Equations for Lossy Media

Previous estimates of the EM properties for sandy soilbed system under different conditions were performed using the equations of the transmission coefficient and reflection coefficient for a lossless media [Serrano 2008]. This means that there was no energy loss from the transmitter antenna to the receiver antenna. Since the s-parameters measurements were performed for the soilbed under different conditions (dry and wet), losses on the media are likely to be present. The equations considered for the estimates of the EM properties were developed by Nicolson [1970]. The reflection coefficient (Γ) and transmission coefficient (T) equations used for lossy media are;

$$\Gamma = (\mu_c/\epsilon_c)^{1/2} - (\mu_o/\epsilon_o)^{1/2} / ((\mu_c/\epsilon_c)^{1/2} + (\mu_o/\epsilon_o)^{1/2}) \quad 3.1$$

where μ_c is the complex permeability, ϵ_c is the complex permittivity, μ_o is the permeability at free space ($4\pi \times 10^{-7}$ H/m) and ϵ_o is the permittivity at free space (8.85×10^{-12} F/m).

$$\mathbf{T} = \mathbf{e}^{-(\alpha + j\beta)d} \quad 3.2$$

where α is the attenuation constant, β is the phase constant, and d is the separation between the transmitter antenna and the receiver antenna. α and β are defined as;

$$\alpha = 2\pi f (\mu_r \epsilon_r)^{1/2} (0.5 * (1 + (\sigma / 2\pi f \epsilon_r)^2)^{1/2} - 1)^{1/2} \quad 3.3$$

where f is the operating frequency, σ is the medium electrical conductivity, μ_r is the relative permeability and ϵ_r is the relative permittivity.

$$\beta = 2\pi f (\mu_r \epsilon_r)^{1/2} / c \quad 3.4$$

where c is the speed at free space (3×10^{10} cm/s).

For these experiments, the media used were air and sandy soil. Both mediums are non-magnetic and can be concluded that the μ_r is equal to unity. The s-parameters (S_{11} , and S_{21}) measurements taken correspond to the reflection and transmission coefficients respectively. This means;

$$S_{11} = \Gamma \quad 3.5$$

$$S_{21} = T \quad 3.6$$

Equations 3.2 and 3.6 were used to determine the EM properties (ϵ_r and σ). Equations 3.2 and 3.6 were combined and then solved for ϵ_r and σ . This lead to;

$$\epsilon_r = (\text{phase}(S_{21}) * c / 2\pi f d)^2 \quad 3.7$$

$$\sigma = (2\pi f \epsilon_r \epsilon_0 / d) * ((2 * (-\ln(\text{magnitude}(S_{21}))) * c / 2\pi f d (\epsilon_r)^{1/2})^2 + 1)^2 - 1)^{1/2} \quad 3.8$$

3.7.2 EM Properties Estimates using Two Frequency Points

Estimates of the EM properties of the soilbed were considered by using equation 3.7 with two different frequency points. To estimate the relative permittivity using two frequency points, two phase values of the transmission response were selected at two different frequencies. To avoid overestimation of the relative permittivity, it is recommended to select the two close frequencies, since the phase is expected to change slowly for small changes in frequency. A modification of equation 3.7 leads to;

$$\epsilon_r = \frac{(\text{phase}(S_{21f_2}) - \text{phase}(S_{21f_1}))^2 c^2}{2\pi(f_2 - f_1)^2 d^2} \quad 3.9$$

where f_1 is the first frequency selected, f_2 is the nearest frequency value of f_1 , S_{21f_1} is the insertion loss at f_1 and S_{21f_2} is the insertion loss at f_2 .

3.7.3 Channel Transfer Function Method

The Channel Transfer Function (CTF) method is a technique used to eliminate the antenna effects present of the s-parameters measurements [Farid 2004]. By removing the antenna effects from the s-parameters measurements, the newly computed s-parameters are expected to only represent the soil medium parameters. This newly s-parameters are applied to estimates the EM properties of the soilbed. In order to determine the CTF matrix, the s-parameters matrix in a single two-port network (equation 3.10) is rearranged to yield a system of cascade matrices (equation 3.11):

$$\begin{bmatrix} V_1^- \\ V_2^- \end{bmatrix} = \begin{bmatrix} S_{11} & S_{12} \\ S_{21} & S_{22} \end{bmatrix} \begin{bmatrix} V_1^+ \\ V_2^+ \end{bmatrix} \longrightarrow \begin{bmatrix} V_1^- \\ V_1^+ \end{bmatrix} = \begin{bmatrix} 1/S_{12} & -S_{22}/S_{12} \\ S_{11}/S_{12} & S_{12} - S_{11}S_{22}/S_{12} \end{bmatrix} \begin{bmatrix} V_2^- \\ V_2^+ \end{bmatrix} \quad 3.10$$

$$\begin{bmatrix} 1/S_{12} & -S_{22}/S_{12} \\ S_{11}/S_{12} & S_{12} - S_{11}S_{22}/S_{12} \end{bmatrix}_{Total} = \begin{bmatrix} 1/S_{12} & -S_{22}/S_{12} \\ S_{11}/S_{12} & S_{12} - S_{11}S_{22}/S_{12} \end{bmatrix}_T \begin{bmatrix} 1/C_{12} & -C_{22}/C_{12} \\ C_{11}/C_{12} & C_{12} - C_{11}C_{22}/C_{12} \end{bmatrix}_{SOIL} \begin{bmatrix} 1/S_{12} & -S_{22}/S_{12} \\ S_{11}/S_{12} & S_{12} - S_{11}S_{22}/S_{12} \end{bmatrix}_R \quad \mathbf{3.11}$$

where $[S]_{Total}$, $[S]_T$, $[C]_{SOIL}$, $[S]_R$ represents the equivalent s-parameters matrices of the measurements, the transmitting antenna characteristics, the soilbed, and the receiving antenna characteristics, respectively on the cascade matrices. $[C]_{SOIL}$ represent the corrected s-parameters for antenna's effects, and are subsequently applied for the estimation of the EM properties using equations 3.7 and 3.8.

3.8 Time Domain Modeling

A simulated soilbed model was developed to study the behavior of the electromagnetic wave propagation through an assigned medium using HFSS's transient network analysis option. The transient network analysis is based on Discontinuous Galerkin Time Domain (DGTd). DGTd analysis gives a full understanding of the EM characteristics of the simulated model over a time period. The soilbed model used for the transient analysis is the same used for the design of the helix antenna and for the soilbed studied in frequency domain (Figure 3.20). The input signal is a broadband waveform between 500 MHz to 1.5 GHz (Figure 3.21).

The simulated results of the soilbed model were used to estimate the EM properties of the studied medium. The resulted reflected and transmitted response of the transient EM wave is obtained, and the EM properties for the model are estimated. The

simulations performed were for different assigned EM properties (Table 3.4). For time domain simulations, the relative permittivity was the only EM property of interest.

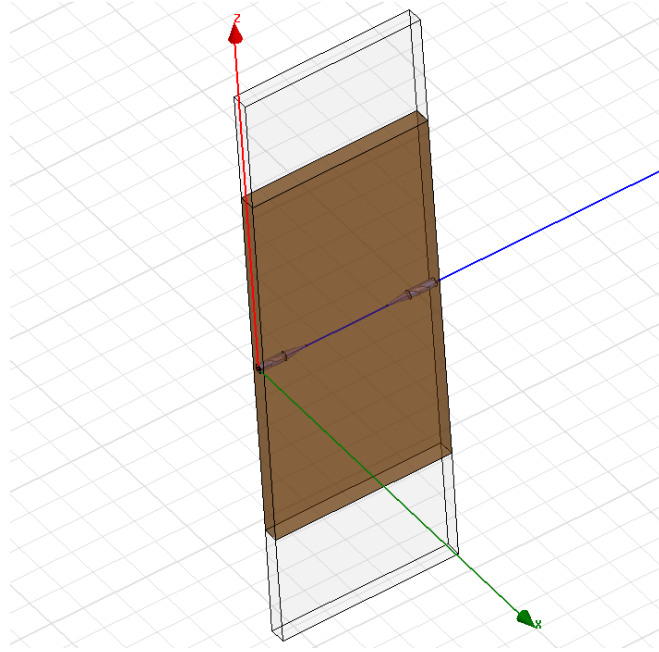


Figure 3.20 Simulated Testbed Model Used for Transient Network Analysis.

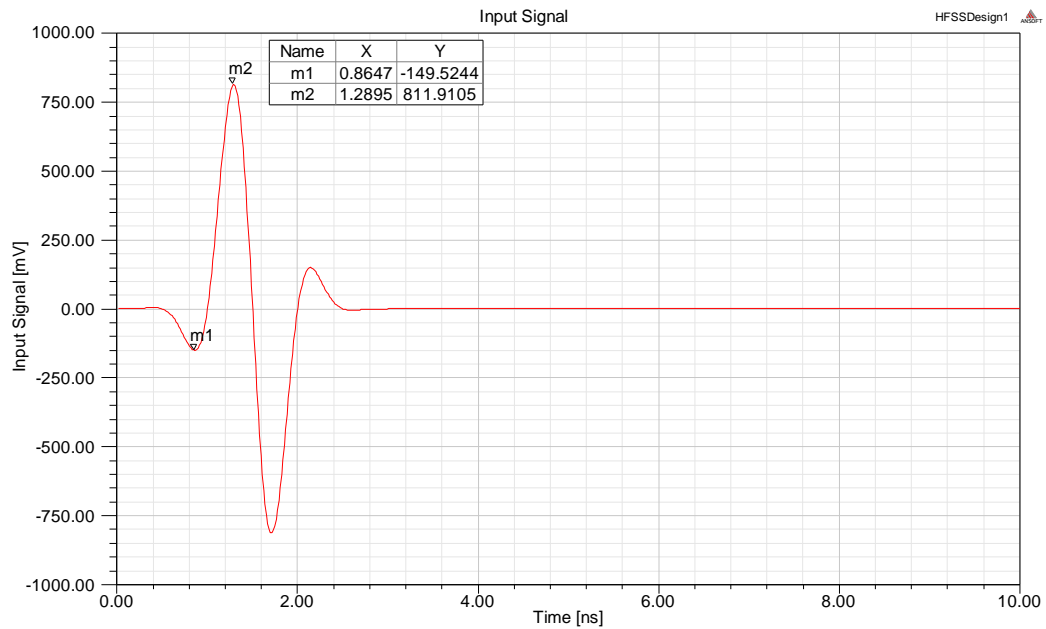


Figure 3.21 Input Signal Used for Transient Network Analysis of the Simulated Testbed Model.

Table 3.4 Assigned Relative Permittivity of the Simulated Testbed Model Using Transient Network Analysis

Type of material	Assigned Relative Permittivity
Air Medium	1
Dry Sand	4
Test Property #1	10
Test Property #2	20

3.9 Estimation of Electromagnetic Properties in Time Domain

Estimates of the relative permittivity were performed from the reflected and transmitted response of the transient analysis for the simulated soilbed model. To determine the relative permittivity from time domain measurements a relationship between the relative permittivity with the reflected and transmitted signal response must be established. The following equations (equations 3.12 and 3.13) were used to relate the reflected and transmission response with the relative permittivity.

$$\mathbf{T}_r=(2\mathbf{d}_r\sqrt{\epsilon_{r1}})/c \quad \mathbf{3.12}$$

where T_r is the time of return or the reflected response time, d_r is the distance from the excitation point to the end of the antenna, ϵ_{r1} is the relative permittivity of the material which the signal travels through (i.e., coaxial line dielectric, antenna dielectric) and c is the speed of light

$$\mathbf{T}_t=(\mathbf{d}_t\sqrt{\epsilon_{r2}})/c; \quad \mathbf{3.13}$$

where T_t is the time of arrival from the transmitter antenna to the receiving antenna or the transmission response time, d_t is the separation between antennas, and ϵ_{r2} is the relative permittivity of the studied medium.

The reflected signal includes multiple reflections caused by different elements on the testbed. Such elements are the antenna, the transmission line, boundaries, and also the studied medium. For this analysis, the antenna reflected response is the primary element

and the coaxial transmission lines are secondary (if present). The time of return for the simulated model accounts for the input signal which requires subtracting it to obtain the reflected response of the testbed. The result is a shift in time of the simulated reflection response.

The time of arrival of the transmitted signal is used to estimate the relative permittivity. The transmitted signal includes the input signal and the reflected signal. The reflection response must be, therefore, subtracted from the transmission response to obtain the travel time in the studied medium. The separation between antennas is fixed ($d_t=19.4$ cm) for the simulated model using different EM properties. Using equations 3.12 and 3.13 to solve for the relative permittivity of the medium gives;

$$\epsilon_r = [(T_t - T_r) * c / d_t]^2 \quad 3.14$$

Since both T_r and T_t require the subtraction of the input signal time, it is not necessary to perform the input signal time subtraction because they will cancel out automatically in equation 3.14.

The selection of T_t and T_r take place from the transmitted and reflected response of the simulated model, respectively. The first peak of the transmission response is selected as T_t (Figure 3.22). In Figure 3.22 the value of T_t selected is marked as m1. For the analyzed simulated models, the first peak is usually very small since the intensity of the direct path is small compared to the entire energy inside the testbed. The selection of the appropriate value of T_r for the analysis come in reference from the input signal waveform (Figure 3.21). Using the simulated reflected response, a waveform with a delay time

similar to the input signal is obtained. The first peak of that delayed time waveform is considered as T_r and marked as m4 (Figure 3.23). The expected reflected and transmission response results using transient analysis for the soilbed model are illustrated in Figures 3.24 and 3.25, respectively.

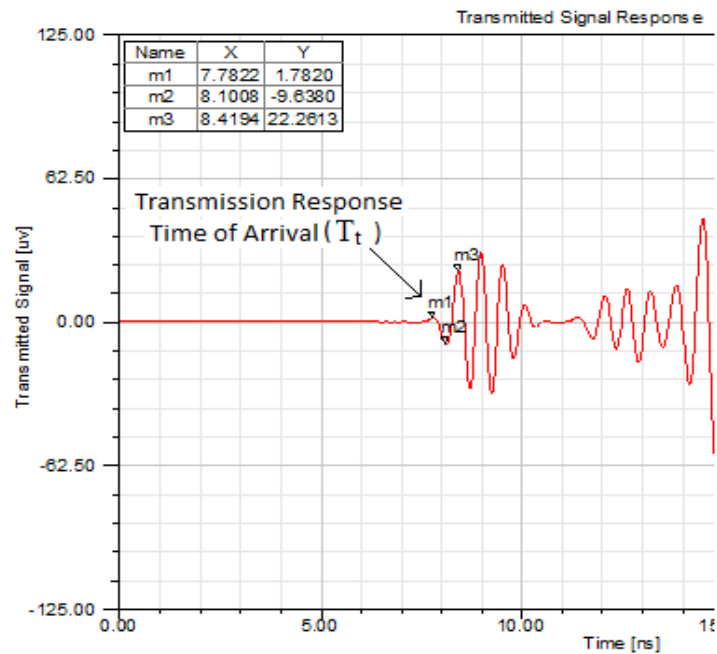


Figure 3.22 Transmission Response and Variable Selection for the Simulated Model Using Transient Network Analysis.

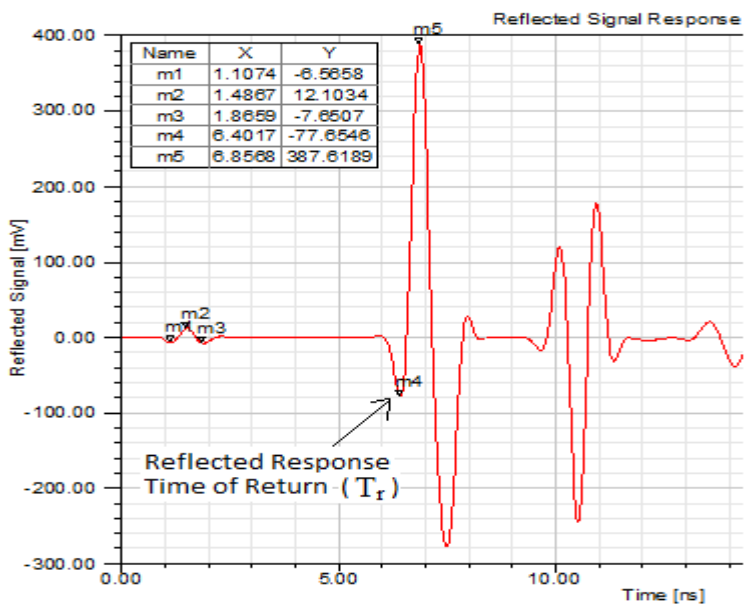


Figure 3.23 Reflection Response and Variable Selection for the Simulated Model Using Transient Network Analysis.

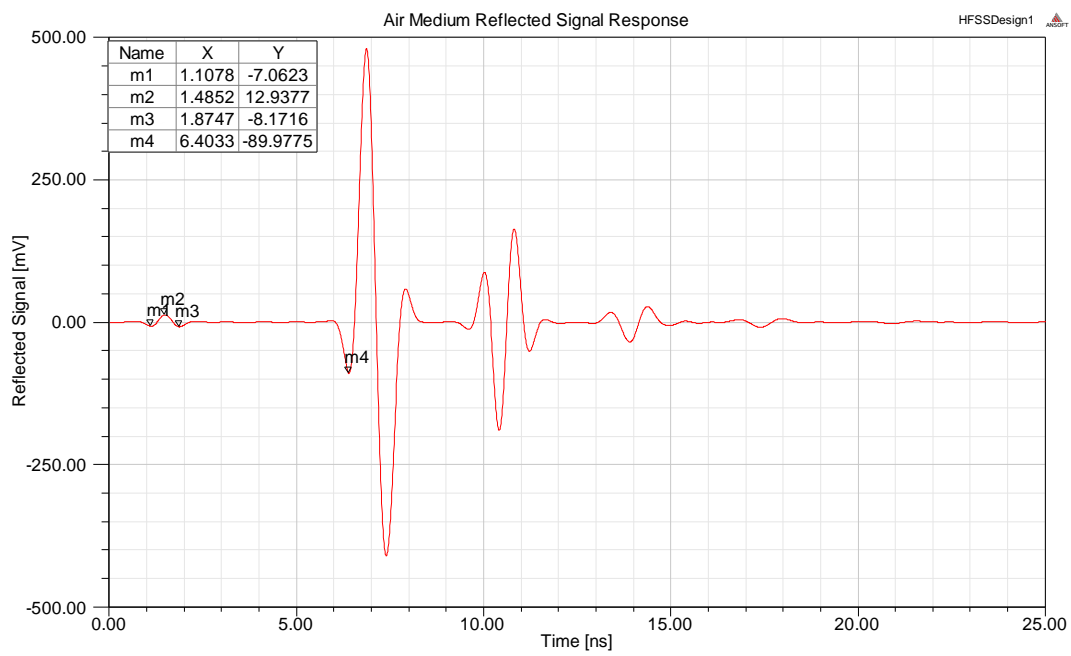


Figure 3.24 Reflection Response for the Simulated Model of Air Medium Testbed.

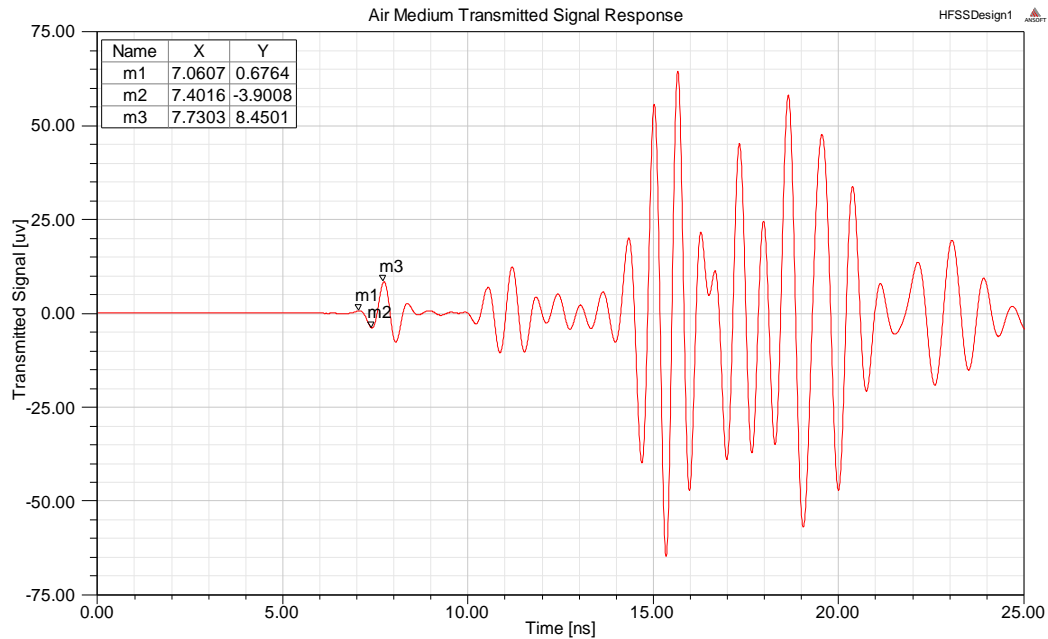


Figure 3.25 Transmission Response for the Simulated Model of Air Medium Testbed.

4 ANALYSIS AND RESULTS

4.1 Overview

This chapter discusses the results for the estimates of the relative permittivity using different frequency and time domain methods from s-parameters measurements. Relative permittivities were estimated using: transmission and reflection equations for lossy media; two frequency points; the channel transfer function method; the phase component of the transmission response; a modified phase-shift; and time domain methods. Experimental measurements and simulated results for the designed helix antennas for different EM properties and boundary conditions are presented and discussed. Analysis of the results leads to a new design of the soilbed for CWR measurements.

4.2 Estimation of the EM Properties

Estimates of EM properties of sand soilbed under different environmental conditions were performed using previous s- parameters measurements taken by Serrano [Serrano 2008]. Measurements of dry sand, dry sand with trichloroethylene (TCE, a DNAPL), wet sand, and wet sand with TCE were used to estimate the EM properties. The estimates were performed for a frequency range from 1 GHz to 2 GHz. The numerical analysis for the three techniques used to estimate the EM properties was performed with a MATLAB code.

4.2.1 Estimates Using Transmission and Reflection Equations for Lossy Media

Estimates of the relative permittivity were performed using equation 3.7. Three different frequencies were selected for analysis. Table 4.1 shows the estimates of the relative permittivity at three different frequencies and for different dry sand soilbed measurements. The results using the three analyzed frequencies show that all the estimated values of the relative permittivity are below unity. Incorrect estimates for relative permittivities (which should never be less than one) can result from inaccurate s -parameters measurements, antenna effects, and/or boundary effects of the tank.

4.2.2 Estimates of the EM Properties Using Two Frequency Points

Estimates of the relative permittivity for the measurements made by Serrano [2008] were also performed by using equation 3.7 at three different frequencies. Since this method requires two frequency points per estimate, the second frequency point corresponds to the value right after the first selected frequency point. The summary for the resulting estimates of the relative permittivity is shown on table 4.2. These results of the relative permittivity show a lot of discrepancies compared to the results in table 4.1. Most of the values obtained were over unity but there were overestimated due to a large phase difference between the two selected frequency points. On the other hand, there are some estimated values that are below unity leading to inaccurate results. This error was initially attributed to a very small phase difference.

Table 4.1 Relative Permittivity Estimates Using the Equations on Lossy Media

S-parameter Raypath	1 GHz	1.5 GHz	2 GHz
S_{51}	0.092	0.036	0.0045
S_{61}	0.081	0.034	0.0014
S_{71}	0.054	0.016	0.0029
S_{81}	0.071	0.014	0.00062
S_{52}	0.015	0.0037	0.0015
S_{62}	0.058	0.0012	0.012
S_{72}	0.00052	0.045	0.0013
S_{82}	0.034	0.016	0.0071
S_{53}	0.00061	0.00012	0.00018
S_{63}	0.014	0.049	0.0086
S_{73}	0.028	0.00093	0.011
S_{83}	0.035	0.039	0.012
S_{54}	0.00012	0.0061	0.0023
S_{64}	0.0097	0.011	0.021
S_{74}	0.0019	0.046	0.0025
S_{84}	0.00072	0.012	0.0016

Table 4.2 Estimates of the Relative Permittivity using Two Frequencies Points

S-parameter Raypath	1 GHz	1.5 GHz	2 GHz
S ₅₁	4.87	86.24	71.52
S ₆₁	0.24	113.76	166.37
S ₇₁	63.41	150.84	4.79
S ₈₁	91.91	223.98	2.27
S ₅₂	13.01	18.25	59.46
S ₆₂	53.59	16.43	114.69
S ₇₂	21.37	133.87	3.84
S ₈₂	45.27	277.30	126.07
S ₅₃	3.31	72.84	17.54
S ₆₃	57.46	106.63	59.24
S ₇₃	130.61	0.29	12.37
S ₈₃	84.49	0.45	61.61
S ₅₄	17.93	82.99	125.76
S ₆₄	25.57	163.14	159.53
S ₇₄	44.92	75.03	0.15
S ₈₄	85.43	70.04	121.59

4.2.3 Estimates of the EM Properties Using Channel Transfer Function

Method

The previous applied methods yielded inaccurate results in the estimates of the EM properties. These inaccuracies could be caused, among other things, by antenna's effect. The channel transfer function (CTF) was applied to the s-parameters measurements taken by Serrano [2008] to eliminate this effect. In this method, the CTF is applied to s-parameters measurements to obtain corrected measurements which represent the studied soilbed. After the corrections were made, estimates of the EM properties were performed using equation 3.7. The resulting estimates of the relative permittivity (Table 4.3) continue to yield relative permittivity values below unity in most cases even though this analysis was supposed to improve the estimates due to the removal of the antenna effects of the raw s-parameters measurements. This suggests that other effects are causing the discrepancies in the estimates.

Table 4.3 Estimates of the Relative Permittivity Using Channel Transfer Function

S- parameter Raypath	1 GHz	1.5 GHz	2 GHz
S ₅₁	0.061	0.030	0.51
S ₆₁	0.16	0.041	0.31
S ₇₁	0.17	0.26	0.13
S ₈₁	0.18	0.24	0.11
S ₅₂	0.64	0.36	0.23
S ₆₂	0.86	0.24	0.31
S ₇₂	0.63	0.022	0.37
S ₈₂	0.43	0.43	0.32
S ₅₃	1.11	0.22	0.32
S ₆₃	2.42	0.23	0.37
S ₇₃	1.71	0.88	0.60
S ₈₃	1.86	0.45	0.44
S ₅₄	0.010	0.098	0.027
S ₆₄	0.39	0.55	0.041
S ₇₄	0.37	0.60	0.17
S ₈₄	0.46	0.75	0.066

4.2.4 Analysis in the Phase Component of the Transmission Response

A theoretical analysis of the transmission coefficient equation (3.2) was performed to understand the behavior of its response. A transmission coefficient value was determined by considering a specific distance and an assigned EM property in the L-band frequency range (1 GHz- 2 GHz). The distance used was 26 cm, which corresponds

to the distance from the transmitter antenna to the receiver antenna in straight path used to take the measurements of the s-parameters. The obtained result of the calculated transmission coefficient was very different compared to s-parameters measurements already taken. This difference could be due to antenna effects and/or the boundary effect present in the testbed. Although the antennas were constructed very similar, the response was not identical. This leads to obtain different s-parameters measurements over the entire frequency range. An estimate of the EM properties was performed using the calculated transmission coefficient and equation 3.7. This analysis was performed to make sure that equation 3.7 was solved correctly and also to that the first analysis were asserted. The estimated values of the EM properties were still below the unity, which required a much more careful analysis on the transmission coefficient equation.

The transmission coefficient equation (3.2) used to estimates the EM properties from the s-parameters measurements represents a complex exponential equation which is composed of the trigonometric functions sine and cosine demonstrated by Euler Rule (Equation 4.1).

$$\mathbf{T} = e^{-(\alpha + j\beta)d} = e^{-\alpha d} (\cos(\beta d) - j \sin(\beta d)) \quad \mathbf{4.1}$$

Because the derived values for sine and cosine functions exists between 0 and 360 degrees in the unitary circle, the values obtained for angles greater than 360 must be the same as the ones that correspond to the values between 0 and 360 degrees with the only difference that they count the times a phase shift over 360 degrees occurs. For example;

$$\text{a) } \cos(45 \text{ degrees}) = 0.707$$

b) $\cos(405 \text{ degrees}) = \cos(360 \text{ degrees} + 45 \text{ degrees}) = 0.707$ (one 360 degree phase shift)

The 360 degrees phase shift is integrated on the trigonometric function which leads to deduce that for a given value obtained from a trigonometric function the times a 360 degrees phase shift occurs will be unknown. The relative permittivity is determined from the electrical length (βd). The electrical length is the argument of the trigonometric function and also is the factor that causes the erroneous permittivity values. The issue is part by the sine and cosine functions because the maximum phase value obtained by determining the inverse of these functions is 2π leading to a 360 degrees phase shift lost in the argument. As an example βd is determined, the cosine function is applied to βd and then the cosine inverse function is determined. For example,

Given the Values

$$f = 1 \text{ GHz}, \epsilon_r = 3, \mu_r = 1, \text{ and } d = 26 \text{ cm.}$$

Electrical Length Calculation

$$\begin{aligned} \beta d &= 2\pi f(\mu_r \epsilon_r)^{1/2} d/c = (2\pi(1 \times 10^9)(26 \times 10^{-2})(3)^{1/2})/(3 \times 10^8) \\ &= 9.4318 \text{ radians} = 540.40 \text{ degrees (original value)} \end{aligned}$$

Applying the Cosine Function

$$\cos(540.40 \text{ degrees}) = -0.9999$$

Applying Cosine Inverse Function

$$\cos^{-1}(-0.9999) = 179.19 \text{ degrees (Value obtained after applying cosine inverse)}$$

Analyzing the original value with the value obtained after applying cosine inverse;

$$540.40 - 179.19 = 361.21 \text{ degrees}$$

After comparing the original value with the value obtained using the cosine inverse there's no doubt that a 360 degrees phase shift was not integrated in the calculation. This result produces incorrect estimates of the EM. By calculating the relative permittivity using the phase value obtained after applying inverse cosine;

Given the Values

$$\beta d = 179.19 \text{ degrees}, d = 26 \text{ cm}, f = 1 \text{ GHz}, \mu_r = 1$$

Estimation of the relative permittivity

$$\begin{aligned} \epsilon_r &= \left(\frac{(\beta d) \cdot c}{2\pi f \cdot d} \right)^2 \cdot \left(\frac{1}{\mu_r} \right) \\ &= \left(\frac{179.19 \cdot \pi \cdot 3 \times 10^8}{180 \cdot 2\pi \cdot 1 \times 10^9 \cdot 26 \times 10^{-2}} \right)^2 = 0.33 \end{aligned}$$

The result demonstrates a value for the relative permittivity less than unity caused by a single 360 degrees phase shift lost. To determine the actual relative permittivity value, the times 360 degree phase shifts occur must be known. A modified phase shift from equation 3.7 was developed in order to determine the EM properties.

4.2.5 Estimates of the Relative Permittivity using a Modified Phase Shift

The phase component of the transmission coefficient is proportional to the EM properties. A plot of the phase of the transmission coefficient, or the insertion loss (S_{21}), is produced to analyze the phase behavior. A plot of the phase component of the transmission coefficient for a wave that traveled 26 cm through dry sand is illustrated in Figure 4.1. From the response, note that the phase shows multiple 360 degrees phase shifts over the desired frequency range (1 GHz- 2 GHz).

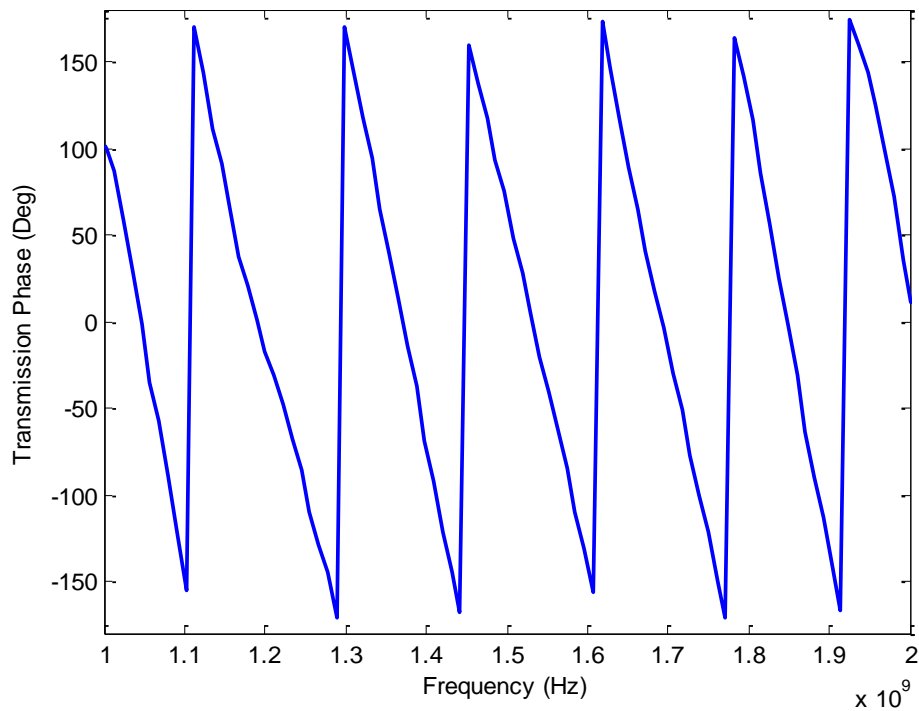


Figure 4.1 Phase Component of the Measured Transmission Response for Dry Sand Soilbed.

From equation 3.7 and using Figure 4.1, the relative permittivity could be determined. Since the phase component value corresponds to a specific frequency, it is possible to go through 360 degrees phase shift on a particular frequency range. This means that

$$\epsilon_r = (\Delta\theta * c / 2\pi\Delta f d)^2, \quad 4.2$$

where $\Delta\theta$ is the phase difference and Δf is the frequency range where the phase difference occurs. From Figure 4.1, a 360 degrees (2π) phase shift occurs for a frequency range of 150 MHz and

$$\epsilon_r = (2\pi * c / 2\pi(150 \times 10^6)d)^2.$$

With a distance of 26 cm from the transmitter to the receiver antenna, the resulting relative permittivity (ϵ_r) for this plot is 59.17, which overestimates the relative permittivity. From the phase component response it is appreciated that the distance traveled by the EM wave is integrated n times over a 360 degrees phase shift in the 1 GHz analyzed range. The phase response gives a specific phase value for a corresponding frequency value. However, there is a relationship between the phase and the frequency which includes the distance implicitly. Considering a phase shift ($\Delta\delta$) over a frequency range (Δf) in equation 4.2, it becomes

$$\Delta\delta = 2\pi\Delta f(\epsilon_r)^{1/2}/c \quad 4.3$$

For this case, the d is incorporated into $\Delta\delta$. From Figure 4.1, a certain number of times a 360 degrees phase shift occurs over the 1 GHz frequency range. With this idea, we can deduce that n times a 360 degrees phase shift occurs over a desired frequency range;

$$2\pi n = 2\pi\Delta f(\epsilon_r)^{1/2}/c \quad 4.4$$

Then by solving equation 4.4 for ϵ_r , we can determine the relative permittivity of the studied medium as;

$$\epsilon_r = \left(\frac{n \cdot c}{\Delta f} \right)^2 \quad 4.5$$

Equation 4.5 gives the relationship between the relative permittivity for a given number of 360 degrees phase shift over a corresponding frequency range.

Estimates of the relative permittivity were performed using equation 4.5 from s-parameters measurements (taken by Serrano [2008]) of sandy soilbed under different environmental conditions. Two identical tanks were constructed and used for sandy soilbed testing. In one of the soilbeds, dry sand conditions measurements were performed while the other tank was used to perform saturated sand conditions measurements. Plots of the phase component of the transmission coefficient measurements are illustrated in Figures 4.2-4.9. By using the plot of the phase component, n and Δf were determined.

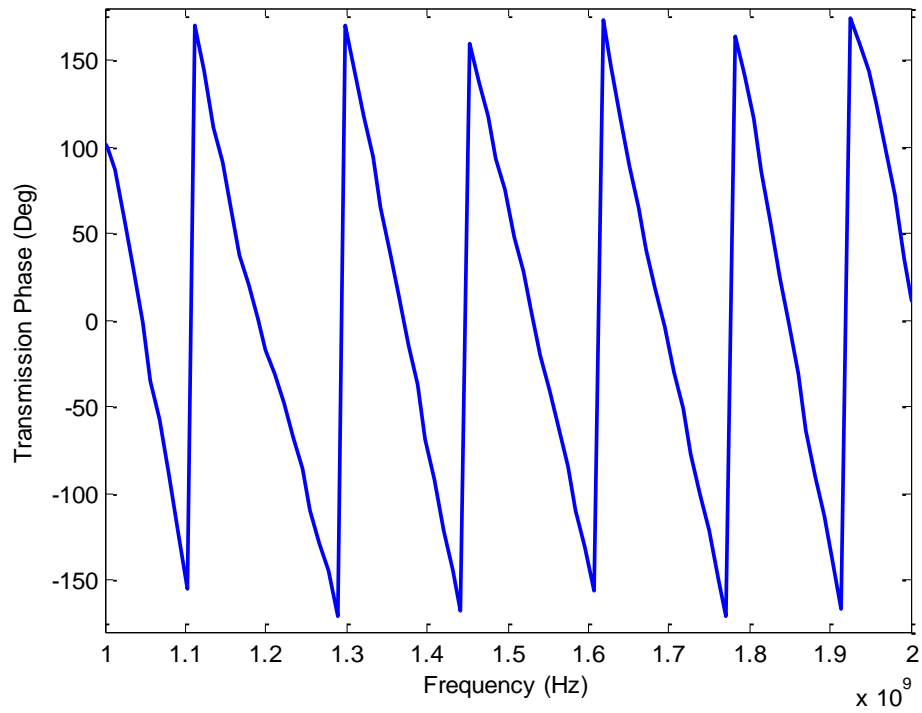


Figure 4.2 Phase Component of the Measured Transmission Response (S_{51}) for Dry Sand Soilbed.

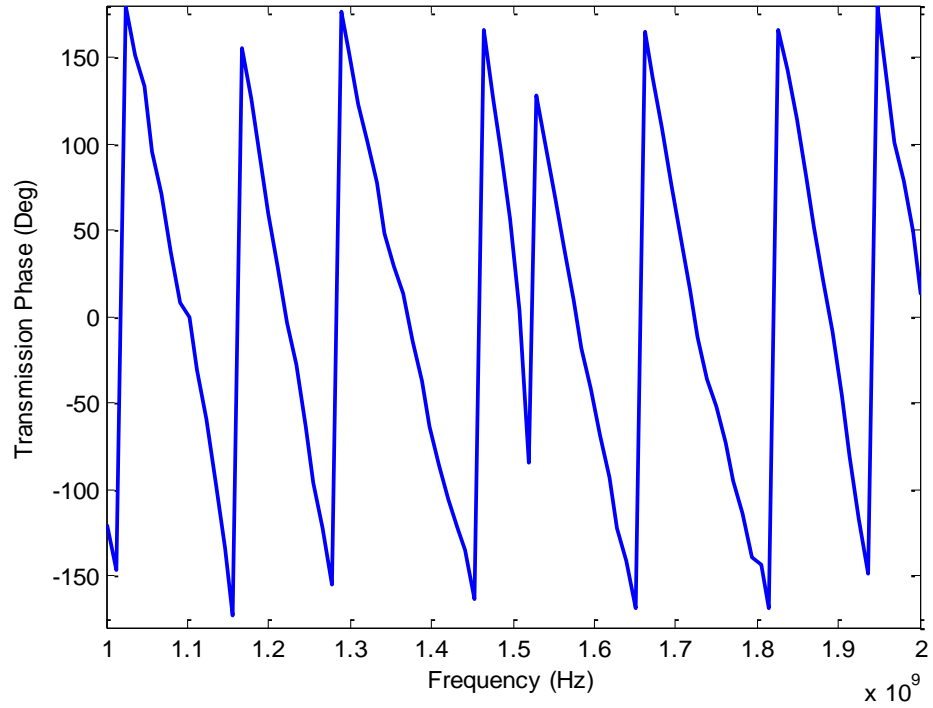


Figure 4.3 Phase Component of the Measured Transmission Response (S_{82}) for Dry Sand Soilbed.

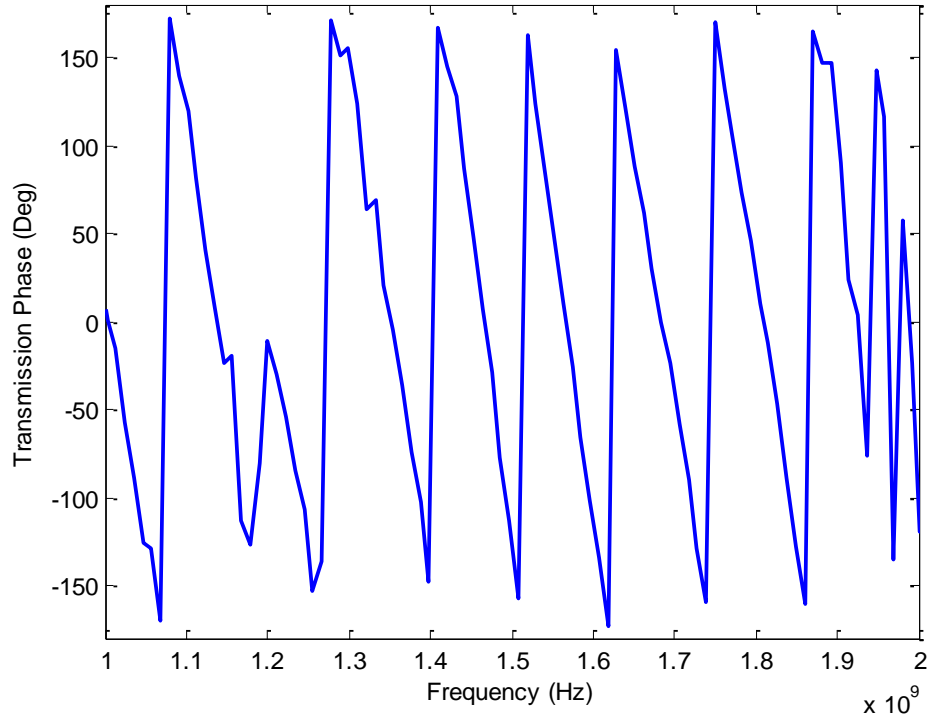


Figure 4.4 Phase Component of the Measured Transmission Response (S_{51}) for Saturated Sand Soilbed.

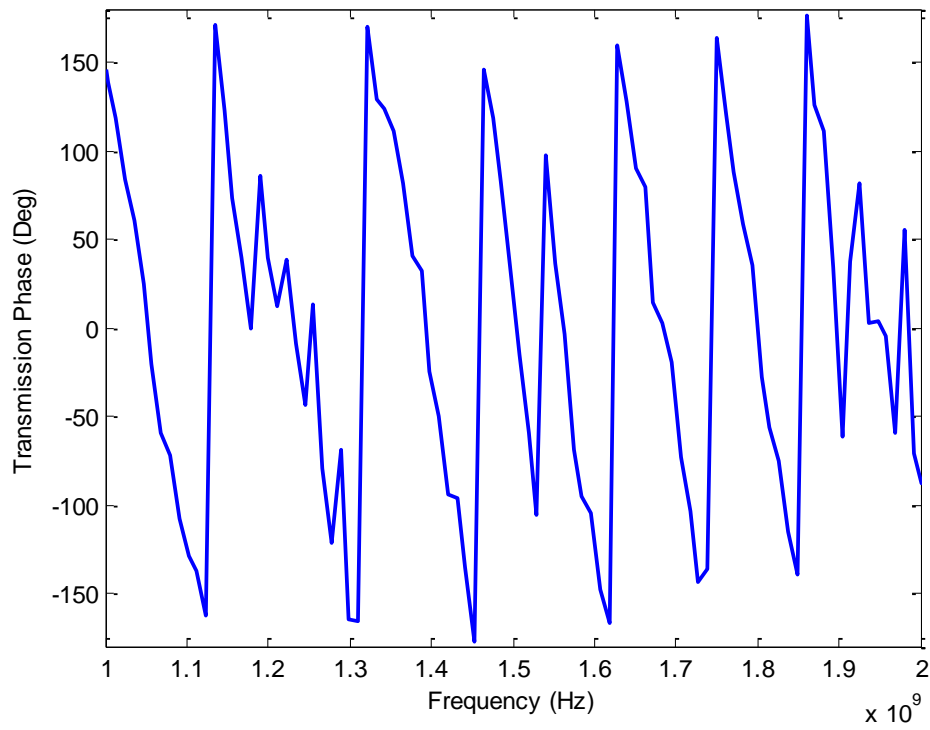


Figure 4.5 Phase Component of the Measured Transmission Response (S_{82}) for Saturated Sand Soilbed.

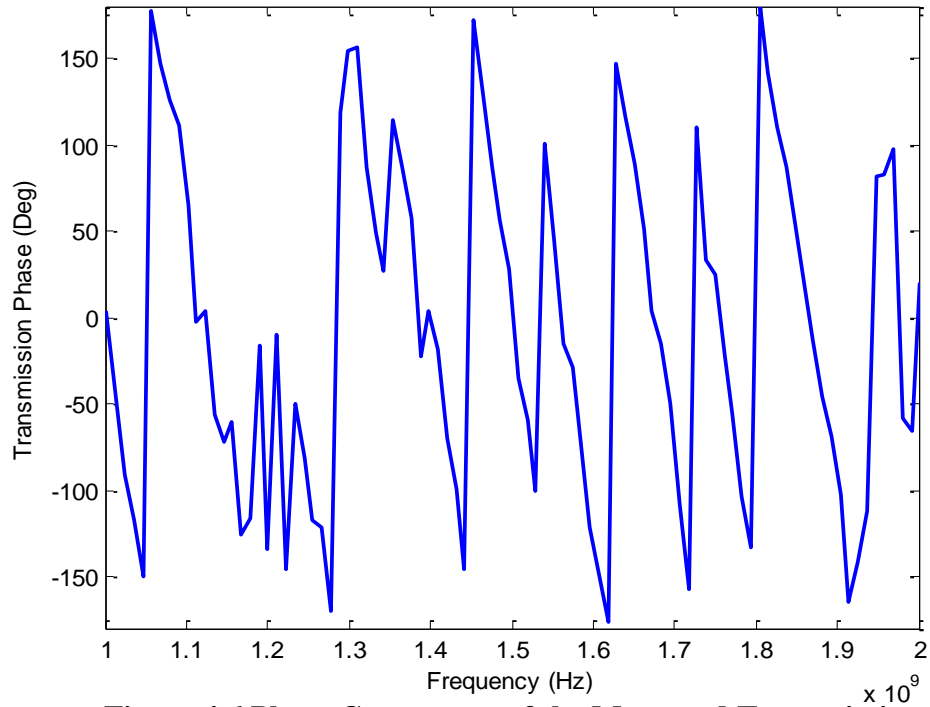


Figure 4.6 Phase Component of the Measured Transmission Response (S_{52}) for Saturated Sand Soilbed.

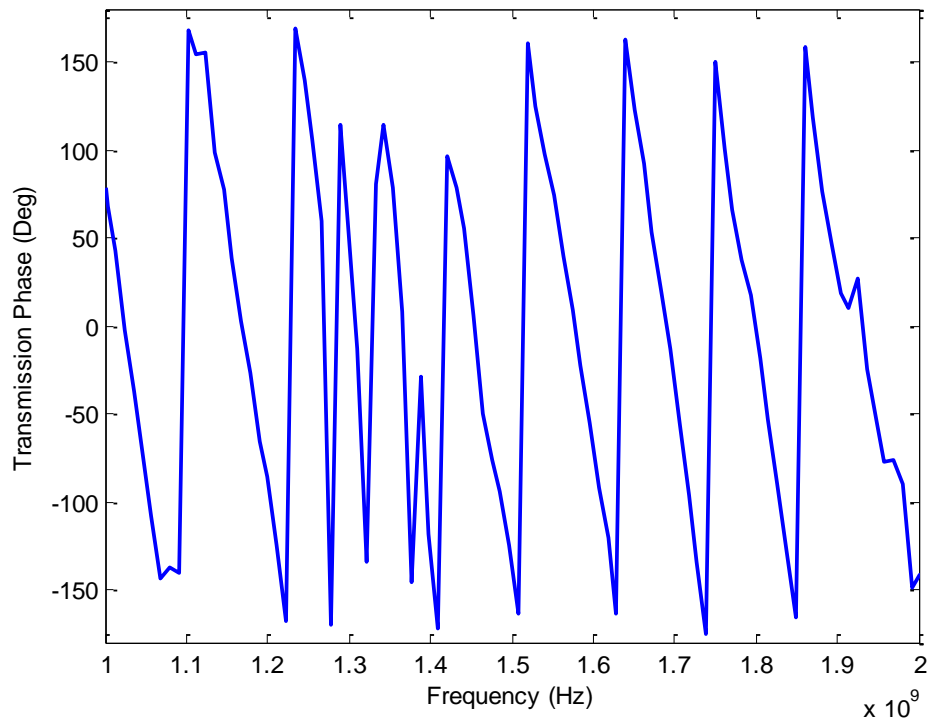


Figure 4.7 Phase Component of the Measured Transmission Response (S_{71}) for Saturated Sand Soilbed.

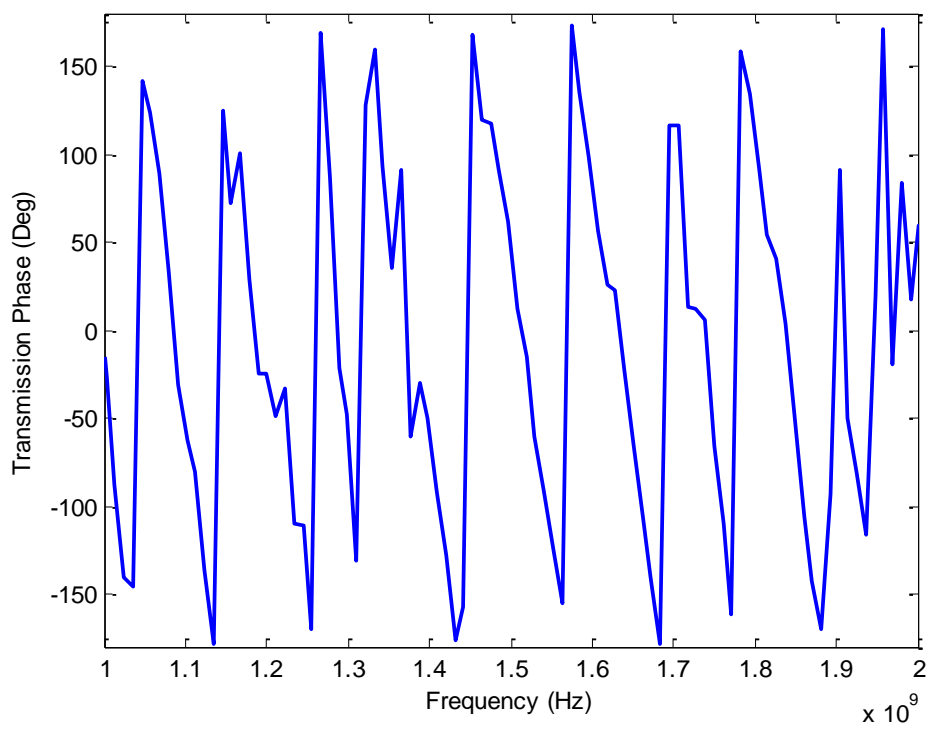


Figure 4.8 Phase Component of the Measured Transmission Response (S_{53}) for Saturated Sand Soilbed With TCE Injected for 45 Minutes.

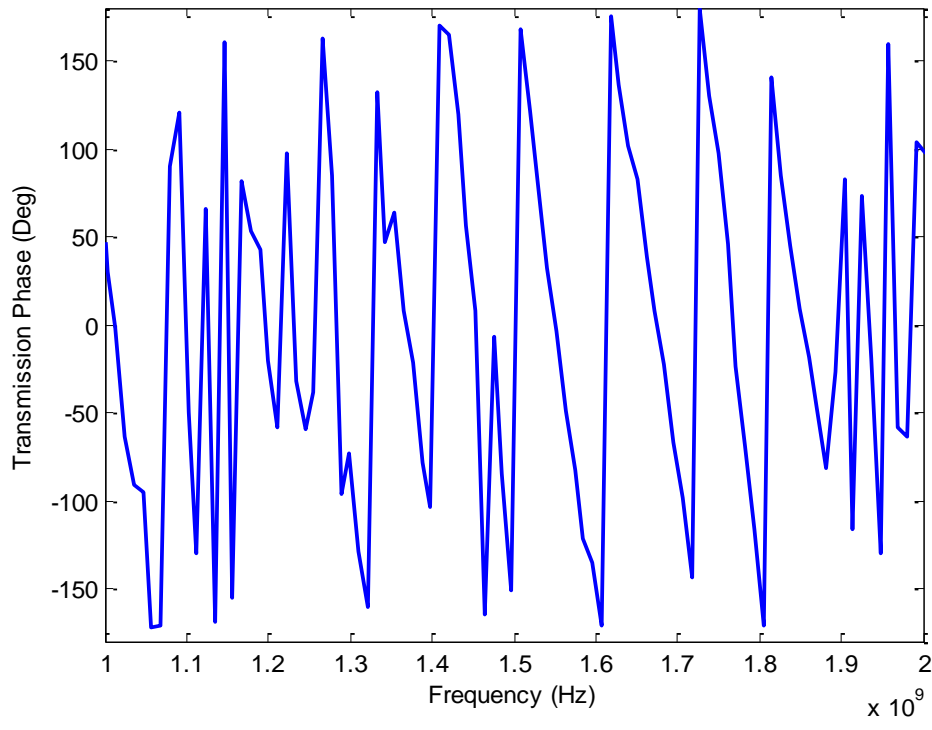


Figure 4.9 Phase Component of the Measured Transmission Response (S_{71}) for Saturated Sand Soilbed With TCE Injected for 45 Minutes.

Estimates of the relative permittivity for dry sand from s-parameters measurements of the dry sand soilbed are shown in tables 4.4 and 4.5. The estimates show pretty good numbers close to the theoretical values (between 2 and 4). The total average over the 16 ray paths for the relative permittivity is 4.38 and the straight path average is 3.95 for the forward transmission while 3.77 for the reverse transmission. The ray paths with the longest distance between the transmitter and the receiver provide the highest numbers on the relative permittivity, causing a large number in the total average compared to the straight path average. For dry conditions after 50 minutes of TCE injected in sandy soilbed, the relative permittivity average increases from 4.38 to 6.12 (Table 4.6). The straight path average for this condition increases from 3.9 to 4.81, which are a little bit higher under this condition compared to dry sand without TCE.

Table 4.4 Estimates of the Relative Permittivity for Dry Sand Soilbed Measurements

Forward Transmission Response Raypath	# of 360 degrees phase shifts	Δf	ϵ_r
S ₅₁	6	960 MHz	3.52
S ₆₁	4	520 MHz	5.32
S ₇₁	3	350 MHz	6.61
S ₈₁	2	320 MHz	3.52
S ₅₂	6	980 MHz	3.37
S ₆₂	5	740 MHz	4.11
S ₇₂	4	630 MHz	3.63
S ₈₂	5	700 MHz	4.59
S ₅₃	5	700 MHz	4.59
S ₆₃	3	490 MHz	3.37
S ₇₃	6	950 MHz	3.59
S ₈₃	7	1 GHz	4.11
S ₅₄	7	800 MHz	6.89
S ₆₄	5	720 MHz	4.34
S ₇₄	5	780 MHz	3.70
S ₈₄	6	940 MHz	4.59

Table 4.5 Estimates of the Relative Permittivity for Dry Sand Soilbed Measurements

Reverse Transmission Response Raypath	# of 360 degrees phase shift	Δf	ϵ_r
S ₁₅	6	960 MHz	3.52
S ₂₅	6	970 MHz	3.44
S ₃₅	5	700 MHz	4.59
S ₄₅	8	920 MHz	6.81
S ₁₆	3	420 MHz	4.59
S ₂₆	5	720 MHz	4.34
S ₃₆	4	610 MHz	3.87
S ₄₆	5	710 MHz	4.46
S ₁₇	3	350 MHz	6.61
S ₂₇	3	450 MHz	4
S ₃₇	6	970 MHz	3.44
S ₄₇	5	800 MHz	3.52
S ₁₈	2	300 MHz	4
S ₂₈	5	710 MHz	4.46
S ₃₈	6	840 MHz	4.59
S ₄₈	5	770 MHz	3.79

**Table 4.6 Estimates of the Relative Permittivity of Dry Sand Soilbed
Measurements with TCE Injected for 50 Minutes**

Forward Transmission Response Raypath	# of 360 degrees phase shifts	Δf	ϵ_r
S ₅₁	4	600 MHz	4
S ₅₂	5	700 MHz	4.59
S ₅₃	6	680 MHz	7.01
S ₅₄	3	320 MHz	7.91
S ₆₁	2	250 MHz	5.76
S ₆₂	5	530 MHz	8.01
S ₆₃	10	900 MHz	11.11
S ₆₄	4	420 MHz	8.16
S ₇₁	5	660 MHz	5.17
S ₇₂	4	510 MHz	5.54
S ₇₃	4	660 MHz	3.31
S ₇₄	5	660 MHz	5.17
S ₈₁	7	800 MHz	6.89
S ₈₂	5	600 MHz	6.25
S ₈₃	5	660 MHz	5.17
S ₈₄	5	760 MHz	3.89

Estimates for the saturated sand soilbed were performed and their results showed an interesting perspective. Dry sand measurements were used as reference (Table 4.7).

The results were very similar to the previous analyzed estimates of dry sand in the other tank. The total average in this condition is 4.41 and the straight ray path average is 3.74. After completely saturating wetting the sand by pumping distilled water at the bottom of the soilbed, the relative permittivity increases from 4.41 obtained on dry sand to 8.16. The straight path average increased from 3.74 to 7.32 (Table 4.8). TCE then was applied to the wet sand (Table 4.9), the relative permittivity increase just a little bit from 8.16 to 8.60, while the straight path average decrease very slow from 7.32 to 7.14.

The small difference in the obtained value for the estimates of the relative permittivity under dry sand with TCE, saturated sand only, and saturated sand with TCE could be due to the limitation of the selected frequency range to determine a 360 degrees phase shift. Compared to dry sand condition, the selected frequency range values were much less. The disadvantage of selecting different frequency range values leads to great uncertainty when considering the estimates of the relative permittivity values. The limitation in the selection of the frequency range values is illustrated in the phase component of the transmission response from Figures 4.4 to 4.9.

Table 4.7 Estimates of the Relative Permittivity for Dry Sand Soiledbed Measurements (Saturated Sand Background)

Forward Transmission Response Raypath	# of 360 degrees phase shifts	Δf	ϵ_r
S ₅₁	6	960 MHz	3.52
S ₅₂	6	960 MHz	3.52
S ₅₃	6	800 MHz	5.06
S ₅₄	7	820 MHz	6.56
S ₆₁	6	860 MHz	4.38
S ₆₂	5	740 MHz	4.10
S ₆₃	4	660 MHz	3.31
S ₆₄	5	740 MHz	4.10
S ₇₁	4	470 MHz	6.52
S ₇₂	4	630 MHz	3.63
S ₇₃	6	950 MHz	3.59
S ₇₄	5	780 MHz	3.70
S ₈₁	5	600 MHz	6.25
S ₈₂	5	730 MHz	4.22
S ₈₃	7	1 GHz	4.41
S ₈₄	6	930 MHz	3.75

Table 4.8 Estimates of the Relative Permittivity for Saturated Sand Soilbed Measurements

Forward Transmission Response Raypath	# of 360 degrees phase shifts	Δf	ϵ_r
S ₅₁	5	610 MHz	6.05
S ₅₂	3	300 MHz	9
S ₅₃	3	320 MHz	7.91
S ₅₄	4	400 MHz	9
S ₆₁	4	460 MHz	6.81
S ₆₂	6	710 MHz	6.43
S ₆₃	4	400 MHz	9
S ₆₄	5	520 MHz	8.32
S ₇₁	2	180 MHz	11.11
S ₇₂	3	300 MHz	9
S ₇₃	6	630 MHz	8.16
S ₇₄	5	560 MHz	7.17
S ₈₁	4	350 MHz	11.76
S ₈₂	3	380 MHz	5.61
S ₈₃	5	590 MHz	6.46
S ₈₄	5	510 MHz	8.65

**Table 4.9 Estimates of the Relative Permittivity for Saturated Sand Soilbed
Measurements with TCE Injected for 45 Minutes**

Forward Transmission Response Raypath	# of 360 degrees phase shifts	Δf	ϵ_r
S ₅₁	6	780 MHz	5.33
S ₆₁	3	280 MHz	10.33
S ₇₁	4	360 MHz	11.11
S ₈₁	1	100 MHz	9
S ₅₂	1	100 MHz	9
S ₆₂	4	410 MHz	8.57
S ₇₂	6	640 MHz	7.91
S ₈₂	5	600 MHz	6.25
S ₅₃	5	560 MHz	7.17
S ₆₃	6	560 MHz	10.33
S ₇₃	4	480 MHz	6.25
S ₈₃	7	660 MHz	10.12
S ₅₄	5	440 MHz	11.62
S ₆₄	3	300 MHz	9
S ₇₄	5	560 MHz	7.17
S ₈₄	6	620 MHz	8.42

4.2.6 Applying the Channel Transfer Function Method to Estimate the Relative Permittivity using the Modified Phase Shift

The CTF was applied to the s-parameters measurements taken by Serrano [2008] in order to improve the previous estimated EM properties obtained from the modified phase shift method. The phase component of the transmission response was obtained after applying the channel transfer function (Figures 4.10 and 4.11). The resulted plot showed a much more complicated shape and was unable to perform the estimate of the relative permittivity.

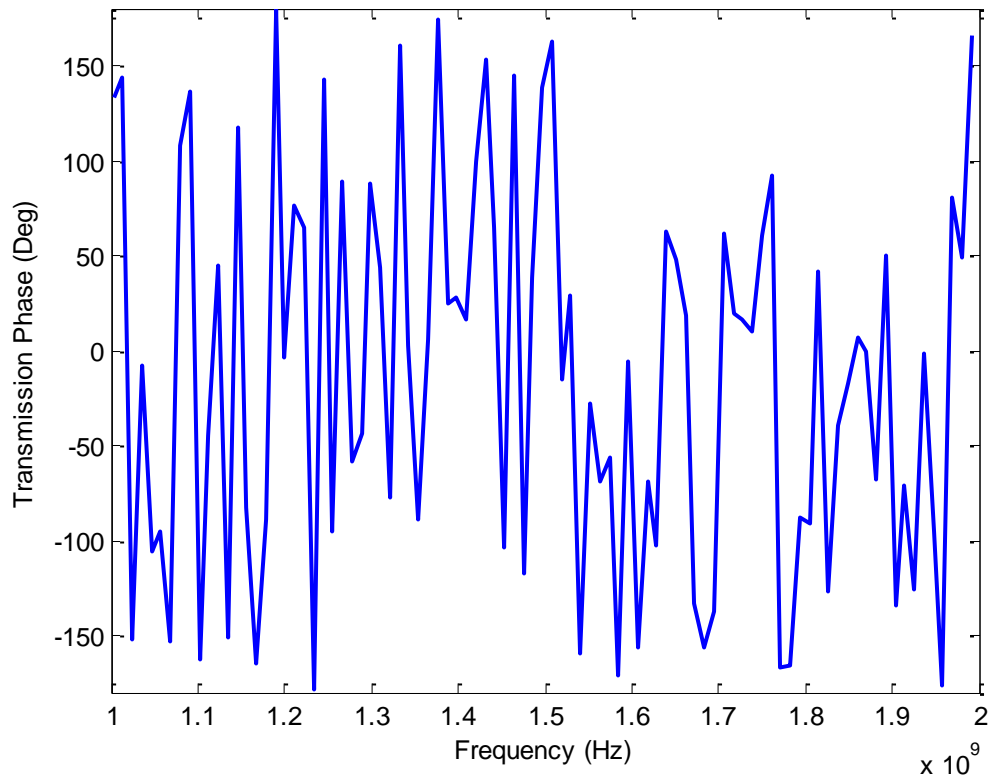


Figure 4.10 Phase Component of the Measured Transmission Response (S_{51}) for Dry Sand Soilbed After Applying Channel Transfer Function Method.

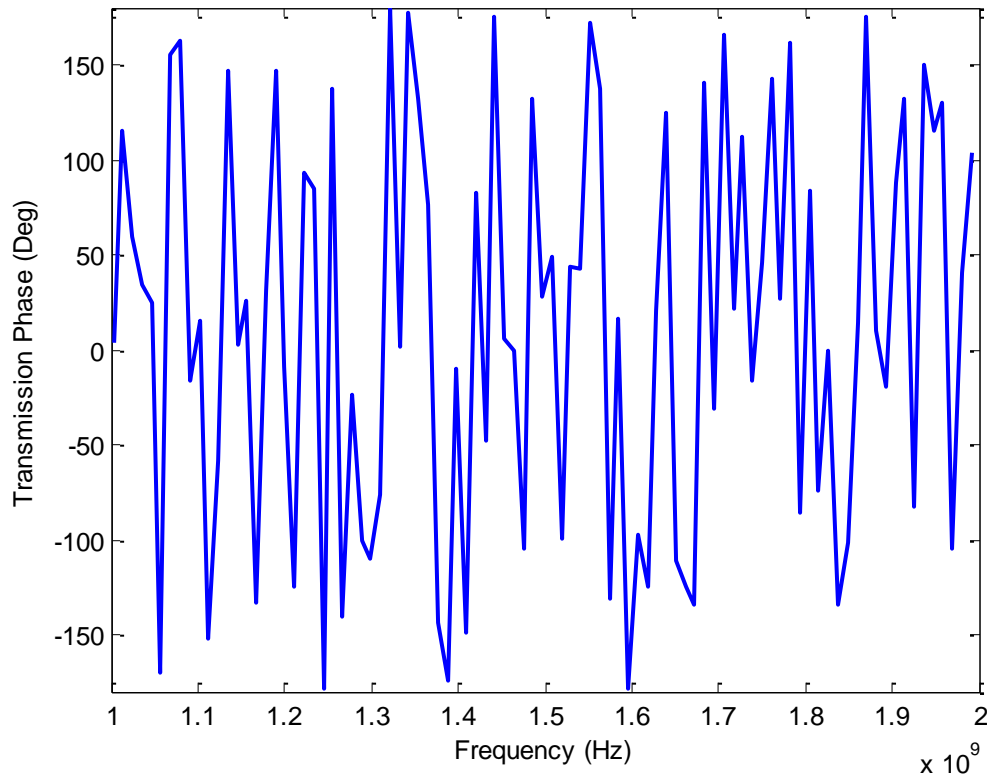


Figure 4.11 Phase Component of the Measured Transmission Response (S_{62}) for Dry Sand Soilbed After Applying Channel Transfer Function Method.

4.3 Design of Helix Antenna for Soilbed Testing

A design of the helix antenna was performed to improve the performance of the s-parameters measurements over the 500 MHz to 1.5 GHz frequency range. Geometry parameters such as the helix diameter, the number of turns of the helix and the width of the strip were used to provide a good impedance matching. The effect of each geometry parameters was performed on dry sand soilbed. For this study, one parameter at a time was changed in the model while the others parameters remained unchanged. The physical limitations of the testbed lead to limit the geometry dimensions for the design of the helix antenna.

4.3.1 Effect of Helix Diameter in the S-parameters Results

The effect of the helix diameter size was significant for s-parameters response over the desired frequency range. By decreasing the helix diameter, the return loss improves significantly and a better performance was achieving over the desired frequency range. An illustration of the return loss response for a diameter of 1.27 cm and a diameter 0.64 cm are shown in Figure 4.12. The final selected value for the helix diameter was 0.64 cm.

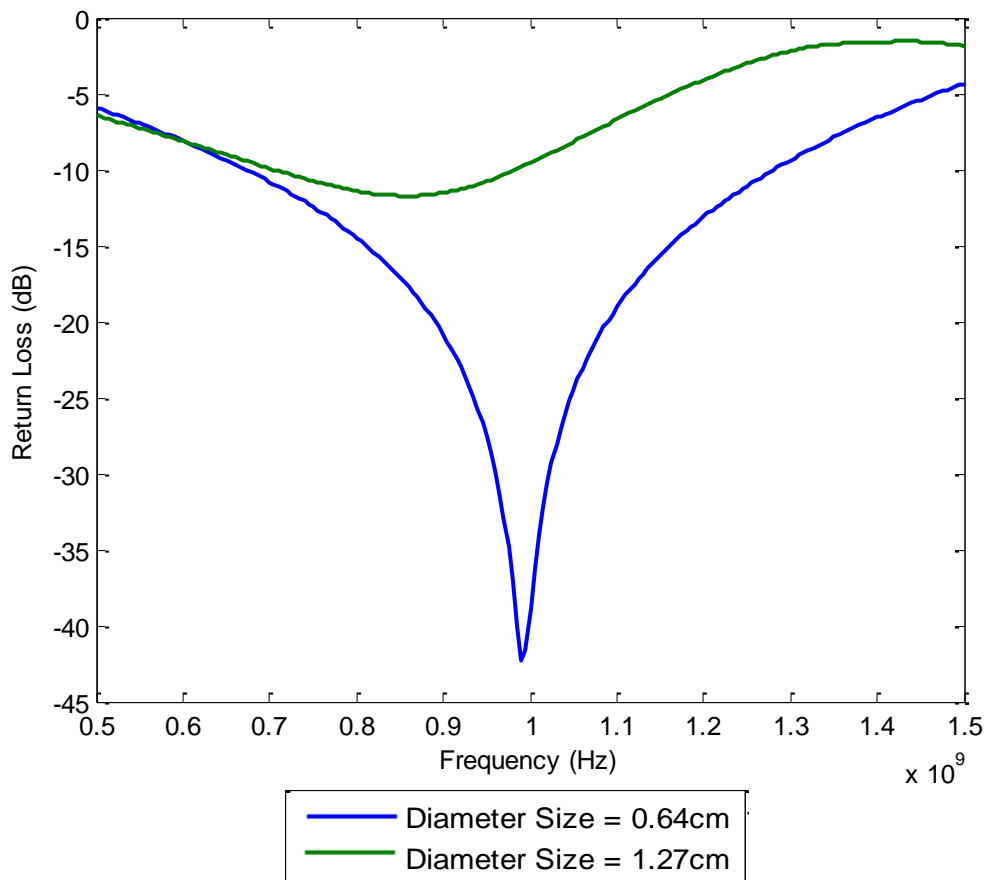


Figure 4.12 Simulated Return Loss Response for the Helix Antenna in Dry Sand Soilbed With a Helix Diameter of 0.64 cm.

4.3.2 Effect on the Helix's Number of Turns

The effect in the number of turns of the helix antenna response was limited by the physical limitations imposed by the testbed. The number of turns affects the return loss matching response as well as the helix diameter affect it. Figure 4.13 shows a decrease for the return loss operation bandwidth as the number of turns increase. Also the center operating frequency shifts to a higher value when the number of turns increases. The selected number of turns for the designed helix antenna was limited to 1 due to helix's length limitations established by the constructed testbed.

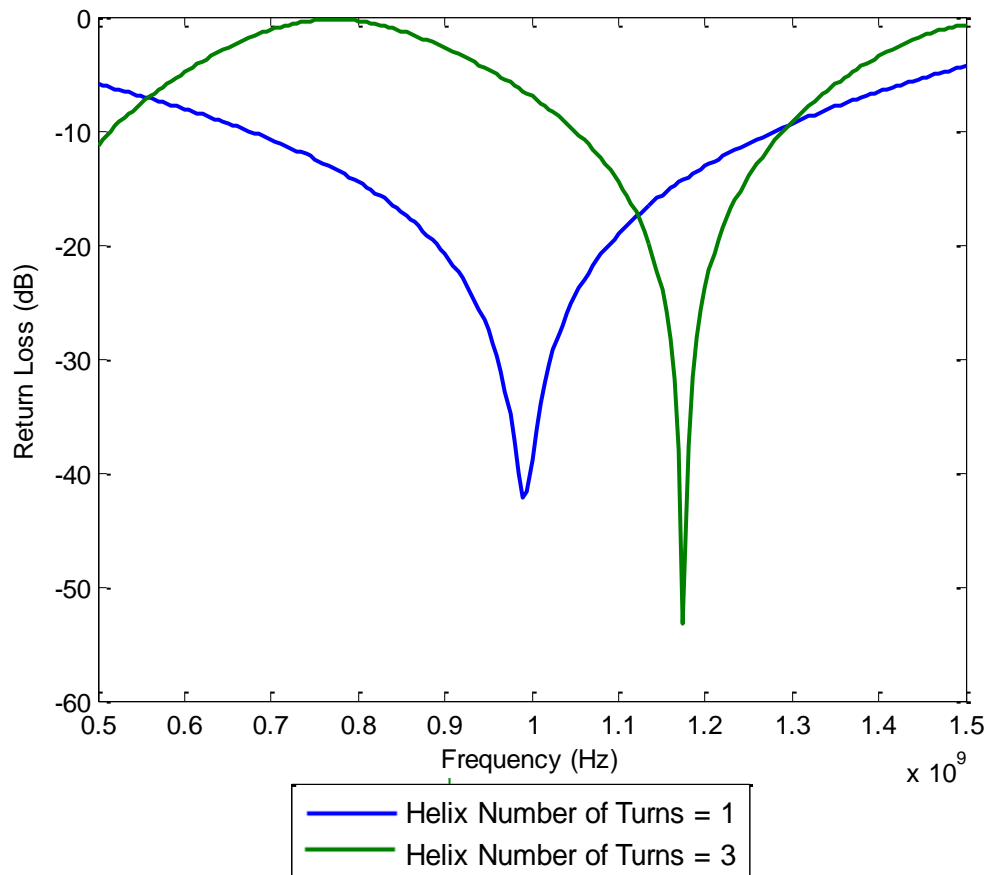


Figure 4.13 Simulated Return Loss Response for the Helix Antenna in Dry Sand Soilbed With a 1 Turn (Blue Trace) and 3 Turns (Green Trace).

4.3.3 Effect of Width Strip in the S-parameters Response

The size of the width strip and the separation between the strips are very significant for the helix antenna to obtain a good performance. For a thin strip and a separation larger than the width of the strip, a poor matching is obtained. However, if the width is wide enough compared to the separation between strips, then a good matching could be achieved. Simulated results for a width size of 0.8 cm and 1.4cm with a width separation of 1.2 cm are shown in Figure 4.14. The results show that as the width increases, the center operating frequency shifts to a lower value. The appropriate selected values of the width size and for the width separation for the designed antenna based on these results were 1.4 cm and 1.2 cm respectively.

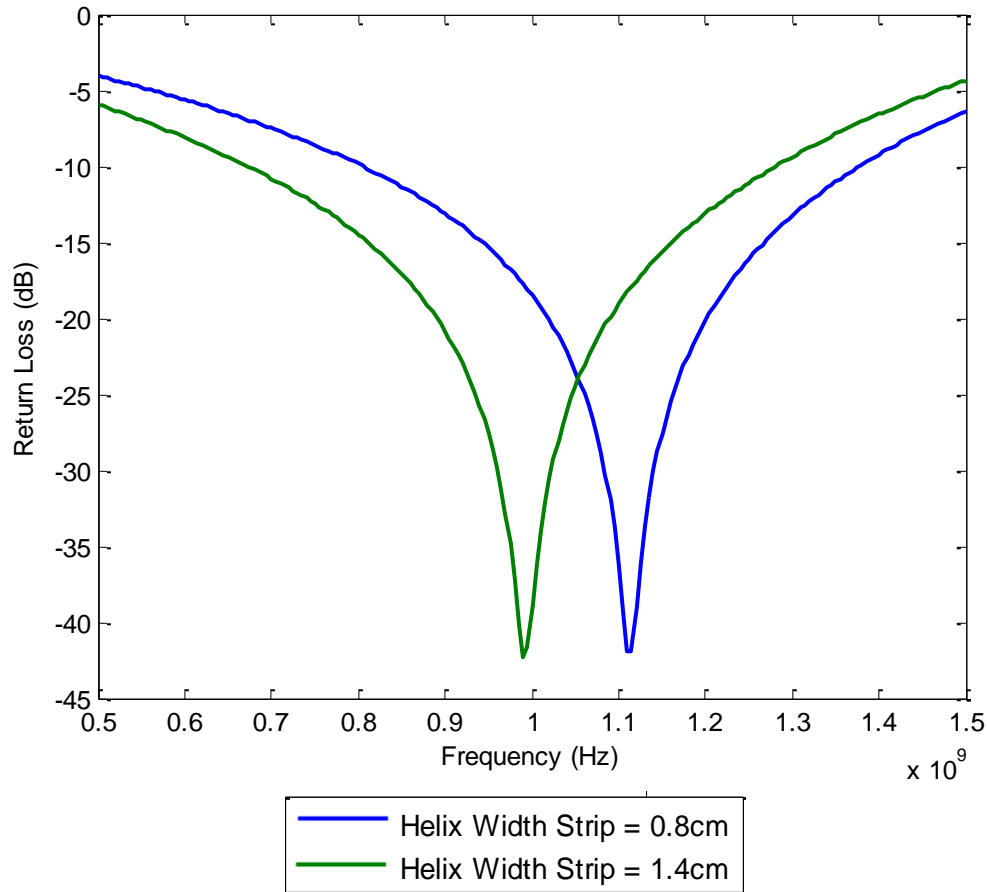


Figure 4.14 Simulated Return Loss Response for the Helix Antenna in Dry Sand Soilbed With a Width Strip of 0.8 cm (Blue Trace) and 1.4 cm (Green Trace).

4.3.4 S-parameters Response under Different Assigned EM Properties

Simulations for the designed helix antennas using the considered geometry parameters were performed under different assigned EM properties of the soilbed. The illustrated s-parameters results for dry sand soilbed, for saturated sand soilbed, and for distilled water showed significant differences (Figure 4.15). Since the helix antennas were surrounded by different mediums, the return loss response lacked a good matching this affect the performance of the antenna for s-parameters soilbed testing.

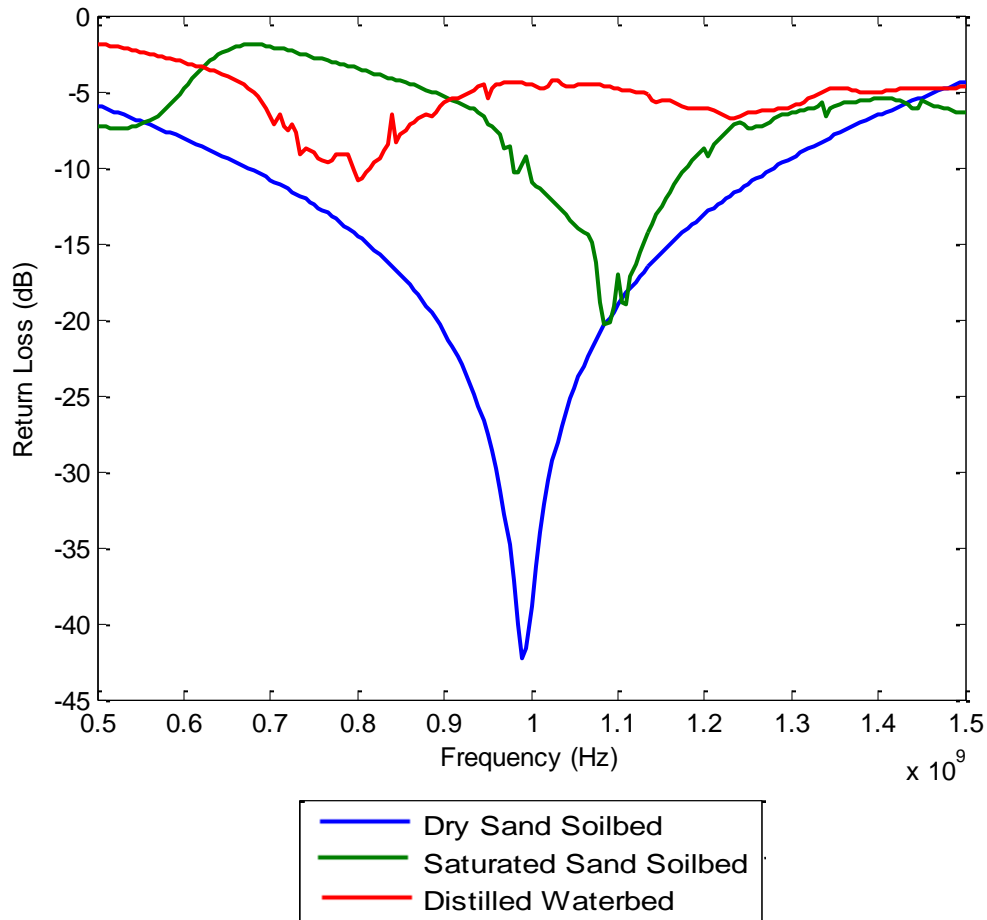


Figure 4.15 Simulated Return Loss Response for the Helix Antenna in Dry Sand Soilbed (Blue Trace), Saturated Sand Soilbed (Green Trace), and Distilled Waterbed (Red Trace).

4.3.5 Final Design of the Helix Antenna

The final geometry of the designed helix antenna is shown in table 4.10. Our objective was to achieve a good performance in the antenna for soilbed testing. The return loss response is affected on different assigned EM properties, and by the imposed physical limitations on the design, over the desired frequency range (500 MHz-1.5 GHz) the selected return loss on dry sand must be less than -6 dB. The simulated results for the selected dimensions on dry sand soilbed model showed at most -5.9 dB for 500 MHz and

1.5 GHz frequencies (Figure 4.16), and show a good performance of the antenna for dry sand conditions.

**Table 4.10 Final Geometry Dimensions of the Designed
Helix Antennas**

Geometry	Size
Length	4 cm
Diameter	0.64 cm
Width Strip	1.4 cm
Separation between Strips	1.2 cm
Number of Turns	1

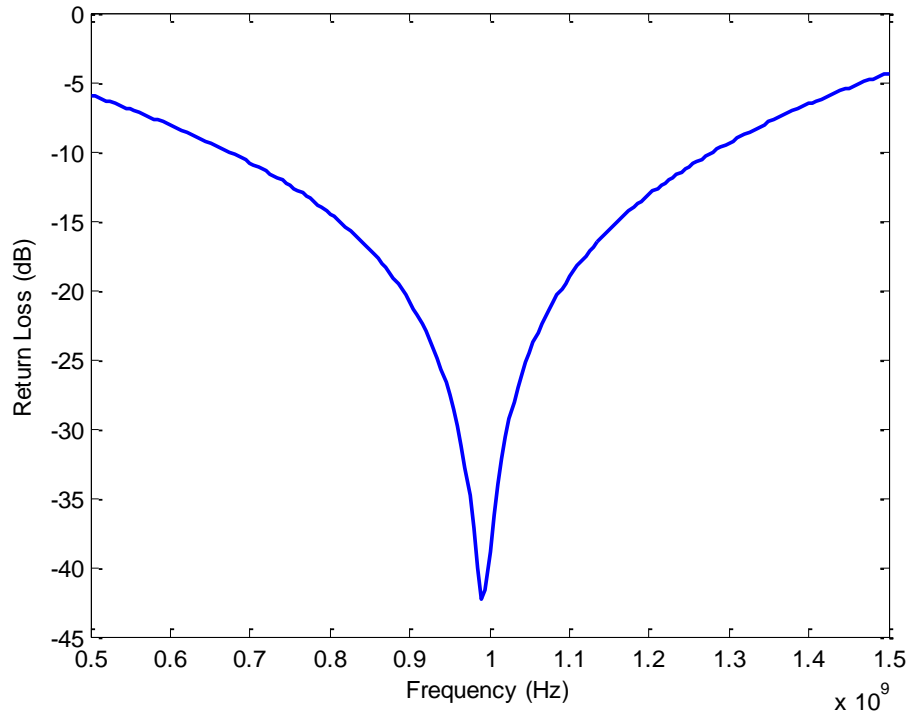


Figure 4.16 Simulated Return Loss for the Designed Helix Antenna in Dry Sand Soilbed.

4.4 Preliminary S-parameters Measurements of Dry Sand Soilbed Using Helix Antennas

4.4.1 Helix Antenna Measurements

Preliminary s-parameters measurements on dry sand soilbed were performed using the designed helix antennas. Comparison of s-parameters measurements with the simulated response (Figures 4.17 and 4.18) show too much discrepancy. The return loss (S_{11}) of the measurements show a poor impedance matching compare to the simulation result which has good matching over the entire frequency range (500 MHz- 1.5 GHz). On the other hand, the insertion loss (S_{21}) shows better response for experimental measurements. Simulation results were very low energy arriving at the receiving antenna. For both, measurements and simulation the values were not compatible. One factor that could affect the response is the presence of a protective well casing pipe (Figure 4.19) in

the boreholes of the testbed where the antenna is placed. In the simulation, this small pipe is not present and it could cause some effect on the antenna response.

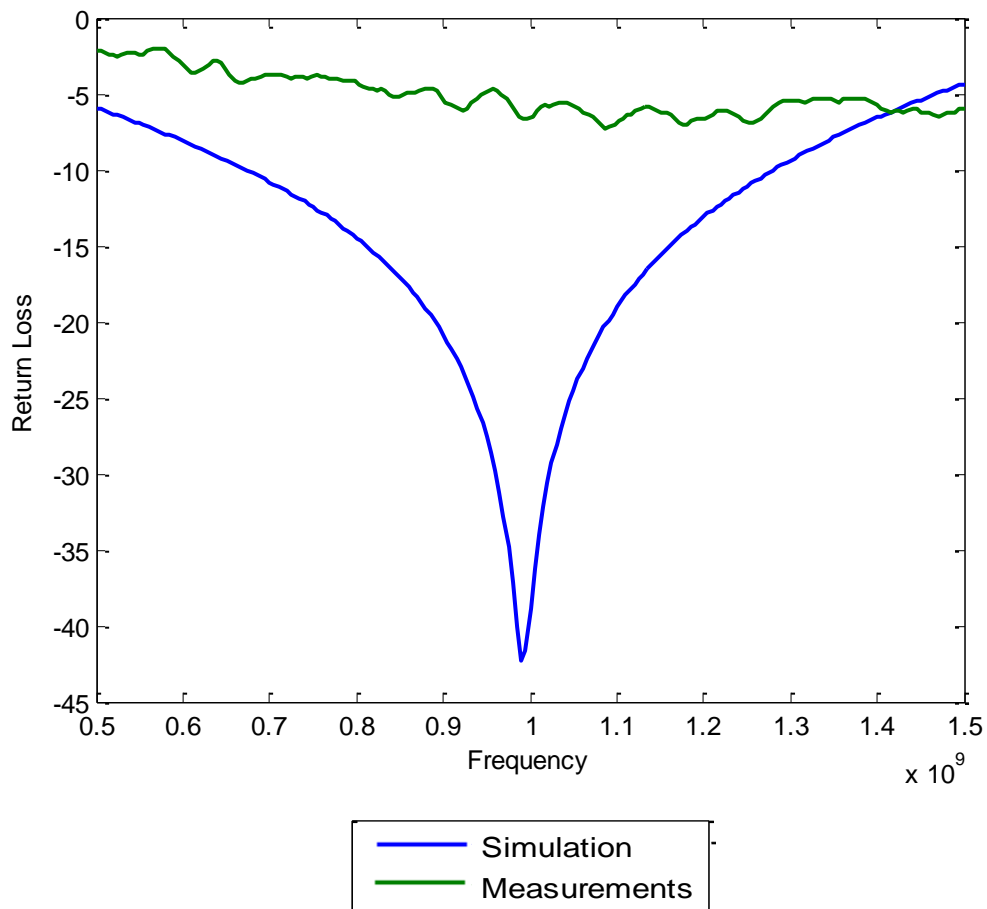


Figure 4.17 Simulated and Measured Return Loss Response of Dry Sand Soilbed.

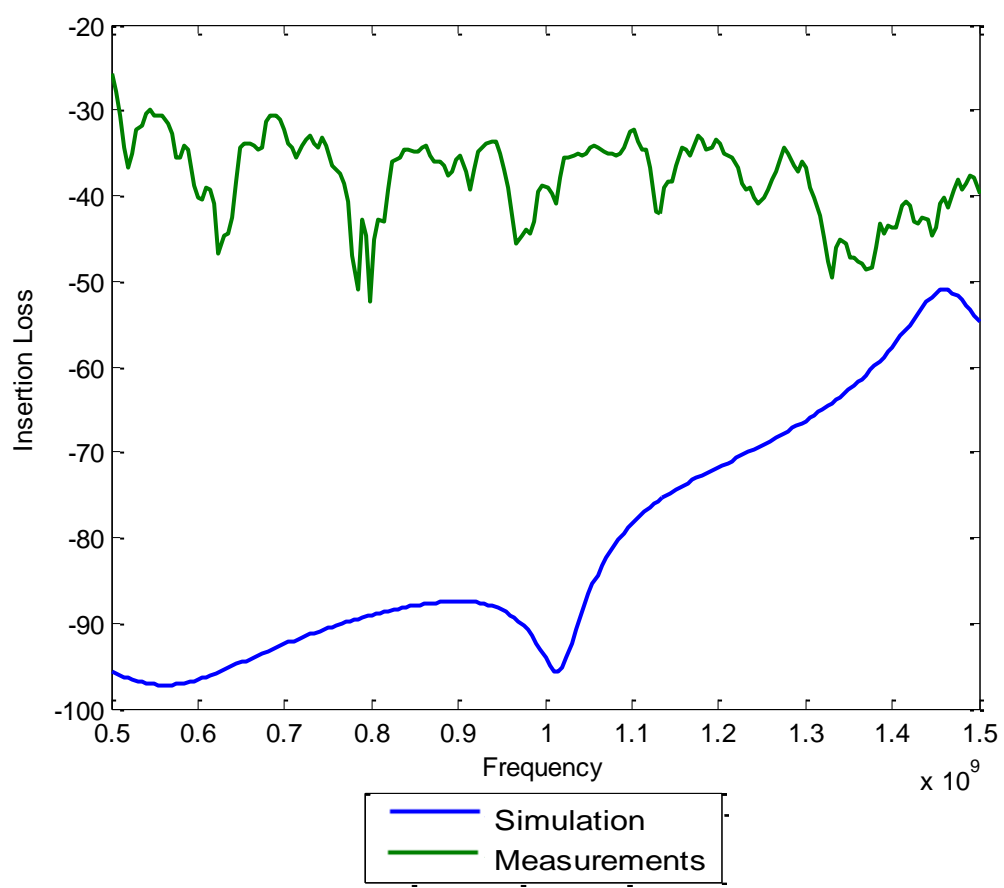


Figure 4.18 Simulated and Measured Insertion Loss Response of Dry Sand Soilbed.



Figure 4.19 Protective Well-Casing Pipe With the Constructed Helix Antenna Used in the S-parameters Measurements.

Simulations of dry sand soilbed including the protective well-casing pipe (Figure 4.20) were performed and it demonstrates that the protective casing affects the return loss of the s-parameters measurements. A similarity is appreciated in a compared plot between the simulated results and the measured response of dry sandy soilbed (Figure 4.21). The similarity of these results is because the helix antenna is surrounded in an air medium (protective well casing pipe), which leads to conclude that the antenna could be designed considering an air medium soilbed model because it is independent on the assigned EM properties of the soilbed. Figure 4.21 shows a discrepancy between frequencies 1.2 GHz and 1.5 GHz. This discrepancy is caused between the helix antenna build in the simulated model and the fabricated helix antenna. The designed antenna was build perfectly uniform in the simulated model, which had no imperfections. On the other hand, the fabricated antenna has imperfections even though it was constructed as most identical as possible to the designed antenna. These imperfections might cause the difference of both responses. The comparison between simulated with the measured insertion loss showed in figure 4.22 remains unchanged by including the well-casing pipe. This result means that the insertion loss is unaffected by including the well-casing pipe and the disagreement is due to boundary effects present in the soilbed.

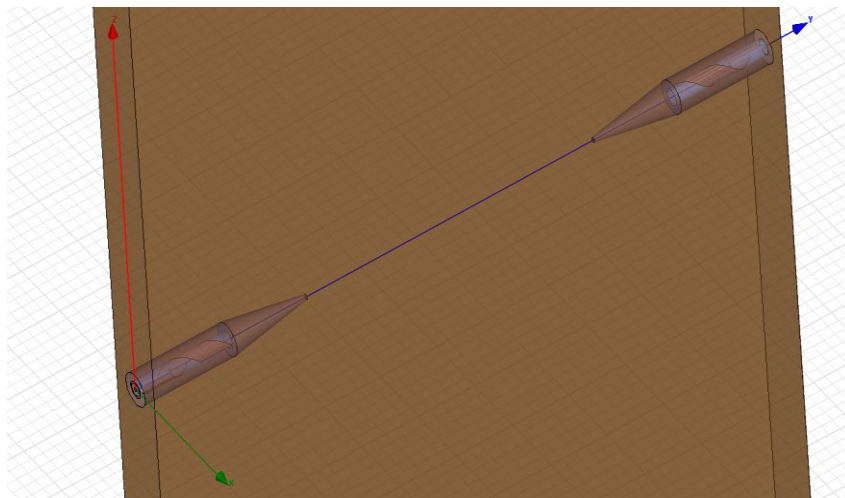


Figure 4.20 Simulated Model Diagram of the Helix Antennas Placed Inside the Protective Well-Casing Pipe.

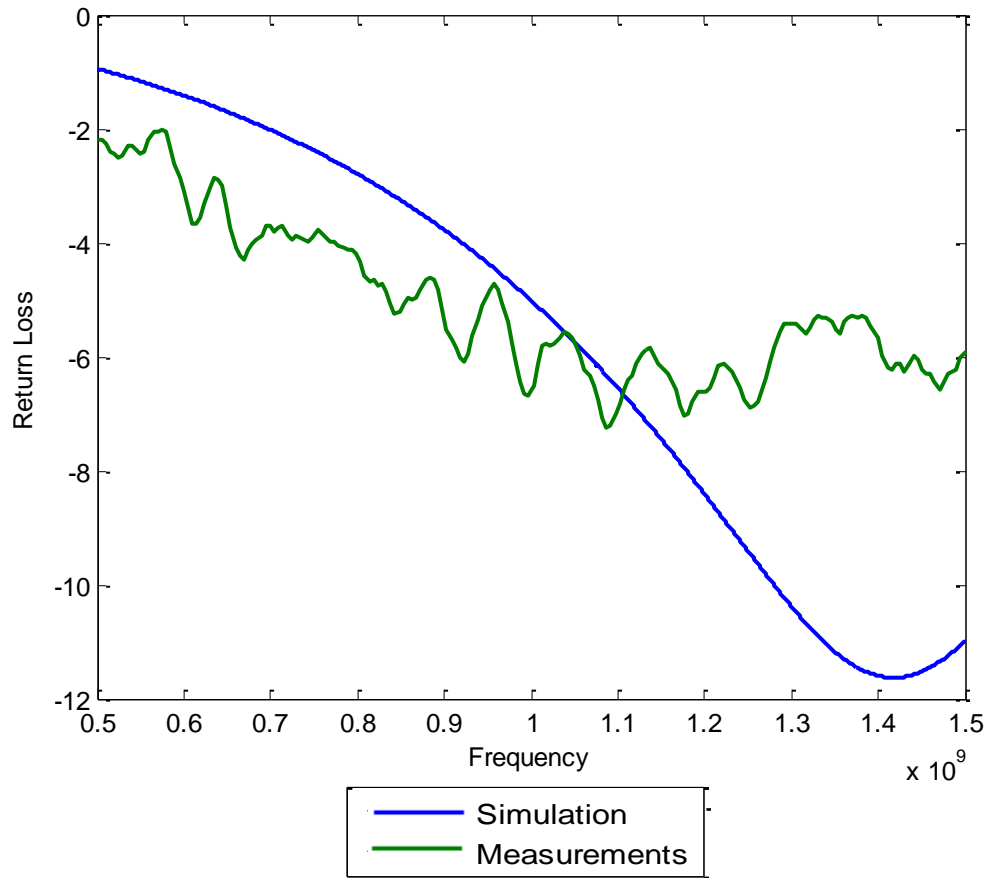


Figure 4.21 Simulated and Measured Return Loss Response of Dry Sand Soilbed Including a Protective Well-Casing Pipe.

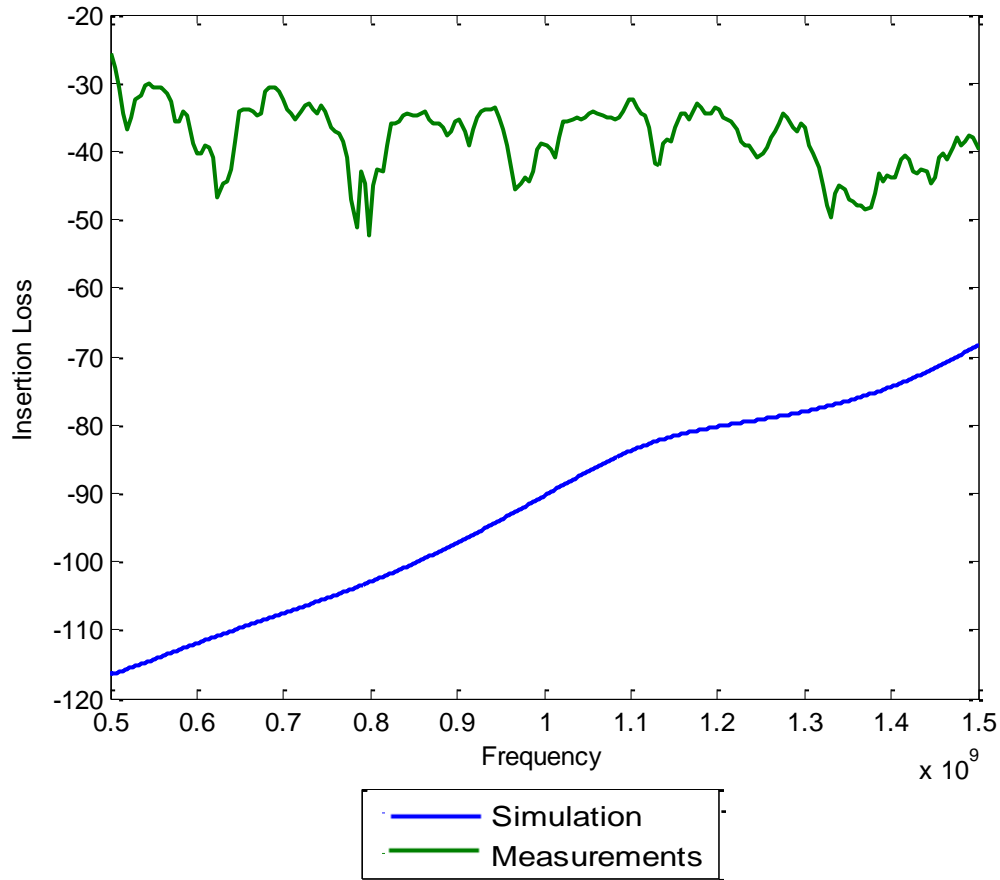


Figure 4.22 Simulated and Measured Insertion Loss Response of Dry Sand Soilbed Including a Protective Well-Casing Pipe.

4.4.2 Estimates of the Relative Permittivity of Helix Antenna

Measurements

Estimates of the relative permittivity for the s-parameters measurements using the fabricated helix antennas were performed. The estimates were performed using the expanded phase option provided by the network analyzer and equation 3.7. The expanded phase is the unwrapped phase angle of the transmission response which accounts the phase ambiguity when a 360 degrees phase shift occurs.

Estimates of the relative permittivity were performed also using the gating option. Gating is a time domain option provided by the network analyzer that eliminates

undesired reflections resulting from different sources, such as boundary effect from the tanks, and any multi-reflection paths affecting the s-parameters measurements. These reflections are eliminated by selecting a time window, and taking the s-parameters measurements over the selected window to represent only the desired portion of time for the analysis.

4.4.2.1 Estimates Using the Expanded Phase Component

Estimates of the relative permittivity from the s-parameters measurements of dry sand soilbed using the helix antennas were performed. Figure 4.23 illustrates the plots for the insertion loss, the expanded phase component of the transmission response, and the estimated values of the relative permittivity over the measured frequency range (500 MHz- 1.5 GHz). The resulted estimates demonstrate reasonable values (between 2 and 4) from 500 MHz to almost 800 MHz. However, approximately from the 800 MHz mark up to 1.5 GHz the estimated values of the relative permittivity were increasing significantly resulting in overestimates (greater than 4). This overestimation is due to the increase expanded phase value at approximately the 800 MHz frequency mark. It can be observed in the expanded phase plot a bump at almost 800 MHz mark and suddenly declines afterwards. The expanded phase trace looks after approximately the 800 MHz mark lower compared to the 500 MHz to almost 800 MHz range. Unwanted reflections or boundary effects may affect the transmission response leading to this overestimation. These unwanted effects in the measurements may be removed using the gating option from the network analyzer and then perform new estimates of the relative permittivity.

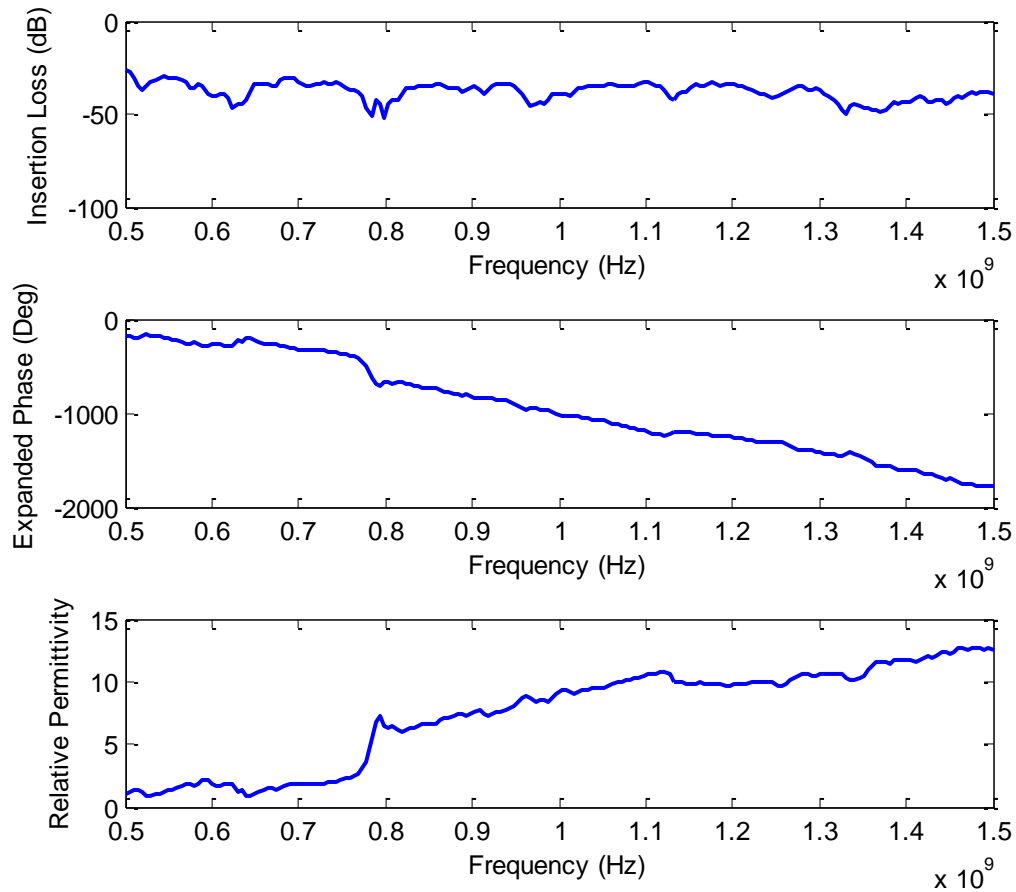


Figure 4.23 Insertion Loss Response (Top), Expanded Phase Component (Middle) and Estimate of the Relative Permittivity (Bottom) for Dry Sand Soilbd with the Helix Antennas Placed at Middle Borehole Location.

4.4.2.2 Estimates Using the Expanded Phase Component with Gating Option

S-parameters measurements of an air medium testbed were taken using the helix antennas and applying the gating option. By applying the gating option, undesired effects that affect the entire response of the system can be eliminated by selecting a time window to avoid inaccuracies in the estimates of the relative permittivity. A time window of 2.5 ns was selected to cover at least twice the time it takes the EM wave to travel at the speed of light through a 19 cm of air medium soilbed. Since the EM properties for the air

medium are well-known, these measurements work as background to see differences in the response as the EM wave propagates through the air medium soilbed. The expanded phase component responses are illustrated in Figures 4.24 to 4.28 with the helix antennas located at different borehole heights. Both the transmitter and receiver antennas were placed at the same height, they were straight pointing one directly to the other.

The estimated relative permittivity values for an air medium testbed at each borehole location were greater than unity, however they were overestimated (greater than 2) in many cases. Although the estimated values are greater than unity, reasonable estimates were for the antennas located at middle borehole location (Figure 4.24) and below middle borehole location (Figure 4.25). The highest estimated values remain with the antennas placed at top, above middle and bottom borehole locations (Figures 4.26-4.28). The top and bottom locations have a very close proximity to the end of the parallel plate waveguide. This boundary proximity may affect the s-parameter measurements leading to inaccuracies of the relative permittivity.

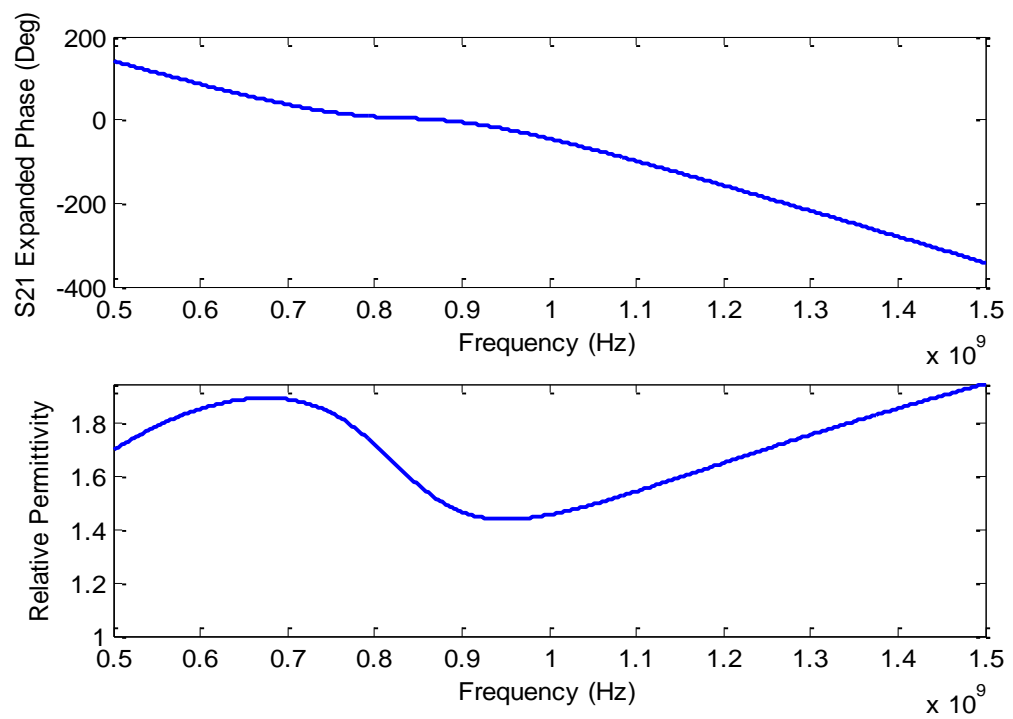


Figure 4.24 Expanded Phase Component (Top) and Estimate of the Relative Permittivity (Bottom) for an Air Medium Testbed Using Gating Option and Antennas Placed at Middle Borehole Location.

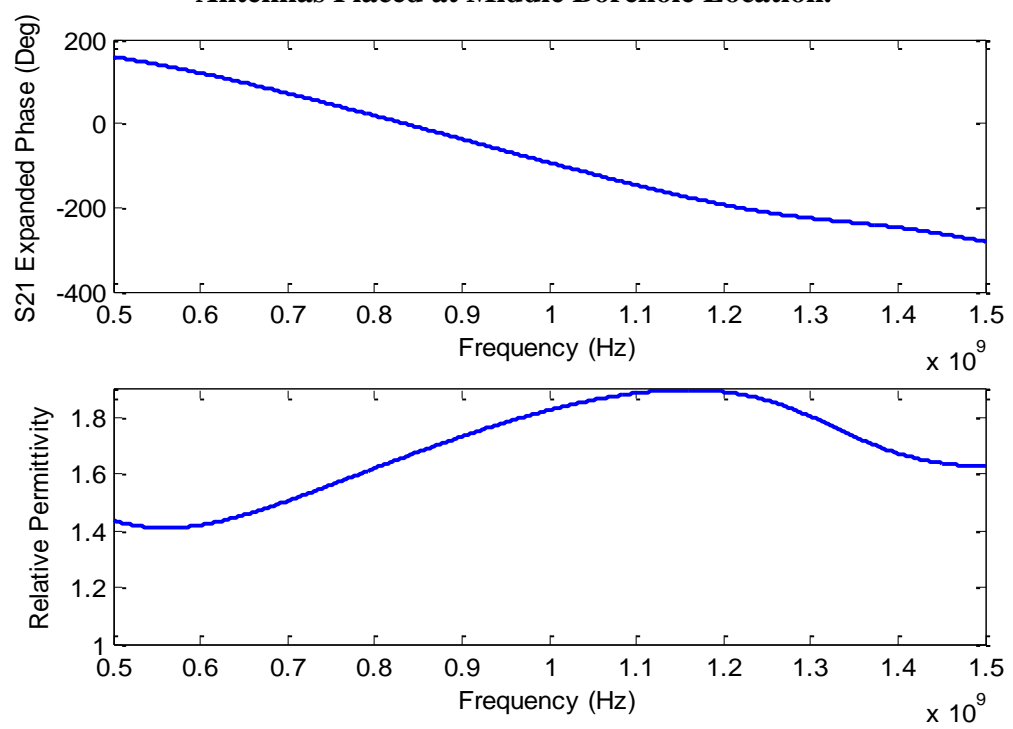


Figure 4.25 Expanded Phase Component (Top) and Estimate of the Relative Permittivity (Bottom) for an Air Medium Testbed Using Gating Option and Antennas Placed Below Middle Borehole Location.

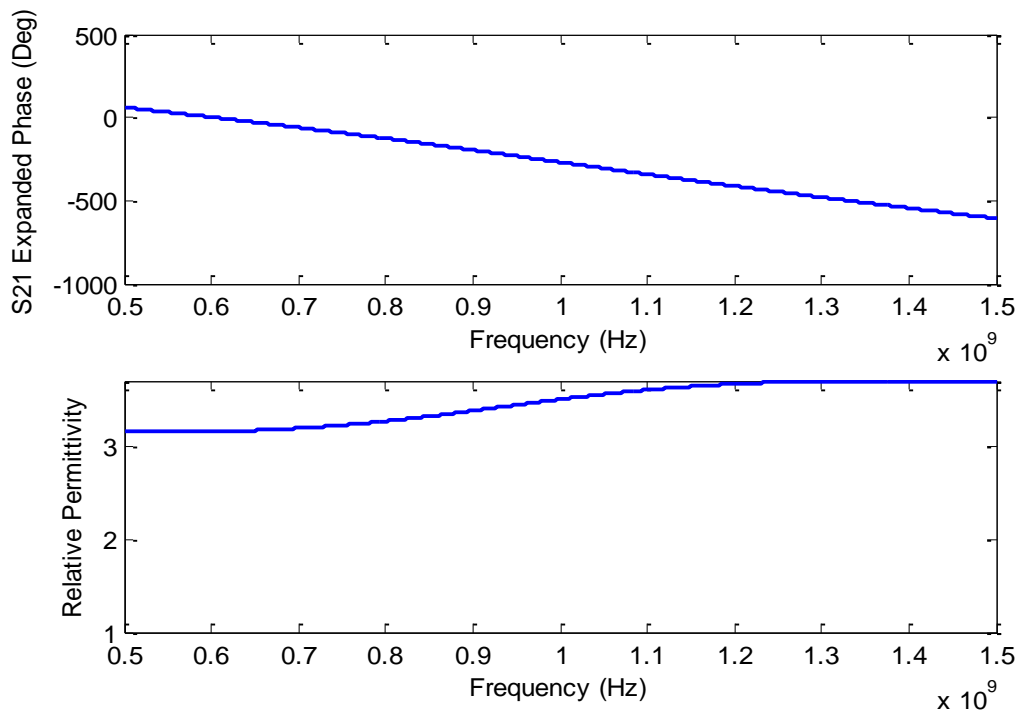


Figure 4.26 Expanded Phase Component (Top) and Estimate of the Relative Permittivity (Bottom) for an Air Medium Testbed Using Gating Option and Antennas Placed at Top Borehole Location.

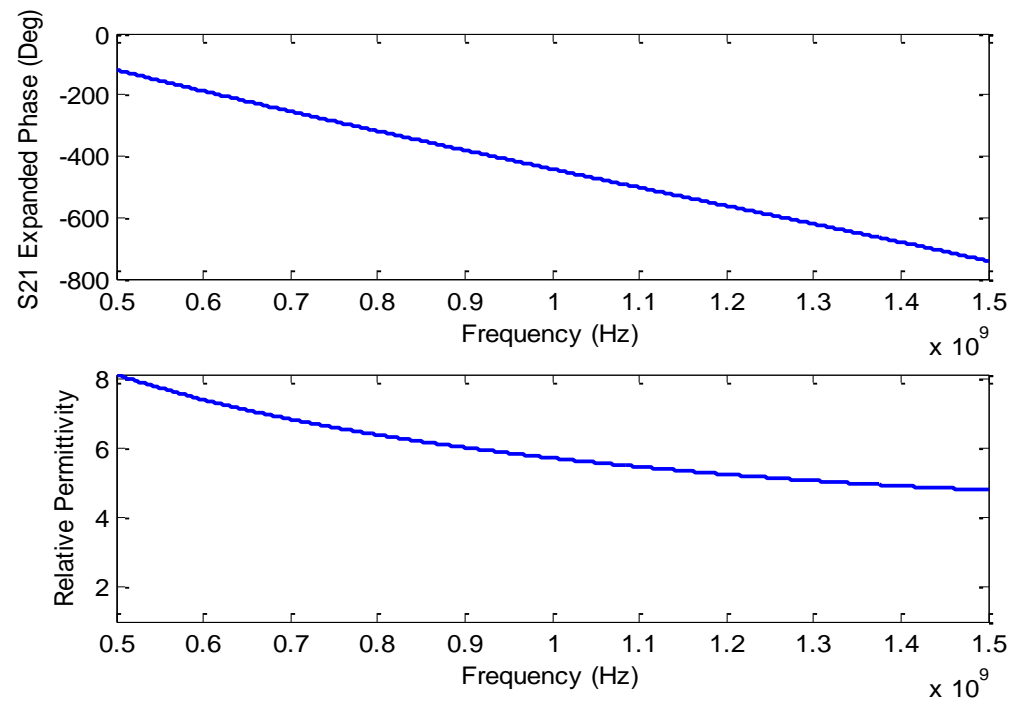


Figure 4.27 Expanded Phase Component (Top) and Estimate of the Relative Permittivity (Bottom) for an Air Medium Testbed Using Gating Option and Antennas Placed Above Middle Borehole Location.

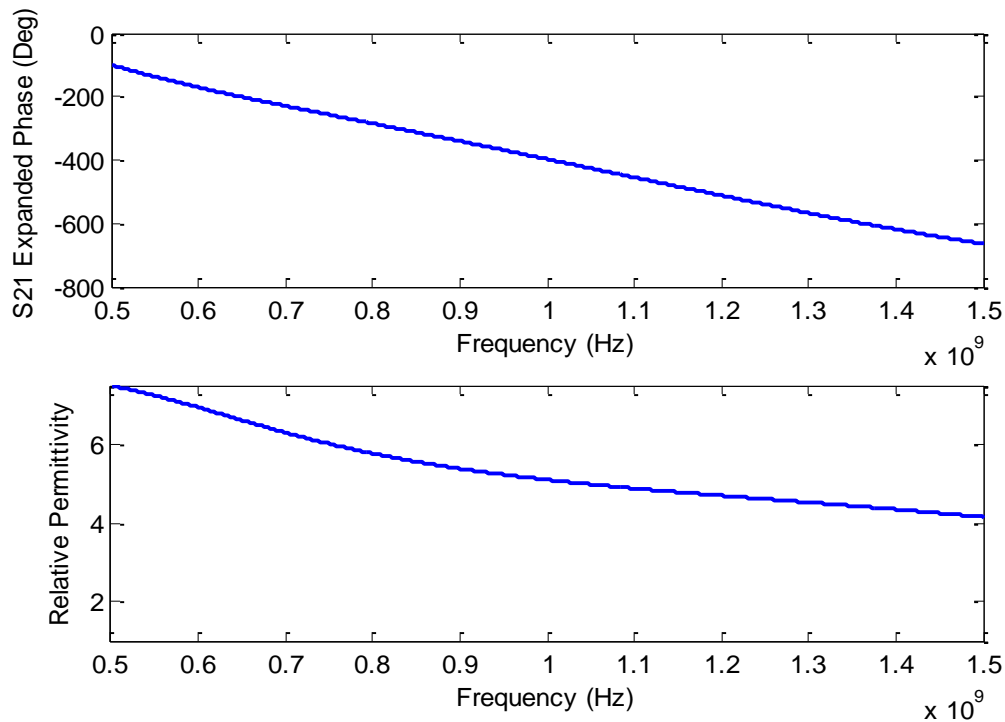


Figure 4.28 Expanded Phase Component (Top) and Estimate of the Relative Permittivity (Bottom) for an Air Medium Testbed Using Gating Option and Antennas Placed at Bottom Borehole Location.

4.5 Time Domain Experiments

Time domain measurement provides a suitable analysis of the EM wave propagation over a time period. Time domain measurements were taken in an air medium for a period of 10 ns with the helix antennas placed at top, middle, and bottom positions. Time domain measurements indicate significant differences between the times of arrival of the propagating wave at different borehole locations of the testbed. The first peak of the reflected response represents the antenna's response. The first peak of the transmission response represents the straight path of the EM wave. For an air medium, the time of arrival is assumed to be the same for all paths at equal distance. Accurate time for the first peak of the reflected response of the EM wave of air medium were obtained (Figure 4.29) at different borehole locations. Accurate times of arrival were obtained for

the antennas located in the middle borehole of the testbed, but inaccurate time was found for the antennas located at the top and bottom boreholes (Figure 4.30). These results suggest that there are boundary effects that affect the measured response. To assess the potential effects of boundary conditions, metal plates were placed over the top of the testbed, and horizontally beyond the extent of the tank.

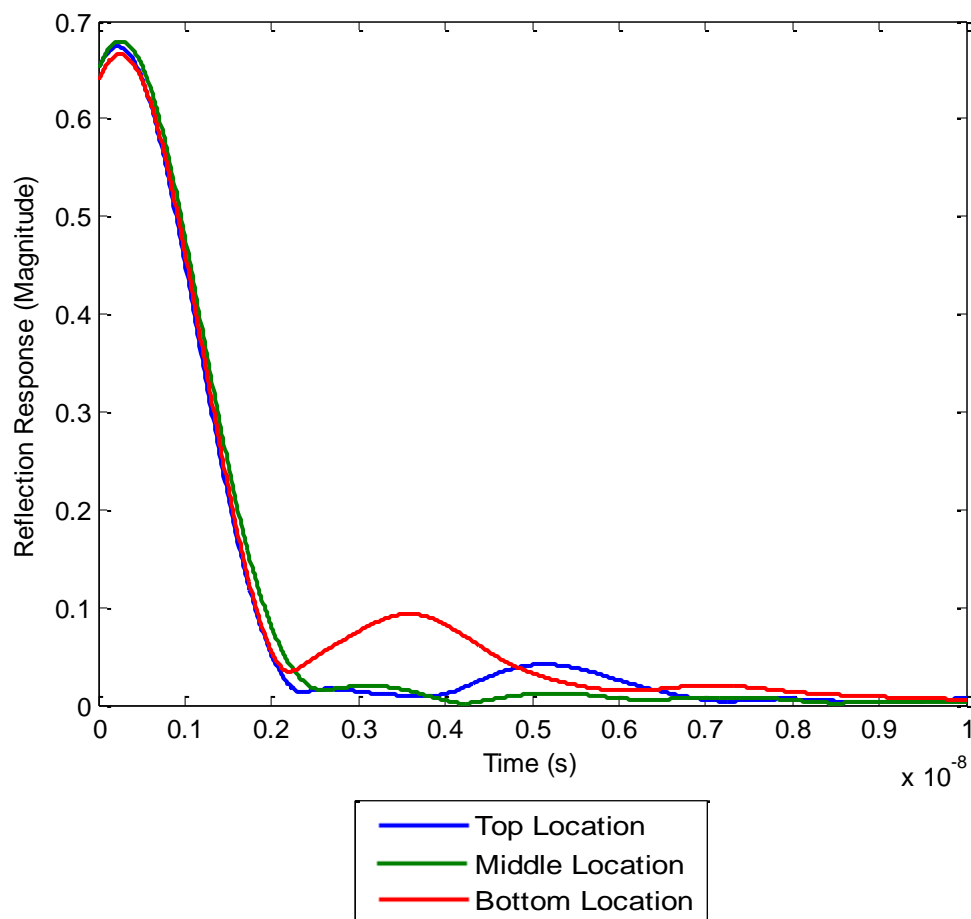


Figure 4.29 Measured Reflected Response of an Air Medium Testbed. Helix Antennas Located at Top (Blue Trace), Middle (Green Trace), and Bottom (Red Trace) Borehole Location.

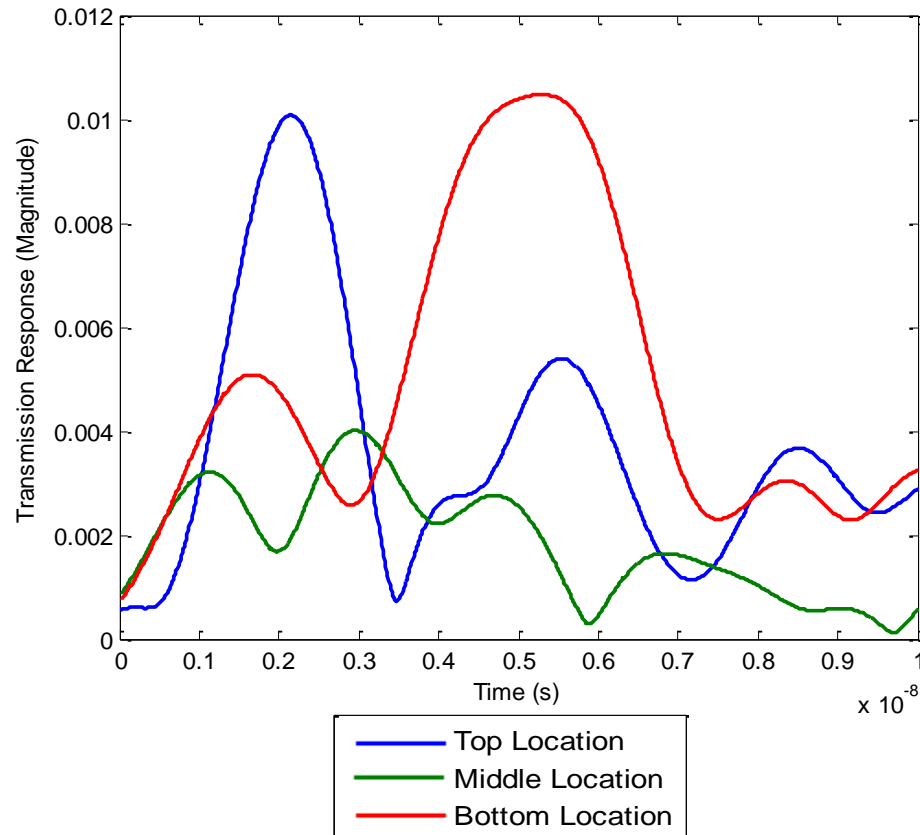


Figure 4.30 Measured Transmitted Response of an Air Medium Testbed. Helix Antennas Located at Top (Blue Trace), Middle (Green Trace), and Bottom (Red Trace) Borehole Location.

Placing a metal plate on top (Figure 3.16) of the testbed suggest that energy is leaving at the top of the testbed when open to the atmosphere. As a consequence, when a plate is place on top and energy cannot leave, and it is concentrated, yielding a higher transmission response (Figures 4.31 and 4.32).

Extended vertical plates placed at both faces of the extent of the tank (Figure 3.17) showed very similar response to the original measured transmission response (with no vertical plate) with slightly difference for a delay time in the first peak (Figure 4.33).

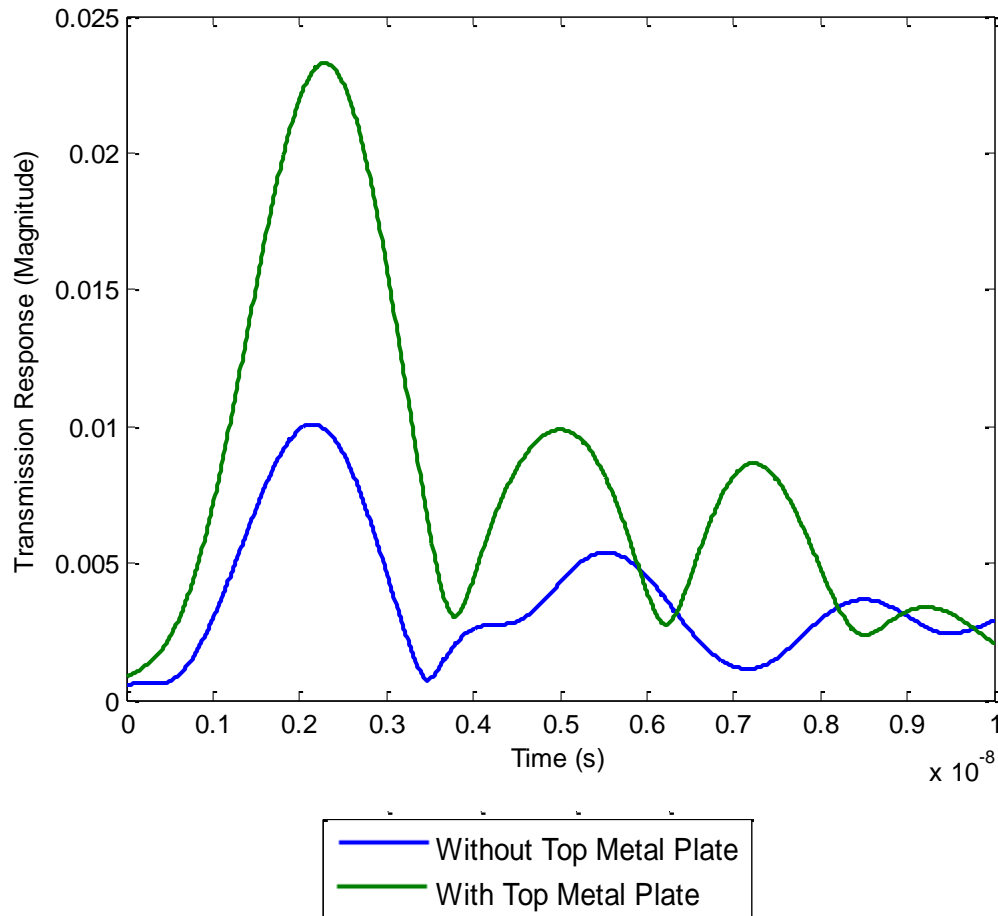


Figure 4.31 Measured Transmission Response of Air Medium Testbed. Helix Antennas Located at Top (Blue Trace) and at Top With Metal Plate Placed on Top (Green Trace) Borehole Locations of the Testbed.

The horizontally extended metal plates placed at the extent of the tank (Figure 3.18) demonstrate excess of energy inside the soilbed tank since the transmission response (Figure 4.34) is much higher in the presence of the horizontal extended plates. This suggests that energy is escaping the tank horizontally when no horizontal plates are placed. These results suggest that a simulation of the soilbed model with and without the horizontal extended metal plates is necessary and a comparison of the simulated results to assess changes of the transmission response. This simulation will lead to possible

potential effects affecting the measurements and consequently the estimates of the relative permittivity of the bulk soil.

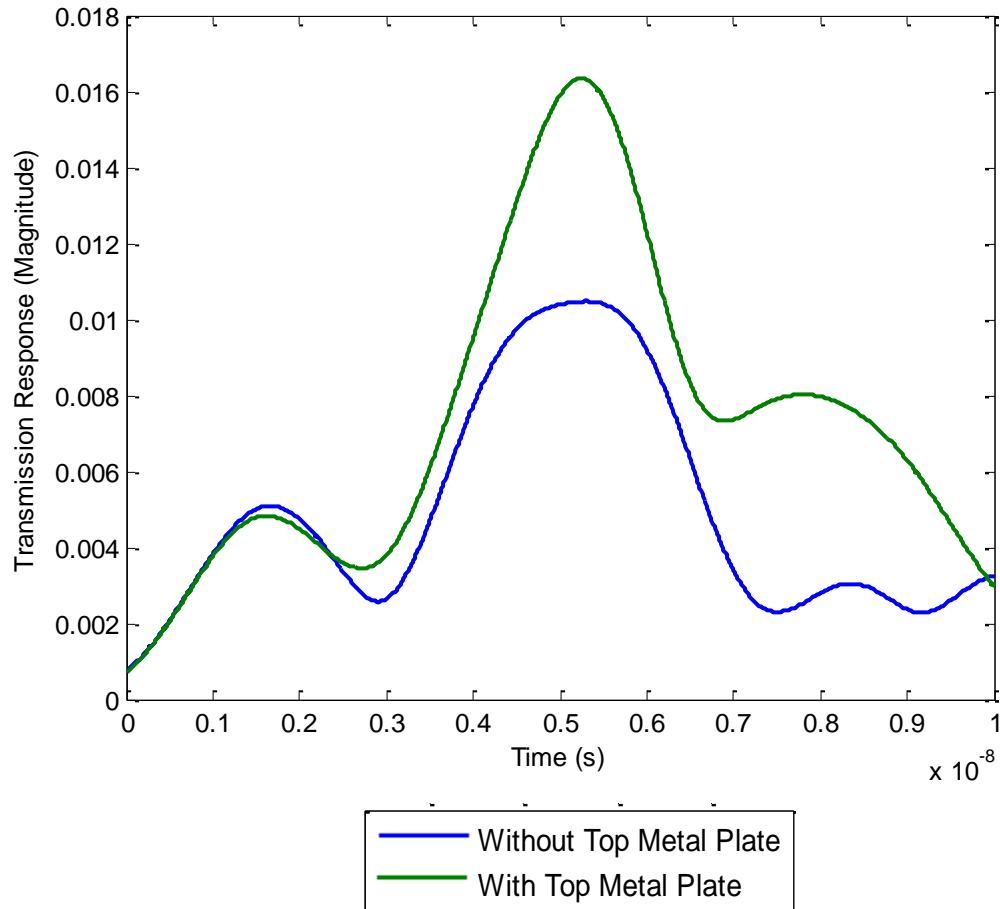


Figure 4.32 Measured Transmission Response of Air Medium Testbed. Helix Antennas Located at Bottom (Blue Trace) and at Bottom With Metal Plate Placed on Top (Green Trace) Borehole Location of the Testbed.

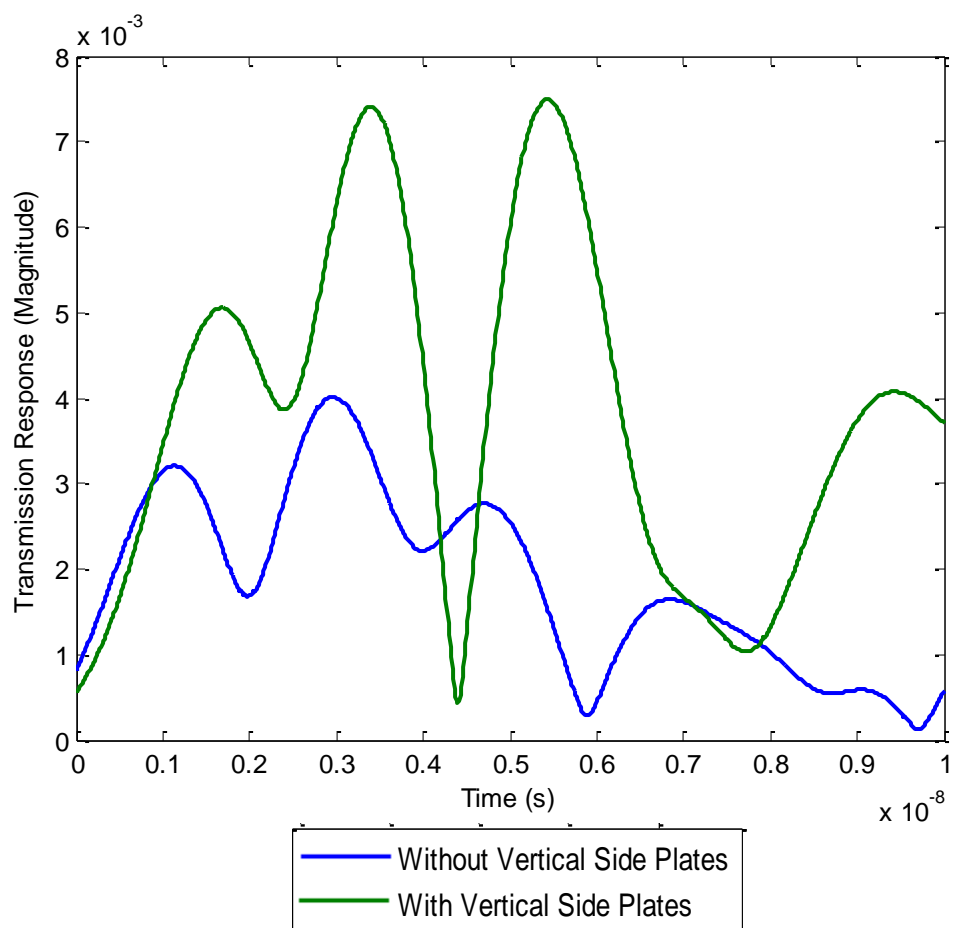


Figure 4.33 Measured Transmission Response of Air Medium Testbed. Helix Antennas Located at Middle (Blue Trace) and at Middle With Extended Vertical Metal Plates (Green Trace).

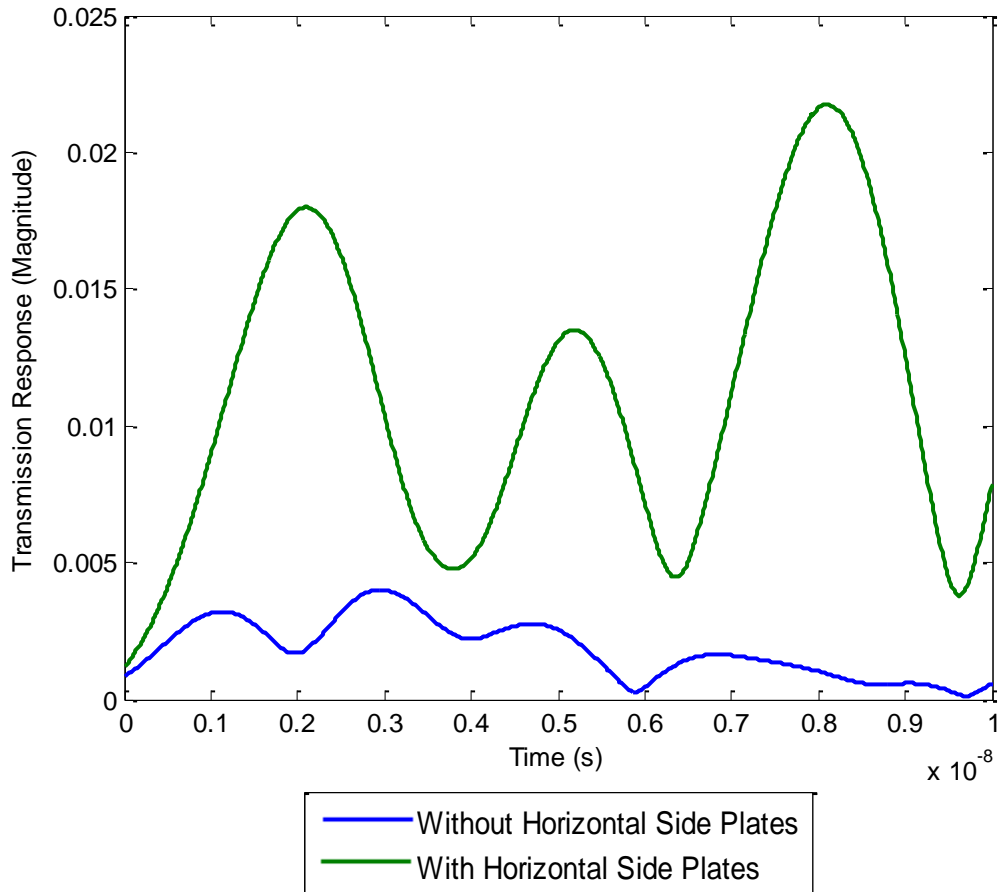


Figure 4.34 Measured Transmission Response of Air Medium Testbed. Helix Antennas Located at Middle (Blue Trace) and at Middle With Extended Horizontal Metal Plates (Green Trace) Borehole Location.

4.6 Frequency Modeling of the Extended Testbed

Simulations were performed for the air medium testbed model including the horizontal metal plates at the faces of the extent of the tank (Figure 4.35). The results show a good agreement in the transmission response compared with the measured response (Figure 4.36). The result suggests that energy was escaping from the tank near the plate discontinuities, causing the wave to propagate through the air along paths

outside the waveguide system. As a result, receiving antennas responded to wave propagation along the waveguide system paths in the tank and to waves propagating outside the waveguide system and re-entering across the top, bottom, and edges of the tank. This was confirmed by removing the horizontal plates and placing air radiation boundaries at the faces of the metal mesh plates (Figure 4.37). The energy entering the soilbed model was comparable with the previous experimental measurements of the sand soilbed (Figure 4.38). It was concluded that an alternative to decrease the excess of energy entering the testbed is by extending the metal mesh plates.

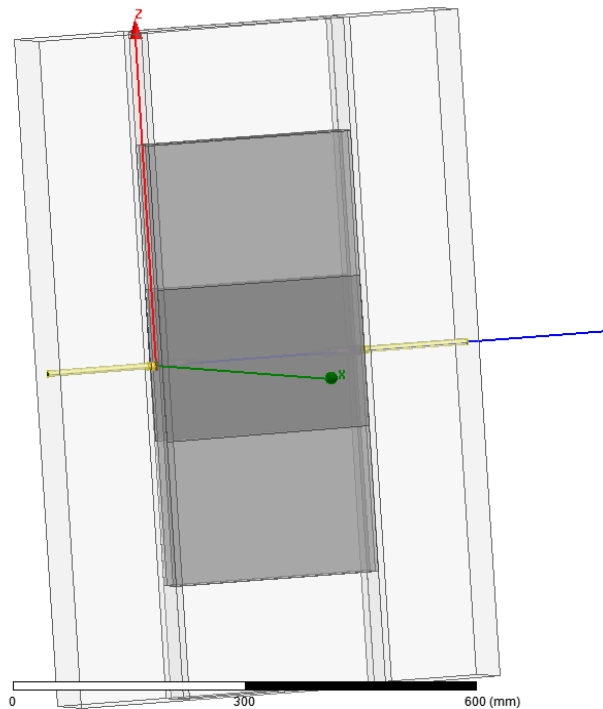


Figure 4.35 Simulated Model Diagram of Air Medium Testbed With the Horizontal Metal Plates Placed at the Faces of the Mesh Plates.

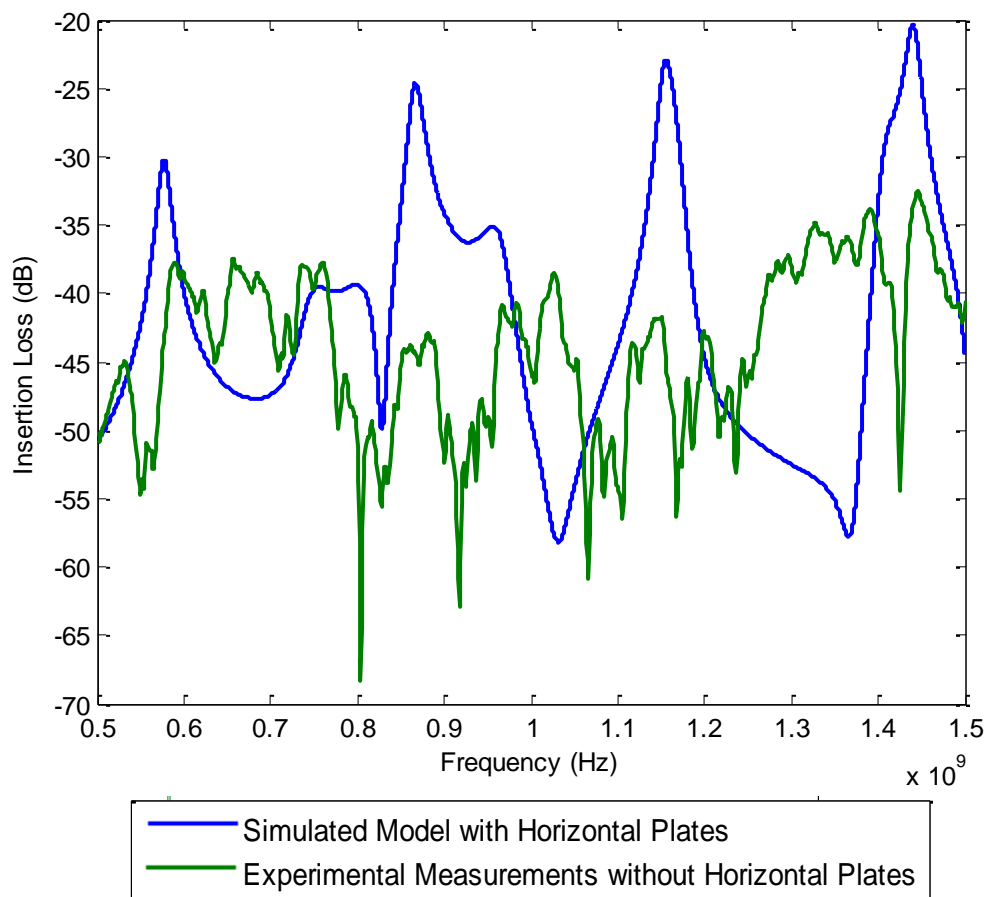


Figure 4.36 Measured (Green Trace) and Simulated (Blue Trace) Insertion Loss Response of an Air Medium.

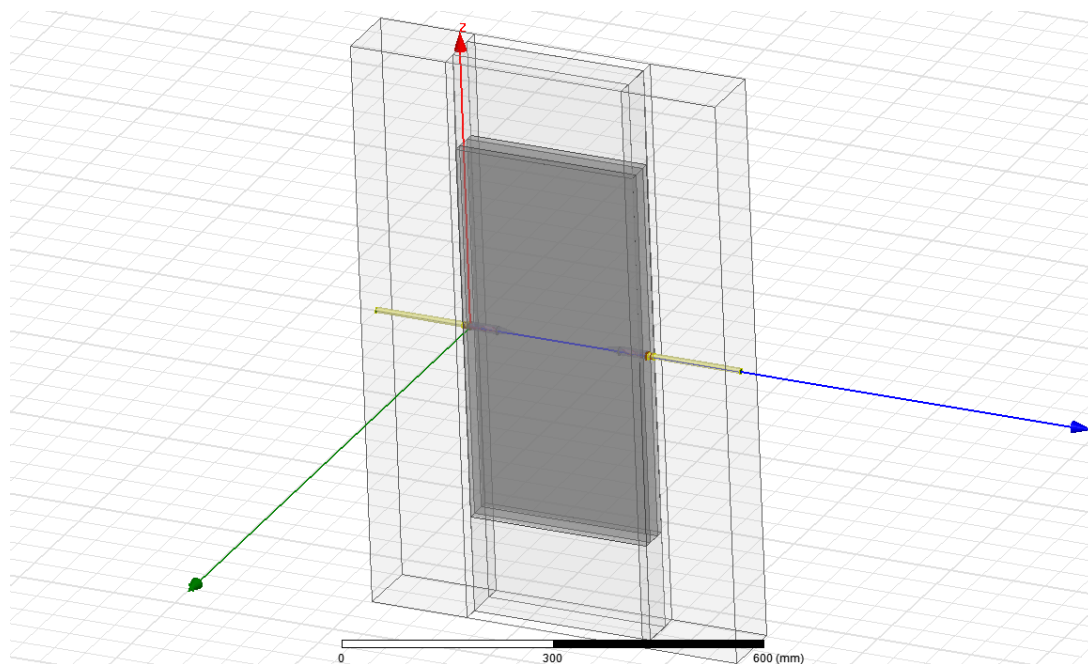


Figure 4.37 Simulated-Model Diagram of an Air Medium Testbed.

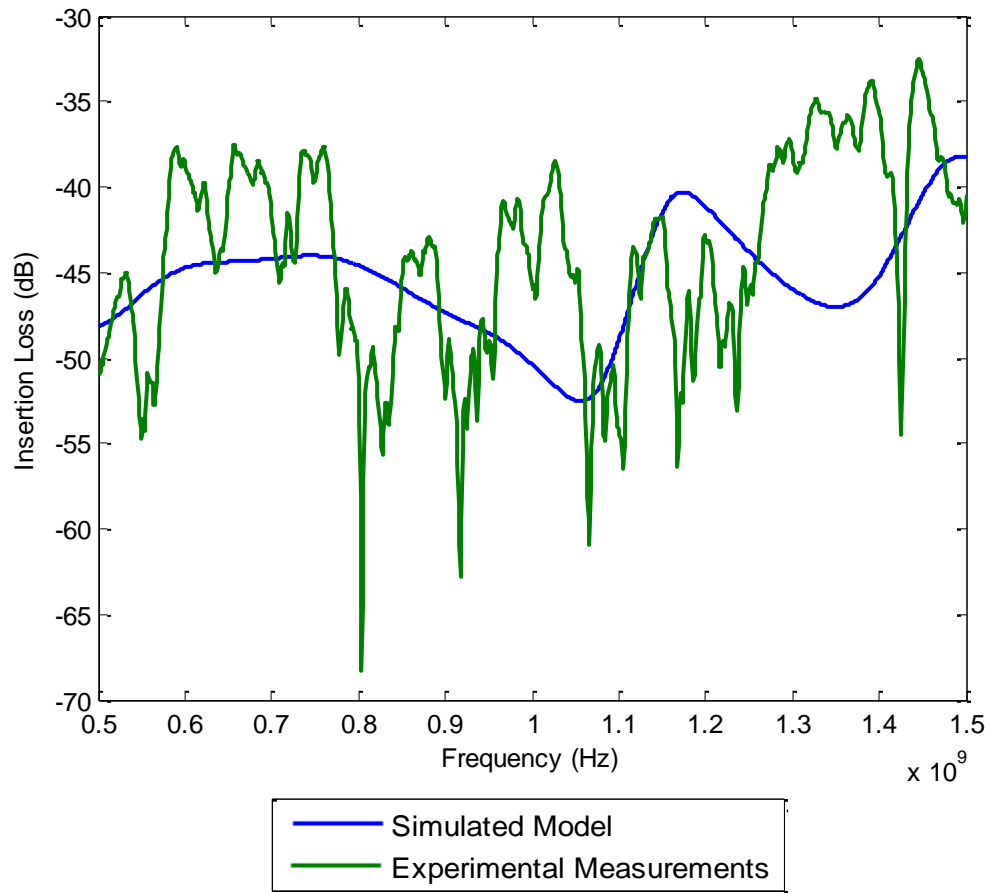


Figure 4.38 Measured (Green Trace) and Simulated (Blue Trace) Insertion Loss Response of an Air Medium.

The simulations were performed for an air medium testbed model to determine the transmission response as the mesh plates are extended horizontally. The testbed model (Figure 4.37) used for these simulations was the same model used for the performed simulations applying the horizontal metal plates to the testbed. For this case, the applied metal plates were removed and the mesh plates were extended horizontally. The height of the mesh plates was unchanged for these simulations. Simulations were performed for mesh plates with a length of 28 cm, 56 cm, 92 cm, 120 cm, and 148 cm. These selected lengths are multiples of the original size of the mesh plates (28 cm). The

simulated results demonstrate a decrease of the transmission response when the mesh plates were extended. As a result, less energy enters the testbed through the edge boundaries and less energy is present at the antennas when the mesh plates length increases, leading to accurate s-parameters response of the soilbed model (Figure 4.39). The reflection response was also affected as result of extending the mesh plates horizontally; causing multiple resonance frequencies in according to the dimensions of the mesh plates (Figure 4.40).

A comparison was performed between the mesh plates length of 120 cm and 148 cm results with a simulated model result of an ideal testbed model (Figure 4.41). This ideal testbed model (Figure 4.42) has the same dimensions of the constructed tank but has a different interpretation in the simulator which affects s-parameters results. In the simulator, this ideal testbed is without air radiation boundaries (no box) at the faces of the mesh plates compared to the simulated model used for the 120 cm and 148 cm lengths. Without these radiation boundaries, there is no energy escaping or entering from the edge boundaries of the tank and it is considered perfect radiation of EM energy inside the tank generated only by the helix antennas and the nature of the studied soilbed. It was determined that extending the testbed to 120 cm, would result in more accurate and appropriate s-parameters measurements to estimate the EM properties.

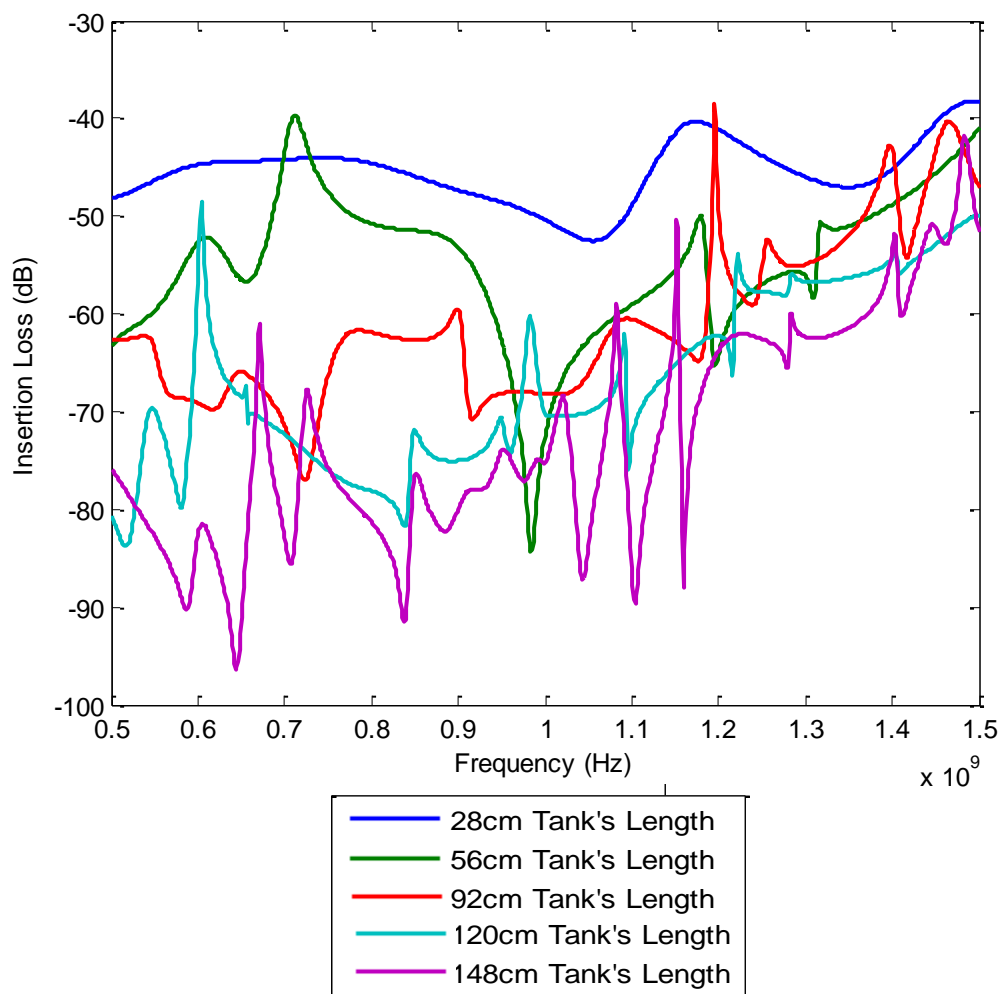


Figure 4.39 Simulated Insertion Loss of Extending the Mesh Plates Length for an Air Medium Testbed. The Mesh Length's are; 28 cm (Blue Trace), 56 cm (Green Trace), 92 cm (Red Trace), 120 cm (Cyan Trace), and 148 cm (Magenta Trace).

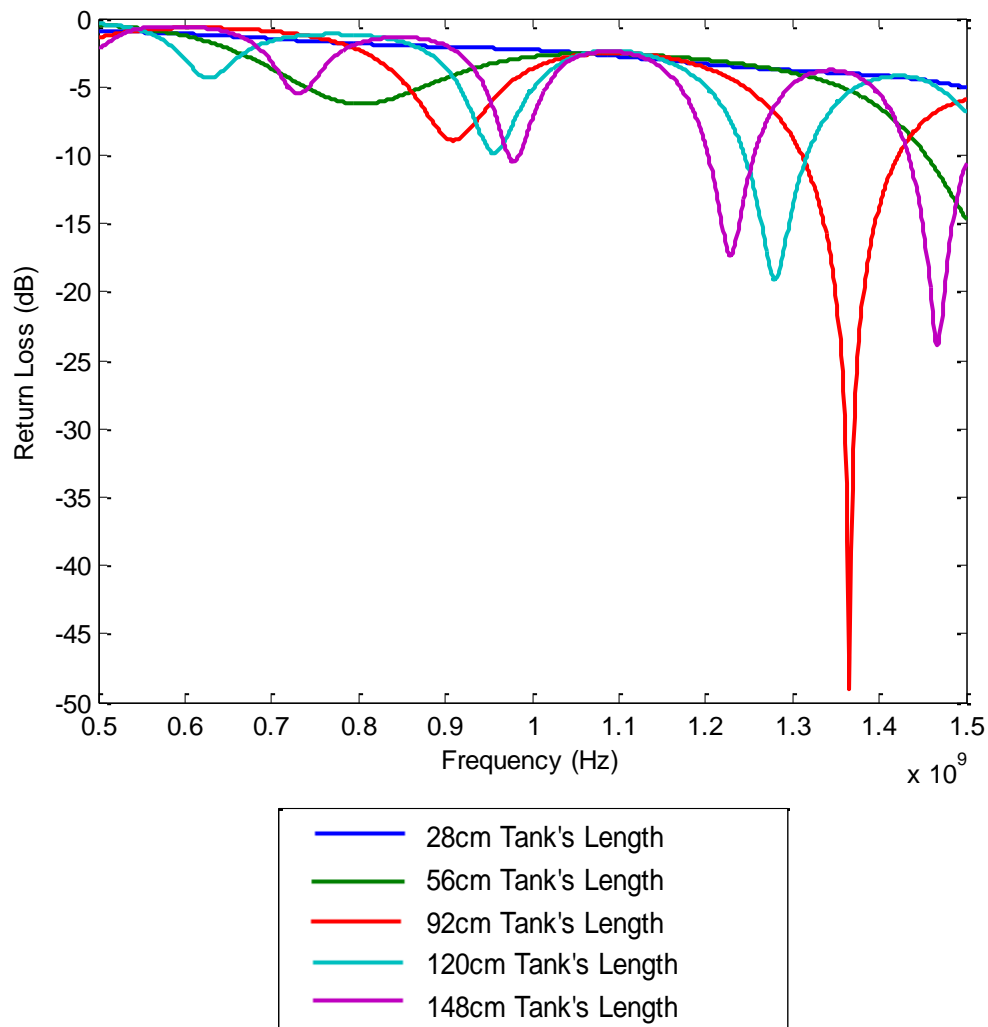


Figure 4.40 Simulated Return Loss of Extending the Mesh Plates Length for an Air Medium Testbed. The Mesh Length's are; 28 cm (Blue Trace), 56 cm (Green Trace), 92 cm (Red Trace), 120 cm (Cyan Trace), and 148 cm (Magenta Trace).

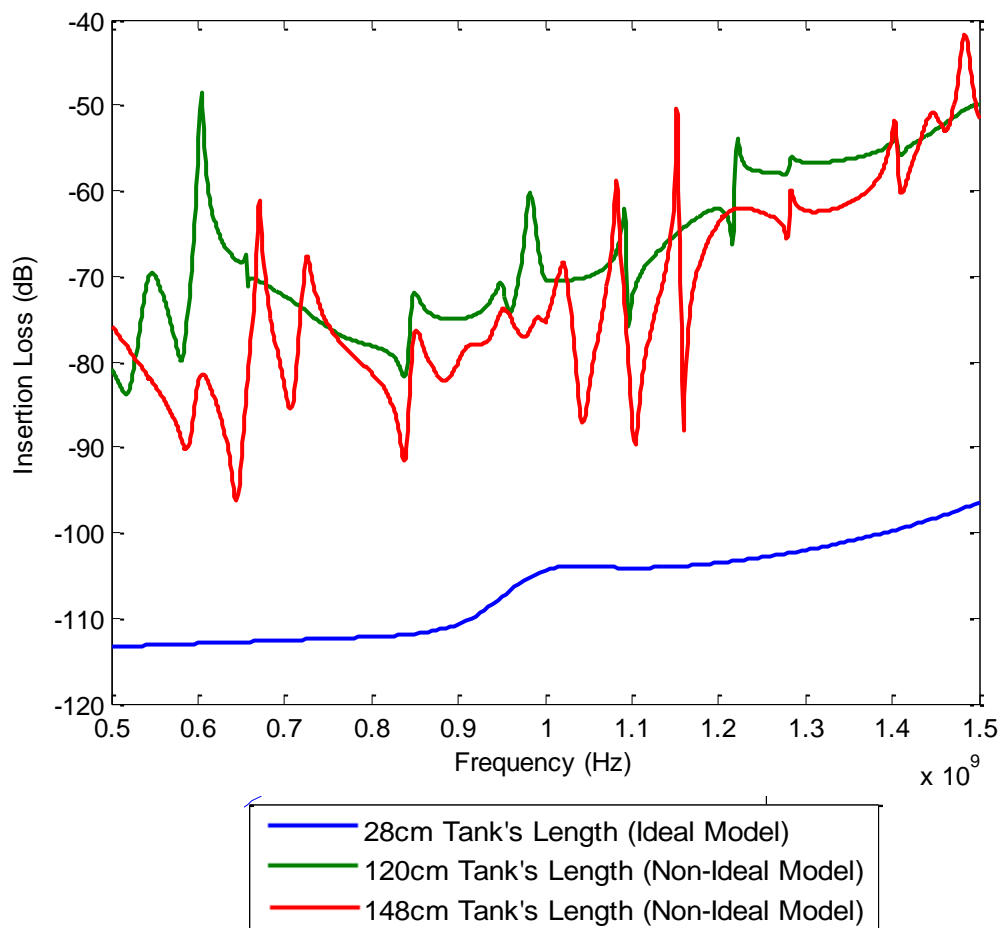


Figure 4.41 Simulated Insertion Loss of an Air Medium Testbed. Ideal Testbed (Blue Trace), 112 cm Long Extended Testbed (Green Trace), and 140 cm Long Extended Testbed (Red Trace).

From previous experimental time domain measurements (Figure 4.30), the first peak of the transmission response with the antennas located at top and bottom boreholes showed a significant delay compared with the antennas located at middle boreholes. For the experiments without vertical extensions, the antennas located at the top and bottom boreholes of the testbed were close to the discontinuity of the waveguide, causing additional undesired wave propagation modes. This results in inaccurate s-parameters measurements and consequently inaccurate EM properties estimates. In order to avoid

undesired wave propagation modes, simulations extending the testbed vertically were suggested.

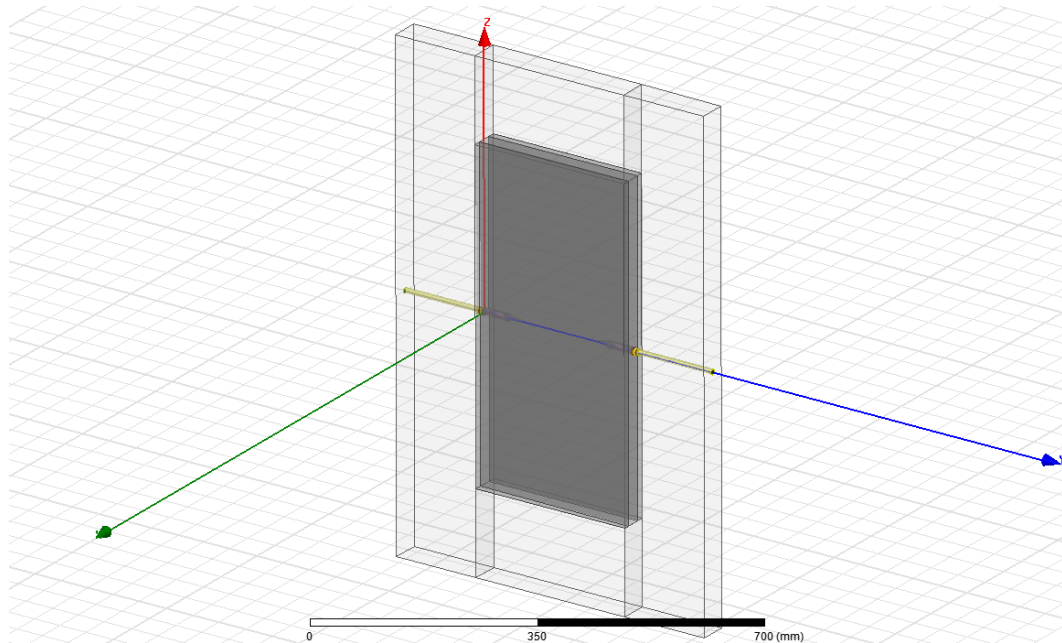


Figure 4.42 Simulated-Model Diagram of an Air Medium Testbed Without Air Radiation Boundaries at the Extent of the Tank.

Simulations of the transmission response extending the testbed vertically were performed on an air medium testbed model. The model used for the simulations was the same model used to perform the simulations to extend the mesh plates horizontally. For these simulations, the length of the testbed remains unchanged (28 cm) while the heights used were 58 cm, 87 cm, 116 cm, and 145 cm. From the simulated results of Figure 4.43, a height of 116cm fulfilled our purpose because there is small difference in the transmission response between 116 cm and 145 cm.

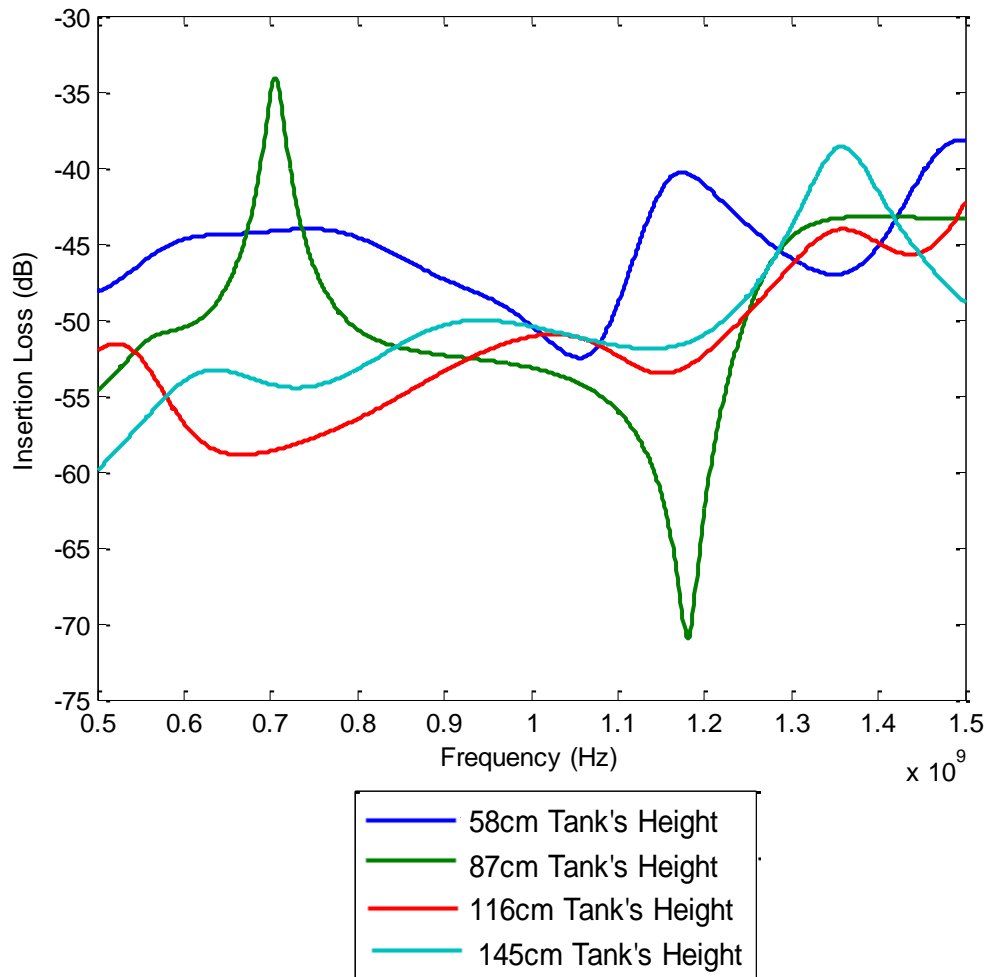


Figure 4.43 Simulated Insertion Loss Response of Air Medium Testbed. Testbed Heights are; 58cm High (Blue Trace), 87cm High (Green Trace), 116cm High (Red Trace), and 145cm High (Cyan Trace).

The suitable dimensions suggested for the testbed to be fabricated is 122 cm wide by 120 cm high (Figure 4.43). Due to physical limitations, the height was limited to 107 cm. Simulations were performed of the suggested dimensions for the extended testbed by placing the antennas at different boreholes locations. The resulted transmission response showed a good agreement (Figure 4.45) for an air medium. These suggested testbed leads to accurate s-parameters measurements and also to good estimates of the EM properties.

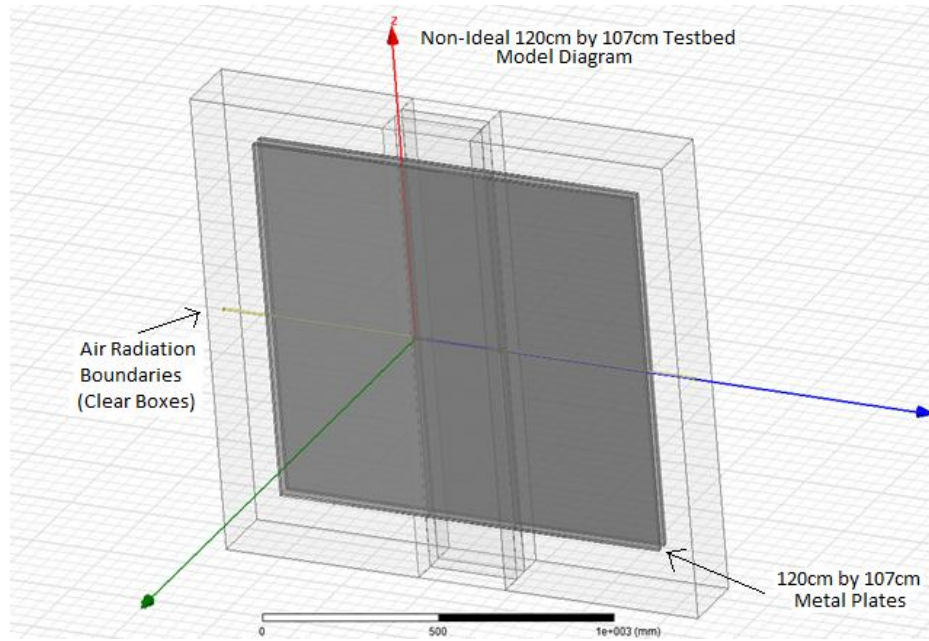


Figure 4.44 Simulated Extended Testbed Model Diagram.

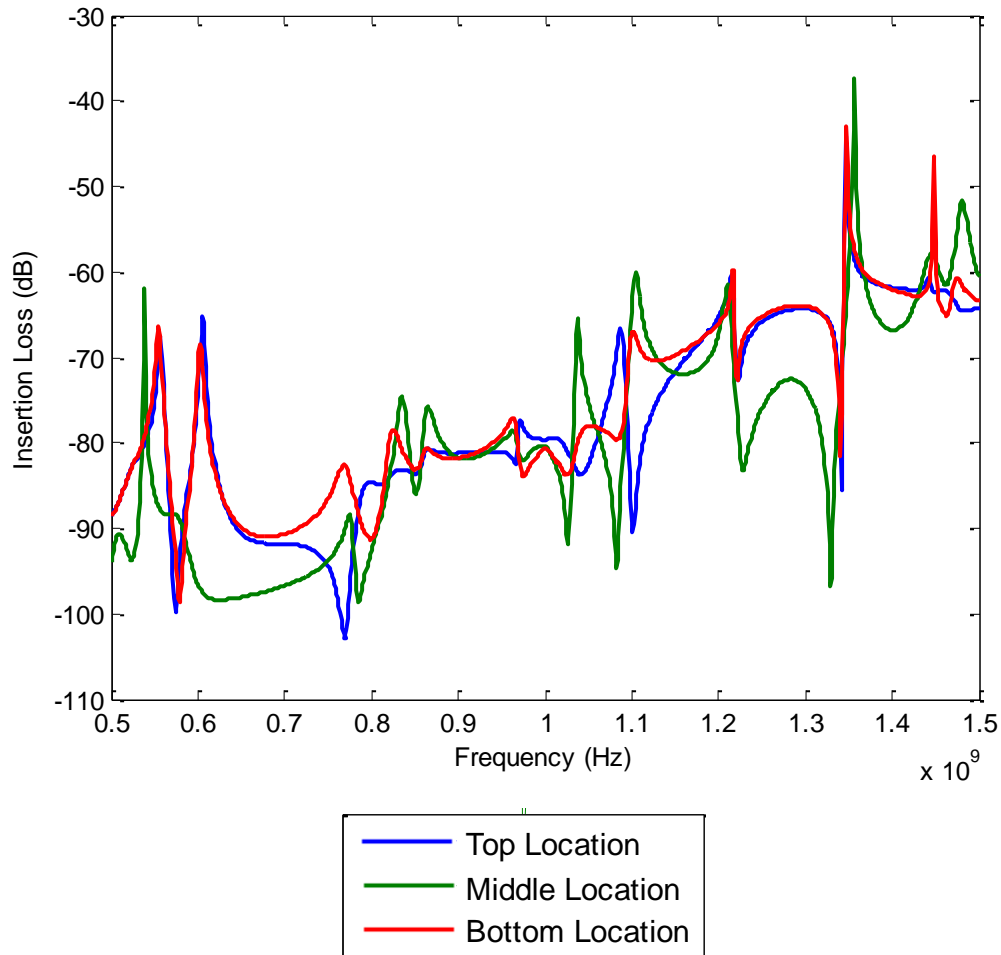


Figure 4.45 Simulated Insertion Loss Response for an Air Medium Extended Testbed (122 cm Wide, 107 cm High, and 2.54 cm Deep). Helix Antennas Located at Top (Blue Trace), Middle (Green Trace), and Bottom (Red Trace) Borehole Locations.

4.7 Estimates of the Relative Permittivity for the Simulated Extended Testbed Model in Time Domain

Estimates of the relative permittivity for the extended testbed simulated model using equation 3.12 for different assigned relative permittivities are shown in table 4.11. The results demonstrate similarities with a slight difference in the estimated values. These differences could be due to the equations used by the Ansoft simulator to analyze

the transmission and reflection response of the extended testbed and the equations used to determine the relative permittivity from the simulated transmission and reflection response of the extended testbed. The simulator uses a combination of Maxwell equations with the finite element method (FEM) to perform a three dimension (3D) full-wave analysis. From the 3D analysis, simulated transmission and reflection response are then extracted. Then, using the simulated transmitted and reflected response, the estimates of the relative permittivity were performed using equation 3.12, which applies for a 2D analysis and limits the accuracy of the estimated values. The reason of using equation 3.12 is to apply method to estimate the relative permittivity considering a controlled testbed system with simplification in the analysis (2D analysis, TEM wave propagation mode, homogeneous medium), and evaluate the possibility of obtaining the EM properties of bulk soil. Transmission and reflection responses of the simulated extended testbed model for different assigned EM properties using transient network analysis are shown in Figures 4.46-4.55.

Table 4.11 Estimates of the Relative Permittivity of the Simulated Extended Testbed Model

Type of material	Assigned Relative Permittivity	Estimated Relative Permittivity	Percentage Error (%)
Air Medium	1	1.04	4
Dry Sand	4	4.56	14
Test Property #1	10	10.8	8
Test Property #2	20	20.16	0.8

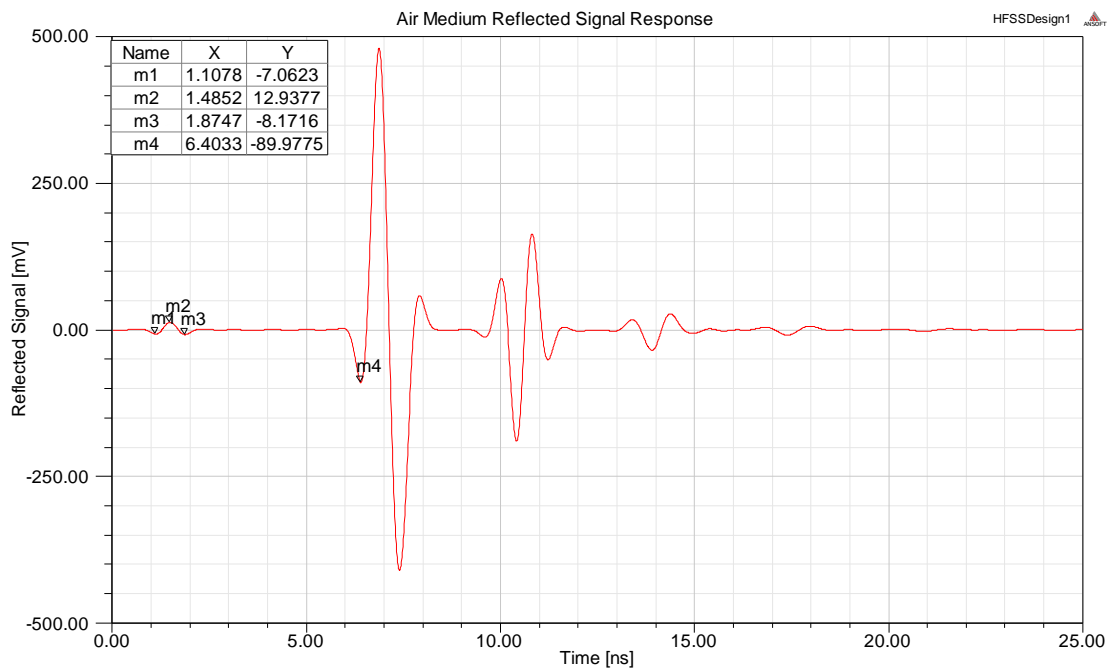


Figure 4.46 Simulated-Model Result of the Reflected Response for Air Medium of the Extended Testbed.

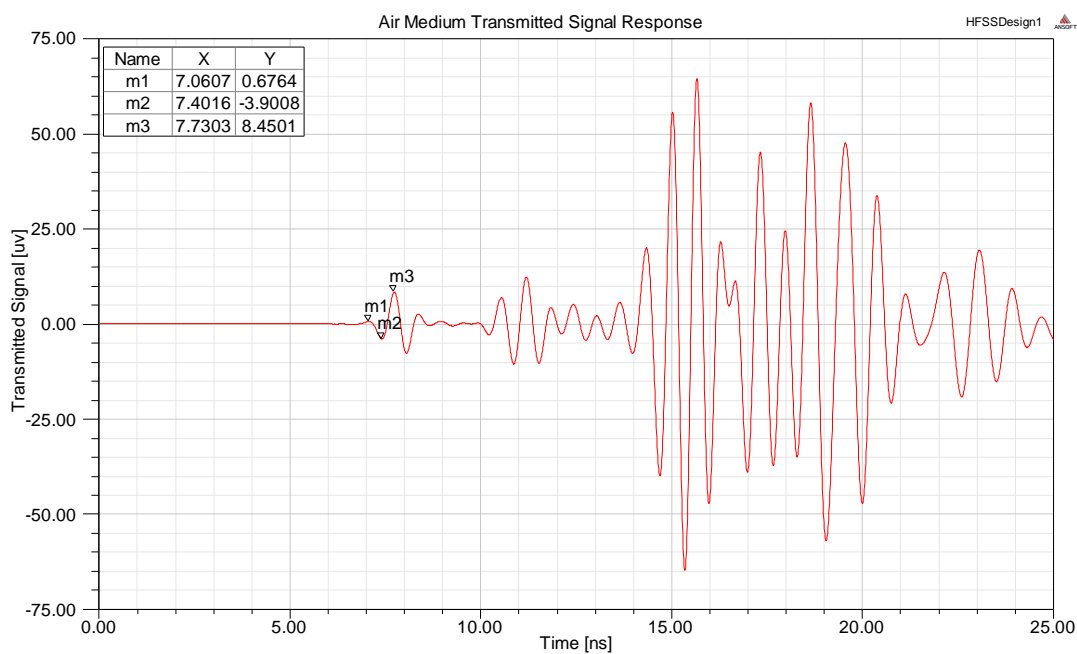


Figure 4.47 Simulated-Model Result of the Transmitted Response for Air Medium of the Extended Testbed.

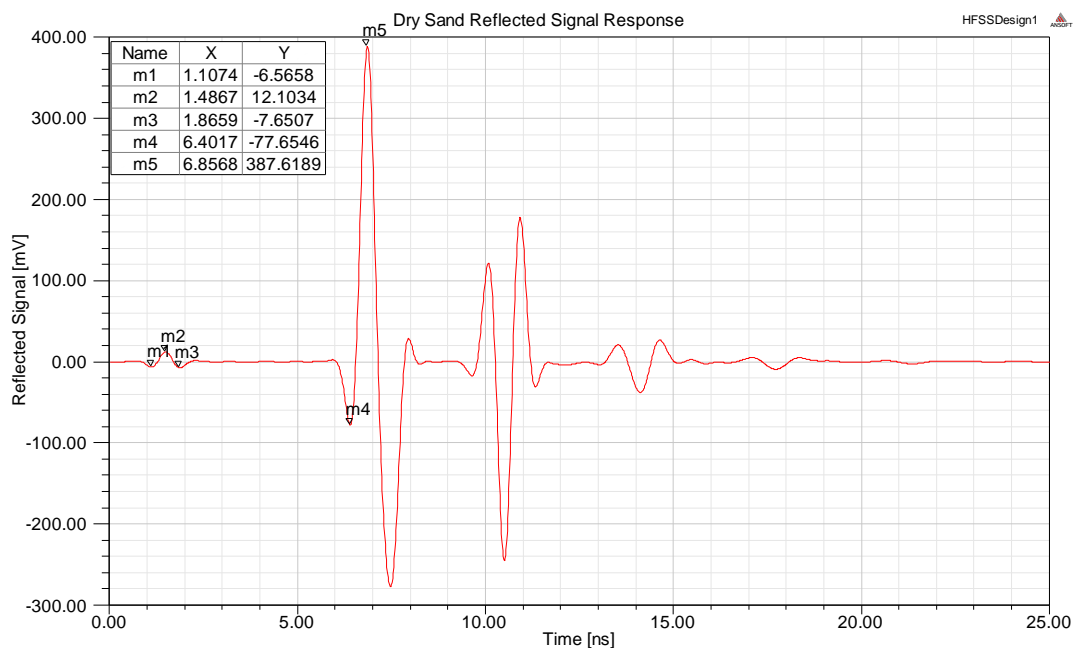


Figure 4.48 Simulated-Model Result of the Reflected Response for Dry Sand of the Extended Testbed.

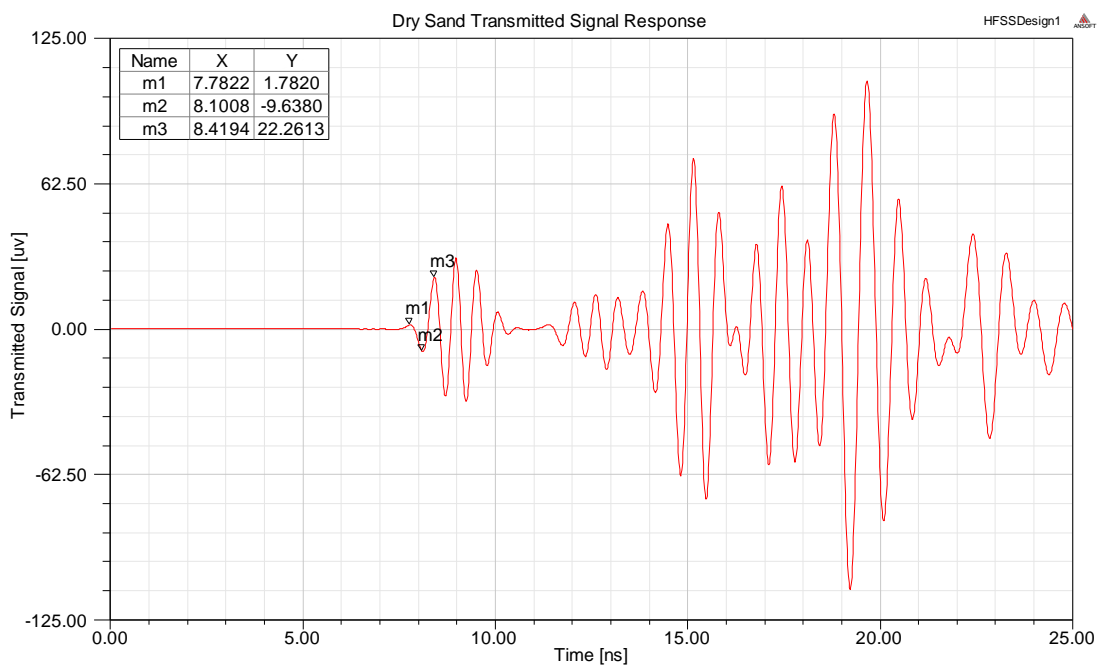


Figure 4.49 Simulated-Model Result of the Transmitted Response for Dry Sand of the Extended Testbed.

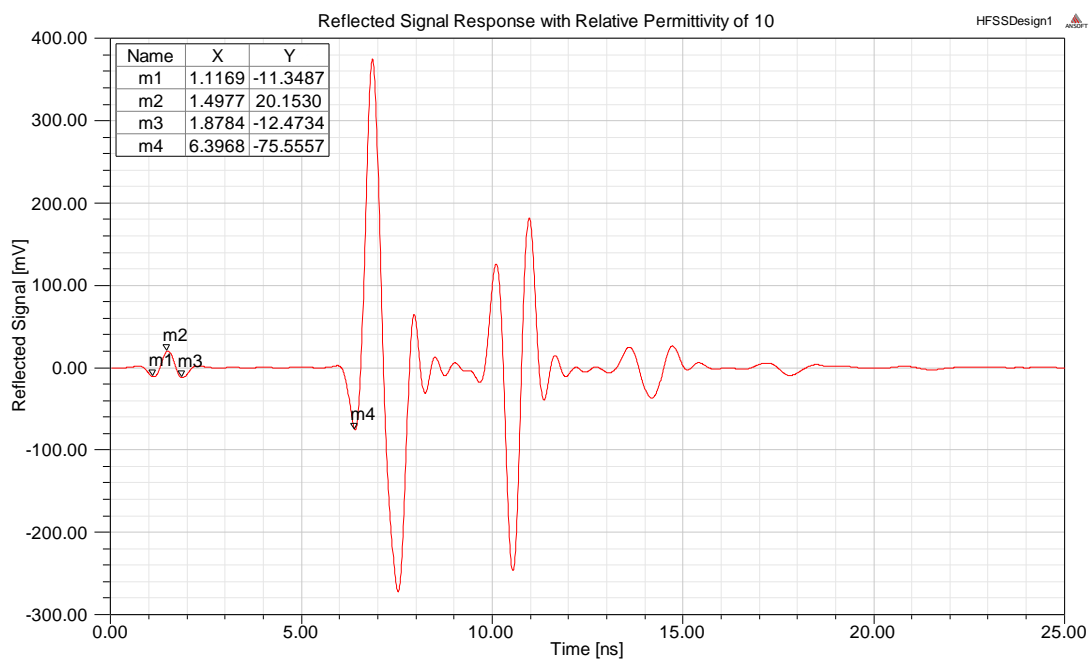


Figure 4.50 Simulated-Model Result of the Reflected Response for a Relative Permittivity of 10 of the Extended Testbed.

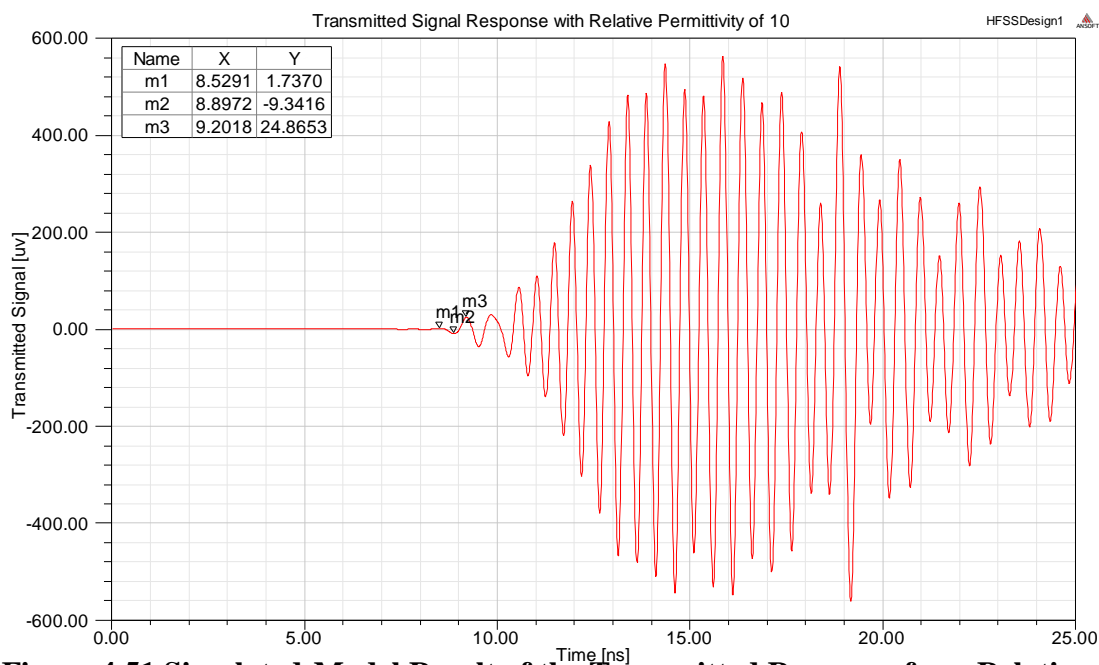


Figure 4.51 Simulated-Model Result of the Transmitted Response for a Relative Permittivity of 10 of the Extended Testbed.

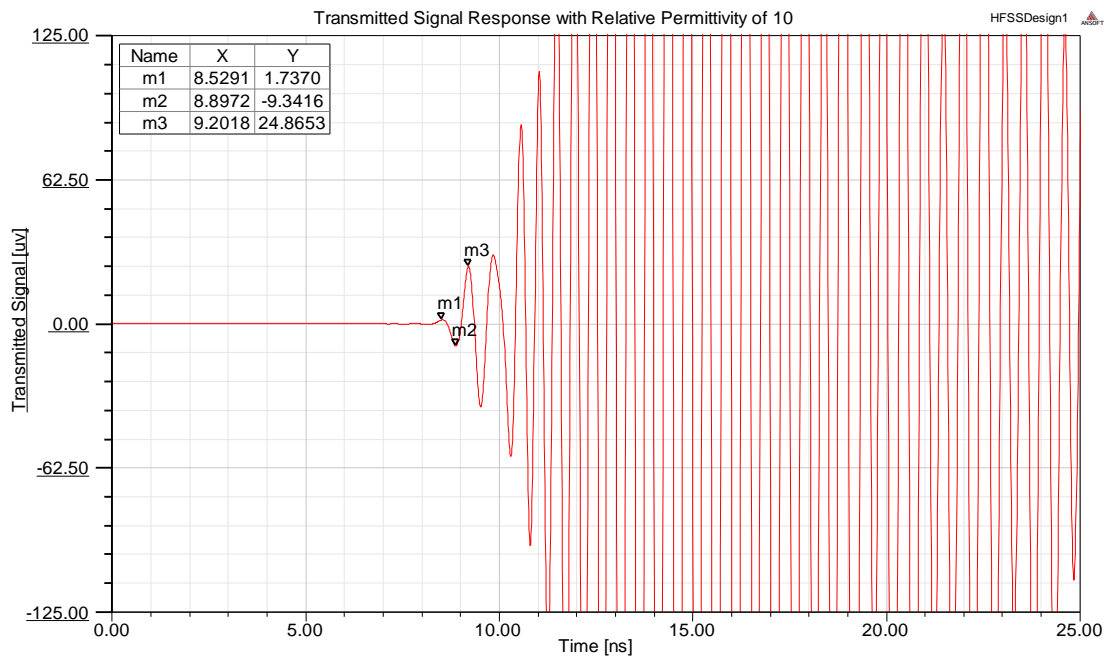


Figure 4.52 Simulated-Model Result of the Transmitted Response for a Relative Permittivity of 10 of the Extended Testbed (Closer Look).

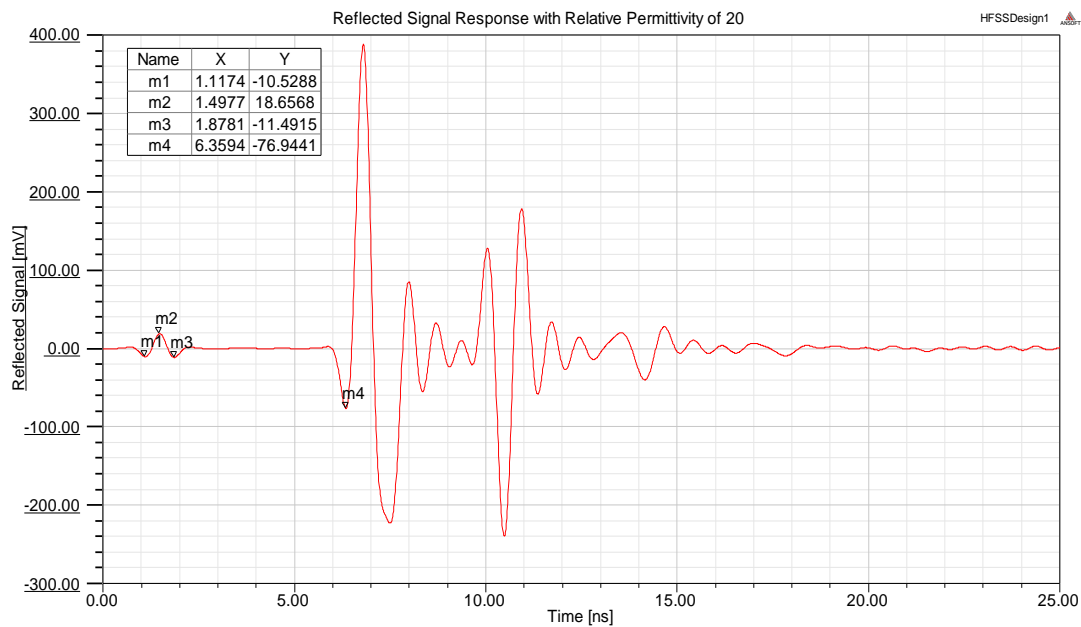


Figure 4.53 Simulated-Model Result of the Reflected Response for a Relative Permittivity of 20 of the Extended Testbed.

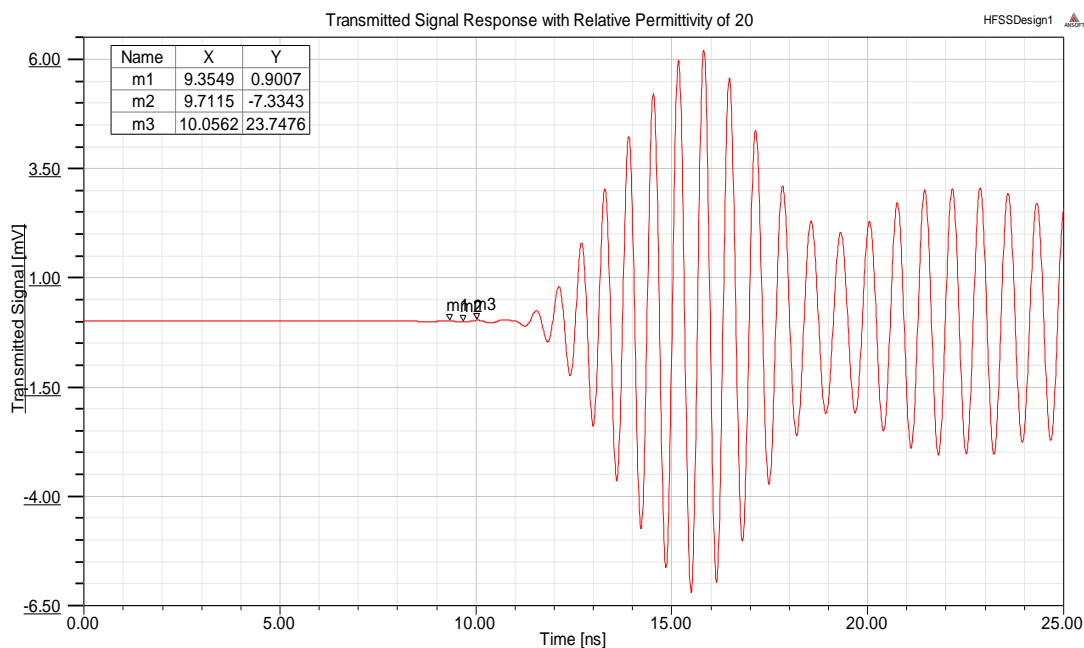


Figure 4.54 Simulated-Model Result of the Transmitted Response for a Relative Permittivity of 20 of the Extended Testbed.

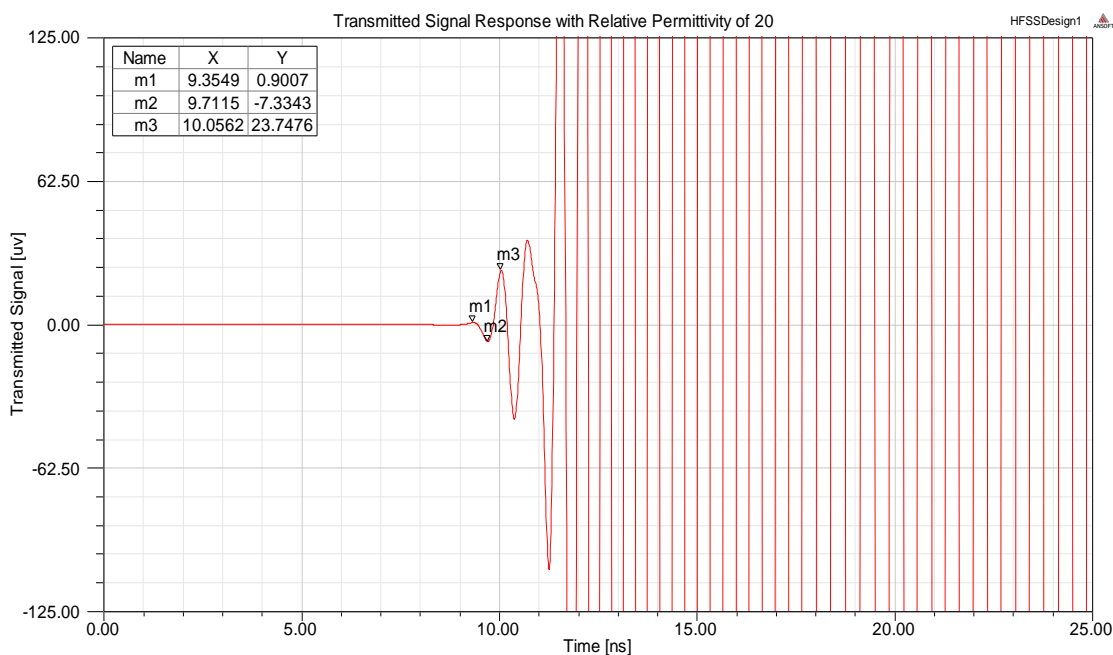


Figure 4.55 Simulated-Model Result of the Transmitted Response for a Relative Permittivity of 20 of the Extended Testbed (Closer Look).

Transient analysis was performed for the previous constructed testbed (30 cm wide, 60 cm high, and 2.5 cm deep) taking into consideration no air boundaries at the face (ideal model) in the extent of the tank and with air boundaries (real model) for an air medium. The simulated results for the reflected and transmitted response for both testbed models are present in Figures 4.56-4.57 and 4.58-4.59, respectively. Estimates of the relative permittivity were performed and compared for both testbed models (Table 4.12). The results of the estimates showed a lesser percentage error when the testbed is without air boundaries at the extent of the tank. This is due to absence of energy entering the testbed through the edge boundaries and through the extent of the tank.

Table 4.12 Estimates of the Relative Permittivity for the Simulated Testbed Model in Air Medium

Type of Material	Estimated Relative Permittivity	Percentage Error (%)
Air Medium (No Air Boundaries)	1.09	9
Air Medium (Air Boundaries)	1.24	24

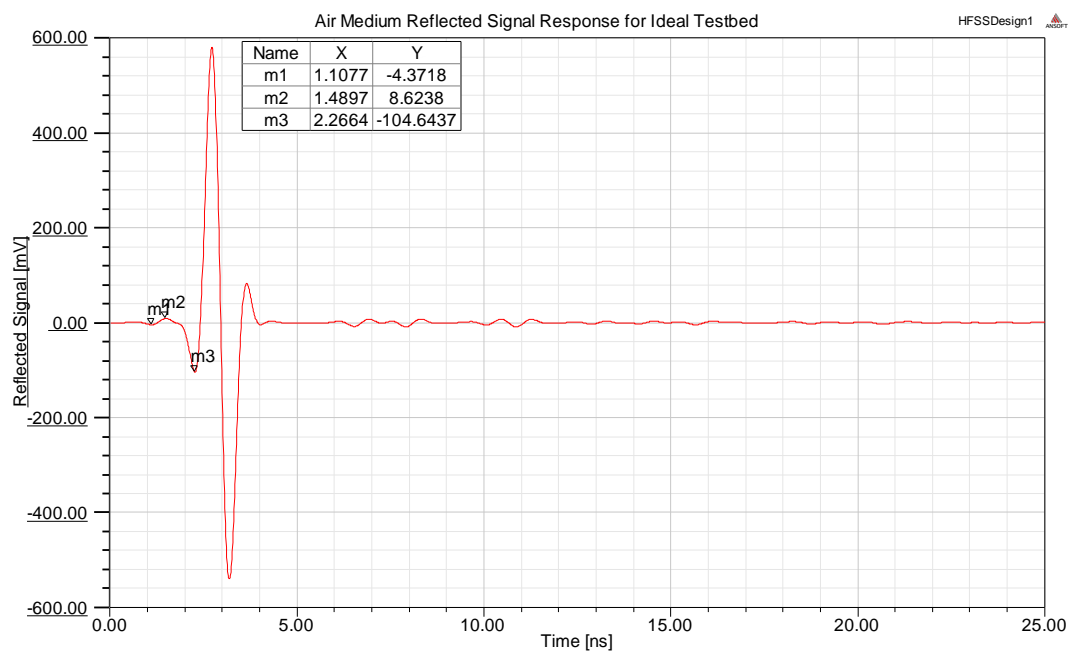


Figure 4.56 Simulated-Model Result of the Reflected Response for Air Medium of the Ideal Testbed.

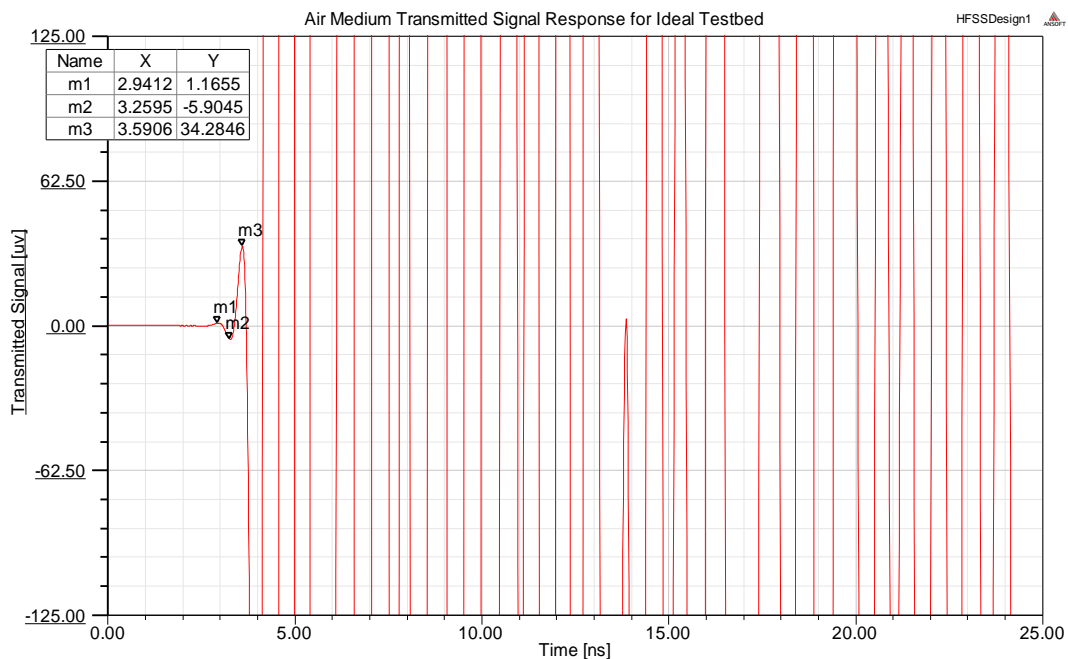


Figure 4.57 Simulated-Model Result of the Transmitted Response for Air Medium of the Ideal Testbed.

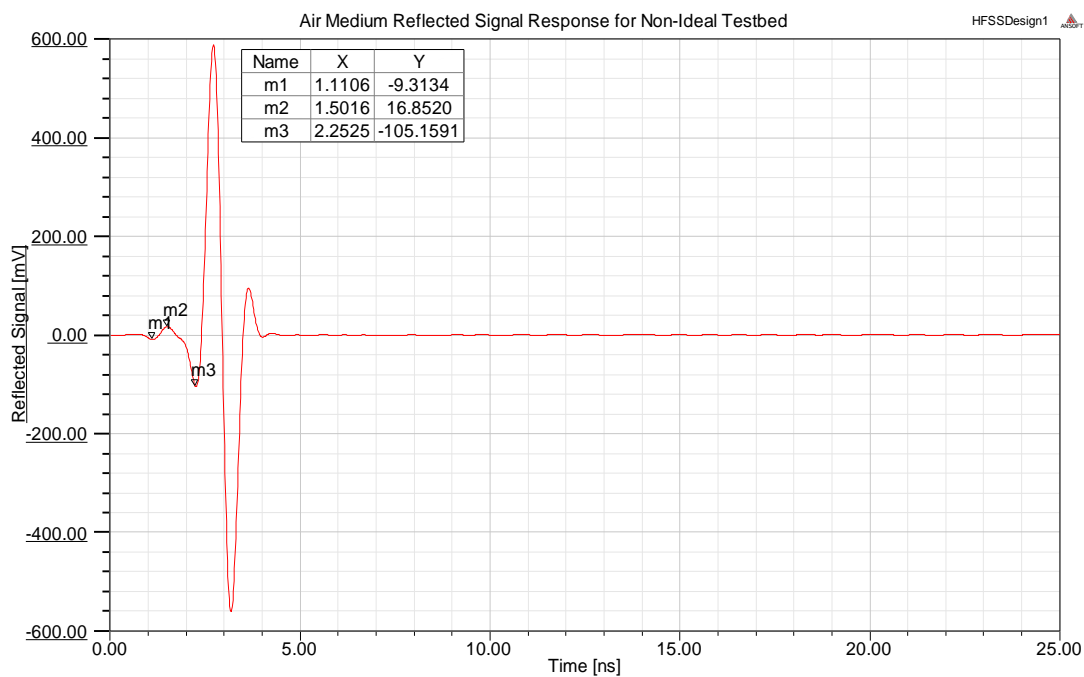


Figure 4.58 Simulated-Model Result of the Reflected Response for Air Medium of the Real Testbed.

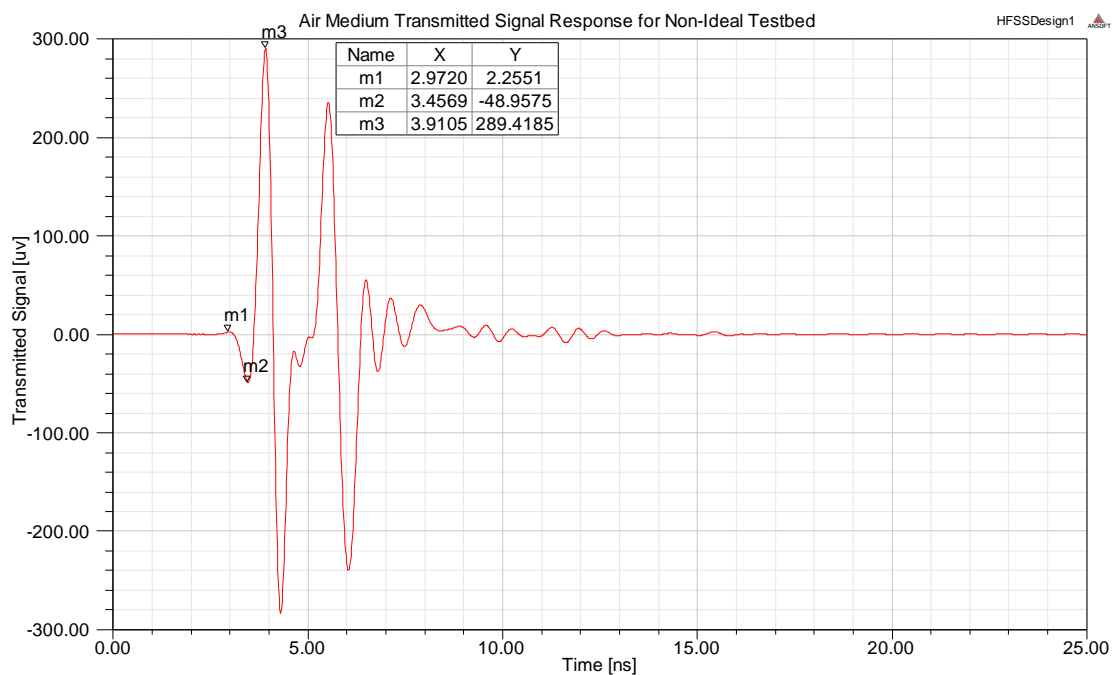


Figure 4.59 Simulated-Model Result of the Transmitted Response for Air Medium of the Ideal Testbed.

Table 4.13 Estimates of the Relative Permittivity for the Simulated Extended Testbed Model of Air Medium with the Antennas Placed at Different Height Boreholes

Antenna Height	Estimated Relative Permittivity	Percentage Error (%)
35.6cm	1.05	5
53.3cm	1.04	4
89cm	1.06	6

Simulations for the extended testbed in air medium with the antennas located at different heights were performed and also results of the estimates of the relative permittivity were determined. Figures 4.60-4.61 and 4.62-4.63 show the simulated response of the extended testbed in air medium with the antennas located at 35.6 cm high and 89 cm high respectively. Results demonstrate similarities in the estimates (Table 4.13) and leads to an improvement of the simulated response because very accurate values were obtain for different heights.

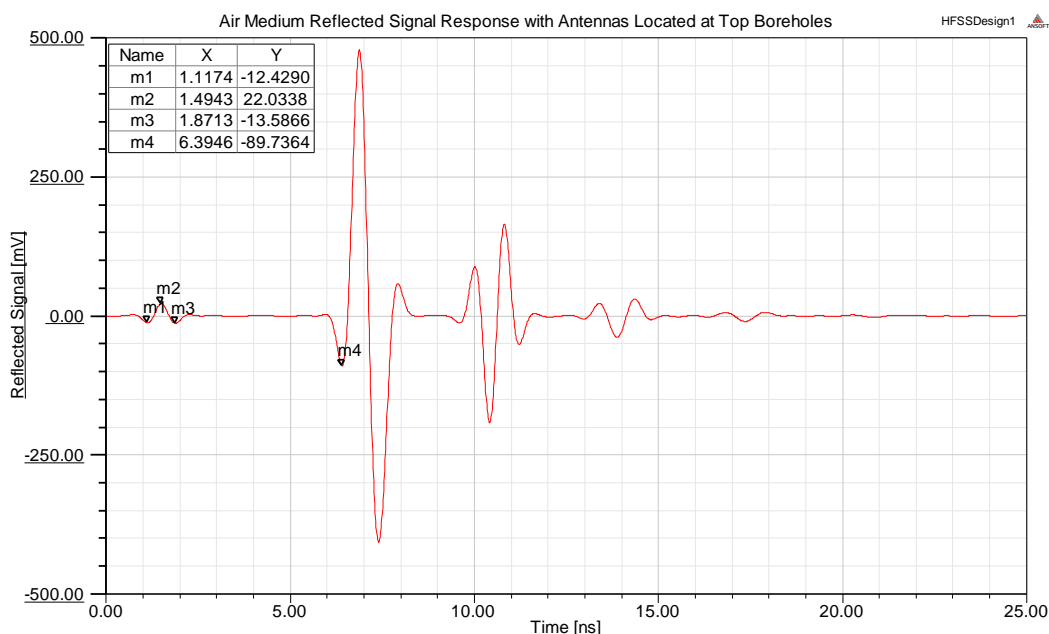


Figure 4.60 Simulated-Model Result of the Reflected Response for Air Medium of the Extended Testbed with Antennas Located at Top Borehole.

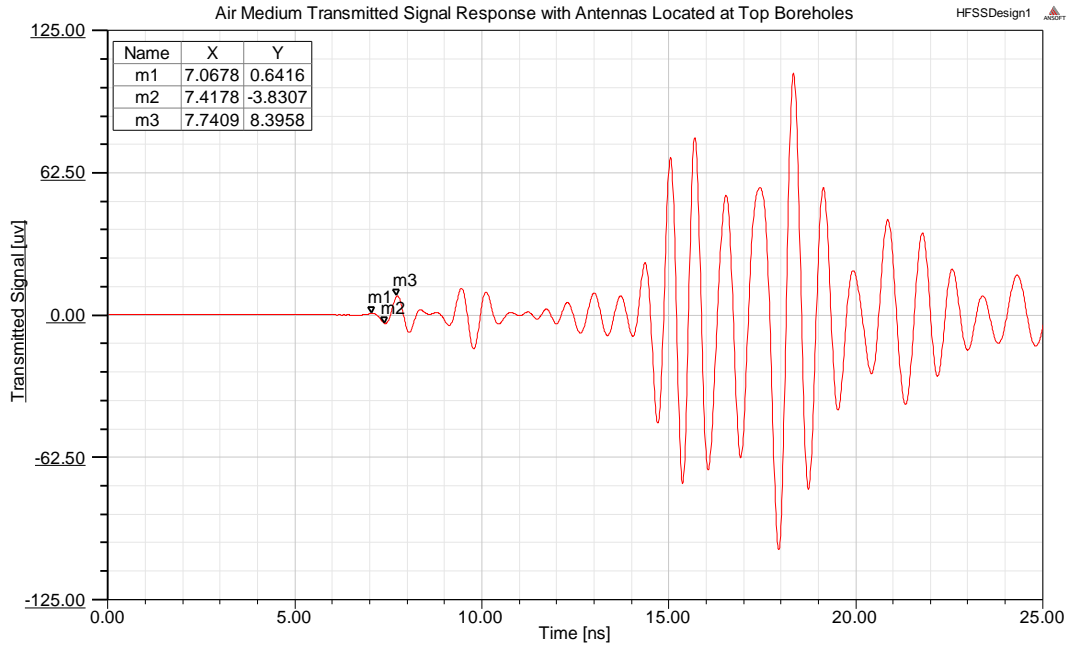


Figure 4.61 Simulated-Model Result of the Transmitted Response for Air Medium of the Extended Testbed With Antennas Located at Top Borehole.

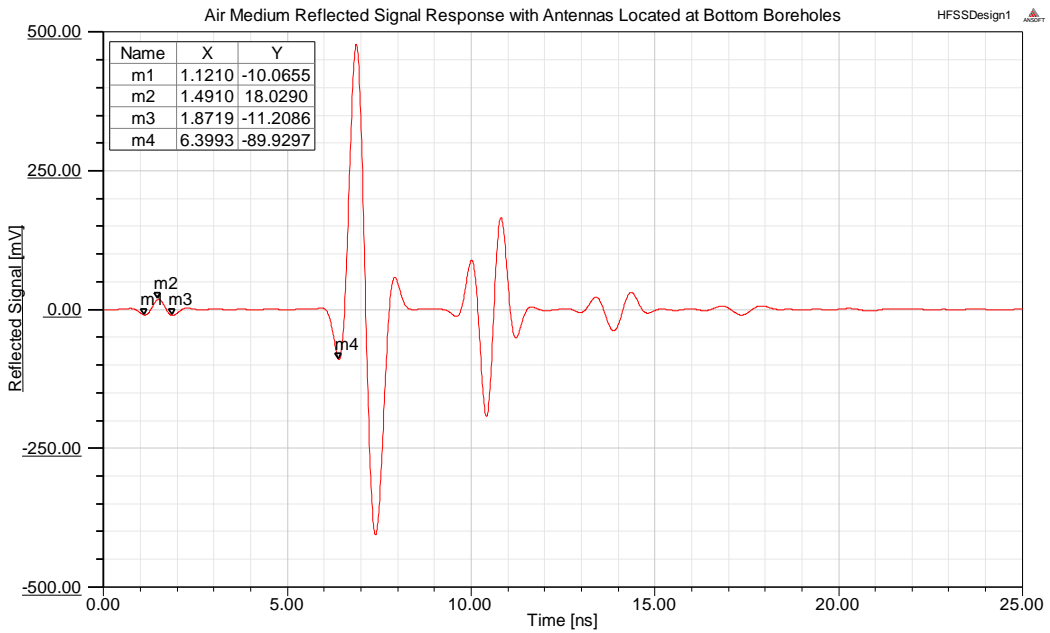


Figure 4.62 Simulated-Model Result of the Reflected Response for Air Medium of the Extended Testbed With Antennas Located at Bottom Borehole.

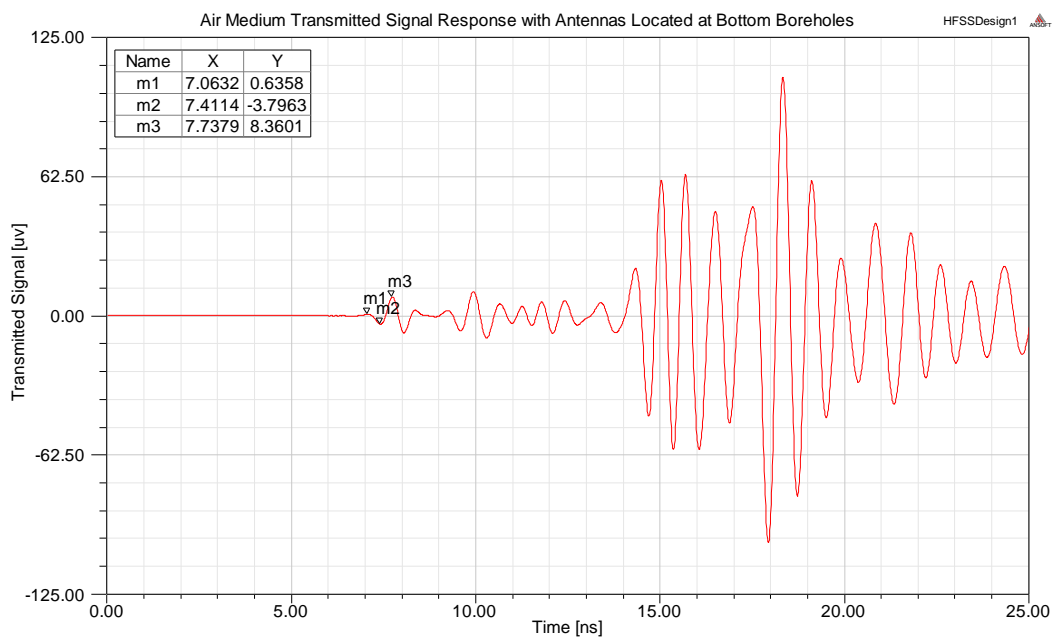


Figure 4.63 Simulated-Model Result of the Transmitted Response for Air Medium of the Extended Testbed With Antennas Located at Bottom Borehole.

5 Conclusion and Recommendations

5.1 Conclusion

CWR transmission and reflection measurements may be applied to detect changes in soil EM properties caused by the presence of underground target elements, such as metal and plastic objects, and DNAPL contamination. Soil testbeds can be used to model CWR systems to interpret EM measurements into meaningful parameters that directly relate to the object of interest, thus enabling CWR technologies for system-wide applications. These testbeds must however, be properly developed to provide accurate s -parameters measurements of the bulk soil and enhance the estimation of soil EM properties under different environmental conditions.

An electromagnetic soilbed was developed to model CWR measurements in soils, and estimate EM properties that can be used to characterize the magnitude and location of DNAPL contamination in underground environments. Experimental and modeling results show that the soilbed developed is applicable for CWR measurements, provided that EM design considerations are met. These considerations include soilbed geometry and boundaries, separation and extension of metal plates, and antennas configuration.

Experimental and modeling efforts to estimate EM properties (i.e., relative permittivities) in a sandy soilbed under different environmental conditions using frequency domain methods show that a minimum extension of the tank is required for proper characterization of the EM properties. At scales smaller than this distance, energy escapes the soilbed near plate discontinuities, causing the wave to propagate through the air along paths outside the waveguide. As a result, receiving antennas respond to wave

propagation along the waveguide paths in the soilbed, and to waves propagating outside the waveguide and re-entering across the top, bottom and edges of the soilbed. It is concluded that the metal plates must extend a minimum distance for accurate measurements. This minimum distance required can be assessed through EM modeling of the system.

The integration of frequency- and time-domain measurements and simulations provided essential tools for proper design. Time-domain analysis applied to the transmission and reflection EM response in the properly developed testbed yielded accurate estimates of soil EM properties.

5.2 Recommendations

- Increase the separation between parallel plates to provide a larger volume of the soilbed to avoid boundaries effects.
- Estimate the EM properties for the extended testbed using the previously frequency domain equations used and compare the results with the estimated results obtained from time domain measurements.

REFERENCES

- Abbas, Z., R. Pollard, and R. Kelsall, "Complex Permittivity Measurements at Ka-Band Using Rectangular Dielectric Waveguide", *IEEE Transaction on Instrumentation and Measurements*, vol. 50 no. 5, pp1334-1341, October 2001.
- Balanis, C., "*Antenna Theory: Analysis and Design*", 3rd ed., Wiley & Sons Publication, New Jersey, pp 1-4, 2005a.
- Balanis, C., "*Antenna Theory: Analysis and Design*", 3rd ed., Wiley & Sons Publication, New Jersey, pp 566-571, 2005b.
- Chen, L.F., C.K. Ong, C.P. Neo, V.V. Varadan, and V. K. Varadan, "*Microwave Electronics: Measurement and Material Characterization*", Wiley & Sons Publication, England, pp 175-207, May 2004.
- Chung, B.K., "Dielectric Constant Measurement for Thin Material at Microwave Frequencies", *Progress In Electromagnetics Research, PIER 75*, 239–252, 2007.
- Day-Lewis, F.D., J. W. Lane, J. M. Harris, and S.M. Gorelick, "Time-Lapse Imaging of Saline Tracer Transport in Fractured Rock using Difference Radar Attenuation Tomography", *Water Resources Research*, vol.39 pp 1290, 2003.
- De Weck, O., Yong Kim, I., "Finite Element Method", Presentation, Massachusetts Institute of Technology, Cambridge, MA, January 2004.
- Ebihara, S., and Y. Hashimoto, "MoM Analysis of Dipole Antennas in Crosshole Borehole Radar and Field Experiments", *IEEE Transactions on Geoscience and Remote Sensing*, vol. 45, no. 8, pp 2435-2450, August 2007.
- Farid, M., C. Kurison, A. N. Alshwabkeh, and C. M. Rappaport, "Tunnel Detection Using Cross Borehole Radar", 2006 Validating TestBED and Research Posters on Real World Problems for I-PLUS Development Conference, Northeastern Univ., Boston, MA, 2006.
- Farid, M., "DNAPL Detection Using Cross Well Radar", Ph.D. dissertation, Department of Civil and Environmental Engineering, Northeastern Univ., Boston, MA, 2004.
- Farid, M., A. N. Alshwabkeh, and C. M. Rappaport, "Laboratory Experimental Setup for Cross-Well Radar", *Symposium on the Application of Geophysics to Engineering and Environmental Problems*, Texas, 2003a.
- Farid, M., A. N. Alshwabkeh, and C. M. Rappaport, "Modeling Borehole Dipole Antenna Patterns for Cross-Well Radar DNAPL Imaging", *Electronic Proceedings of the 12th Pan-American Conference on Soil Mechanics and Foundation Engineering*, Cambridge, MA, 2003b.
- Gunasekaran, S., R. K. Natarajan, A. Kala and R. Jagannathan, "Dielectric of Studies of Some Rubber Materials at Microwave Frequencies", *Indian Journal of Pure and Applied Physics*, vol. 46, pp 733-737, October 2008.

- Hasar, U.C., "Permittivity Determination of Fresh Cement Based Materials by an Open-Ended Waveguide Probe Using Amplitude-Only Measurements", *Progress In Electromagnetics Research, PIER 97*, pp 27-43, 2009.
- Igel, J., K. Takahashi, and H. Preetz, "Electromagnetic Soil Properties and Performance of GPR for Landmine Detection: How to Measure, How to Analyze and How to Classify?", 6th International Workshop on Advanced Ground Penetrating Radar (IWAGPR), pp 1-6, June 2011.
- Jang, H., M. Kyung Park, and H. J. Kim, "Numerical Modeling of Electromagnetic Waveguide Effects on Crosshole Radar Measurements", *Exploration Geophysics*, vol. 38, pp 69-76, 2007.
- Kim, J. S. Cho, M. Yi, and M. Sato, "Anisotropy Borehole Radar Tomography in Korea, Tenth International Conference on Ground Penetrating Radar, Netherlands, June 14-21, 2004.
- Kraus, J., "*Antennas*", 2nd ed., McGraw-Hill Publications, New York, pp 265-271, 1988.
- Lane, J. W., F. D. Day-Lewis, R. J. Versteeg, and C. C. Casey, "Objects-Based Inversion of Cross-well Radar Tomography Data to Monitor Vegetable Oil Injection Experiments", *Proceedings at the Symposium on the Application of Geophysics to Environmental and Engineering Problems SAGEEP, Texas*, 2003.
- Maio, I., P. Savi, and F. Marino, "Estimation of the Permittivity of Dielectrics from the Scattering Responses of TEM Waveguides", 2009 Mediterranean Microwave Symposium (MMS), pp 1-6, February 2010.
- Nakano, M., and P. Savi, "Dielectric Permittivity Estimation via TDR Measurements", *International Conference on Electromagnetics in Advanced Applications, 2009. ICEAA '09*. pp 921-924, November 2009.
- Nicolson, A. M., and G. F. Ross, "Measurement of the Intrinsic Properties of Materials by Time-Domain Techniques" *IEEE Transaction on Instrumentation and Measurements* vol. 19 , no. 4, pp 377 – 382, 1970.
- NRC (National Research Council), *Seeing Into the earth: Noninvasive Characterization of the Shallow Subsurface for Environmental and Engineering Applications*, National Academy Press, Washington D.C., 2000.
- Panzner, B., J. Andreas, and O. Abbas, "Estimation of Soil Electromagnetic Parameters Using Frequency Domain Techniques", 13th International Conference on Ground Penetrating Radar (GPR), pp 1-5, August 2010.
- Rappaport, C. M., S. Wu, M. E. Kilmer, and E. L. Miller, "Distinguishing Shape Details of Buried Non-Metallic Minelike Objects With GPR", *Proceedings of SPIE AeroSense Symposium, Orlando*, vol. 3710, pp 1419-1428, 1999.
- Ratto, C., P. Torrione, and L. Collins, "Estimation of Soil Permittivity Through Autoregressive Modeling of Time-Domain Ground-Penetrating Radar Data", 2010 IEEE International Conference on Wireless Information Technology and Systems (ICWITS), pp 1-4, October 2010.

- Robinson, D.A., "Measurement of the Solid Dielectric Permittivity of Clay Minerals and Granular Samples Using a Time Domain Reflectometry Immersion Method", *Vadose Zone Journal*, Vol. 3 , pp 705-713, May 2004.
- Sagnard, F., F. Rejiba, and M. Froumentin, "Development of Wideband Crosshole and Surface GPR for Soil Characterization: FDTD Modeling and Experiments", *Proceedings of the 40th European Microwave Conference*, pp 331-335, 2010.
- Sagnard, F., "Design of Compact UWB Planar Monopole Antennas for Cross-Hole Radar Application", *IEEE Geoscience and Remote Sensing Letters*, vol. 6, no. 4, pp 816-819, October 2009.
- Sato, M., and T. Takayama, "High Range Resolution Directional Borehole Radar for 3-D Fracture Delineation", *2009 IEEE International Geoscience and Remote Sensing Symposium (IGARSS)*, pp I132- I135 , July 2009.
- Savi, P., I. A. Maio, and I. S. Stievano, "TDR Response Properties and Their use in the Estimation of Soil Permittivity", *Instrumentation and Measurement Technology Conference - IMTC 2007*, pp 1-4, May 2007.
- Serrano, M. F., "Detection and Monitoring of DNAPLs in the Subsurface Under Transient Conditions Using Cross Well Radar", Ph.D. Dissertation, Department of Civil Engineering and Surveying, Univ. Puerto Rico, Mayagüez Campus, Mayagüez, PR, 2008.
- Serrano-Guzman, M. F., I. Padilla, and R. Rodríguez, "Bimodal Detection of Underground Contamination in Two Dimensional Systems", *Proceedings in SPIE on Optics and Photonics in Global Homeland Security III*, vol. 6540 65401O-1-13, 2007.
- Shivandas, D., "Broadband Counter-Wound Helix Antenna for Land Mine Detection", M.S. Dissertation, Naval Postgraduate School, Monterey, CA, 2004.
- Takahashi, K., and M. Sato, "Parametric Inversion Technique for Location of Cylindrical Structures by Cross-Hole Measurements", *IEEE Transactions on Geoscience and Remote Sensing*, vol. 44, no. 11, pp 3348-3355, November 2006.
- Toro-Vázquez, J., Rodríguez-Solís, R., Padilla, I., "Frequency and Time Domain Measurements Using Cross Well Radar to Develop Testbeds for Electromagnetic Properties Estimation", *2011 IEEE International Geoscience and Remote Sensing Symposium (IGARSS)*, Vancouver, BC, pp 850-853, July 2011.
- Will, B., and M. Gerding, "A Time Domain Transmission Method for the Characterization of Inhomogeneous Dielectric Materials", *2009 Asia Pacific Microwave Conference (APMC)*, pp 409-412, December 2009.